The Ribbon Microphone
Multi-Physics Educational Aid

by Marius van Wyk

Thesis presented in fulfilment of the requirements for the degree of Master of Engineering (Electronics) at the Stellenbosch University

Supervisor: Prof. Petrie Meyer

December 2017

DECLARATION

By submitting this thesis electronically, I declare that the entirety of the work contained therein is my own, original work, that I am the authorship owner thereof (unless to the extent explicitly otherwise stated) and that I have not previously in its entirety or in part submitted it for obtaining any qualification.

Date: December 2017

ABSTRACT

Engineering education has historically been mostly mathematics based, with advanced mathematics used to derive simple models for physics phenomena and then using these models to study basic behaviour. However, recent years have seen a proliferation in numerical multi-physics analysis software that performs finite element and finite volume analysis to provide high accuracy solutions to problems. It provides visualisation of solutions that were not possible earlier, thereby giving engineers new insight into problems and solutions. Only using analysis software can however easily cause dissociation from real-world physics and prevent early identification of flawed solutions. To correctly interpret simulation results it is important to first understand how the practical model behaves.

The ribbon microphone is a real-life example that can serve as a laboratory tool for students to make the link between theory, computer simulation and the physical world. Simulation of this seemingly simple device is not trivial. The ribbon microphone is an all-in-one example for simulations in acoustics, mechanics, magnetics and electromagnetics – and the interaction between these disciplines. The value of the ribbon microphone as a teaching aid can be extended by adding transformers and electronic amplifiers to the model. The complete model can be used to illustrate the importance of impedance matching and noise suppression.

The thesis argues a case for the ribbon microphone as a laboratory aid in engineering education. The case for good laboratory examples is supported by related information from engineering education publications. The thesis is structured around a selection of experiments to illustrate how students can learn different aspects of four physics domains through exercises concerned with the ribbon microphone. The experiments consist of computer simulations and real-world exercises. Theory is provided for each physics domain as an introduction to the experiments.

OPSOMMING

Geskiedkundig was ingenieursonderrig hoofsaaklik wiskundig geskoei, met gevorderde wiskunde wat gebruik word om eenvoudige modelle van natuurlike verskynsels af te lei en dan hierdie modelle te gebruik om die basiese gedrag daarvan te bestudeer. Die afgelope tyd is daar egter ‘n klemverskuiwing na die gebruik van numeriese veelvuldige-fisika analisesagteware wat eindige-element en eindige-volume analise uitvoer om hoogs akkurate oplossings vir probleme te verskaf. Dit voorsien die gebruiker met visuele terugvoer wat voorheen nie moontlik was nie. Dit gee ingenieurs dieper insig in probleme en oplossings. Deur slegs analisesagteware te gebruik, kan die gebruiker egter maklik van die werklikheid vervreem word en word foutiewe oplossings nie betyds geïdentifiseer nie. Dit is belangrik om eers die gedrag van die praktiese model te verstaan voordat gesimuleerde oplossings met die nodige insig vertolk kan word.

Die lintmikrofoon is ‘n praktiese voorbeeld wat studente in die laboratorium kan gebruik om die skakel tussen teorie, rekenaarsimulasie en die fisiese wêreld duidelik te verstaan. Simulasie van hierdie oënskynlik eenvoudige toestel is alles behalwe eenvoudig. Die lintmikrofoon is ‘n samevattende voorbeeld van akoestiek, meganika, magnetika, elektromagnetika en die interaksie tussen hierdie dissiplines. Die waarde van die lintmikrofoon as onderrigshulpmiddel kan uitgebrei word deur ‘n tranformator en elektroniese versterker by die model te voeg. Die volledige model kan aangewend word om die belangrikheid van impedansiepassing en ruisbeheer te beklemtoon.

Die tesis stel ‘n saak vir die lintmikrofoon as laboratoriumhulpmiddel vir ingenieursonderrig. Publikasies oor ingenieursonderrig ondersteun die saak vir goeie hulpmiddels. Die tesis is gestruktureer na aanleiding van ‘n aantal eksperimente om aan te toon hoe studente vier verskillende fisika dissiplines kan bestudeer deur middel van die lintmikrofoon. Die eksperimente bestaan uit rekenaarsimulasies en praktiese oefeninge. Die nodige teorie word vir elke dissipline verskaf as inleiding tot die betrokke eksperimente.

ACKNOWLEDGEMENTS

I would like to express my gratitude towards the following persons:

My wife Cornel and my children Marlo, Timo and Lilo for continual encouragement and prayers. Thank you for the days and nights that you allowed me to work on my research when you rather would have spent personal time with me.

Petrie Meyer at SUN for guidance and inspiration. It is surely uplifting and a privilege to have someone with so much insight appreciating my efforts.

Gerhard Roux at SUN for suggesting the research topic and your enthusiasm all along the way.

Willie Perold at SUN for the use of the vapour deposition machine and Frédéric Isingizwe Nturambirwe for helping me to operate the machine. Also for your help to get me up and running with COMSOL®.

Johan van der Spuy at SUN for introducing me to ANSYS®.

Niël, Derrick and Chris at the CSIR “wat my gelei het om hierdie mal perd op te saal”.

Inus at the CSIR for convincing me to write my first conference paper and shedding so much light on various aspects of life.

Alan at the CSIR for the manufacturing of the mechanical parts of the microphone.

Louisa at the CSIR for assisting me with library loans and finding valuable articles that I would have missed otherwise.

The rest of my relatives, friends and colleagues who kept cheering me on (and checking me up) along the road.

And most of all – my heavenly Father, Maker of the universe, for letting me discover even more about the intricate wonders of Your creation and Your grace throughout the journey of this thesis.

TABLE OF CONTENTS

FIGURES

CONTENTS

TABLES

ABBREVIATIONS

ANSYS	Registered trade mark – not an abbreviation
AC	Alternating Current
ASIC	Application-Specific Integrated Circuit
ACTEA	Advances in Computational Tools for Engineering Applications
AWG	American Wire Gauge
CAD	Computer-Aided Design
CAE	Computer-Aided Engineering
CFD	Computational Fluid Dynamics
CGS	Centimetre-Gram-Second
COMSOL	Registered trade mark – not an abbreviation
CSIR	Council for Scientific and Industrial Research
DC	Direct Current
DIY	Do-It-Yourself
ECSA	Engineering Council of South Africa
emf	electromotive force (measured in Volt)
ETK	Electronic Transformer Kit
FEA	Finite Element Analysis
FEM	Finite Element Method
GPIB	General Purpose Interface Bus
IC	Integrated Circuit
IEEE	Institute of Electrical and Electronics Engineers
JFET	Junction Field Effect Transistor
MEMS	Micro Electro-Mechanical Systems
MIL-SPEC	Military Specification
MKSA	Metre-Kilogram-Second-Ampere
PC	Personal Computer
PET	Polyethylene Terephthalate
RC	Resistance Capacitance (filter network)
REW	Room EQ Wizard
RMS	Root-Mean-Square
SI	Système International
SPL	Sound Pressure Level
STEM	Science, Technology, Engineering and Mathematics
SUN	Stellenbosch University
URE	Undergraduate Research Experience
US	United States
USA	United States of America
VA	Volt-Ampere (power)

1 INTRODUCTION

"I hear and I forget, I see and I remember, I do and I understand"

(Confucius)

"Tell me and I forget, teach me and I may remember, involve me and I learn."

(Benjamin Franklin)

The more involved students become with the practical implementation of the theory that they are taught, the more they will learn. Engineering education has historically been mostly mathematics based, with advanced mathematics used to derive simple models for physics phenomena and then using these models to study basic behaviour. However, recent years have seen a proliferation in numerical multi-physics analysis software that performs finite element and finite volume analysis to provide high accuracy solutions to problems. It provides visualisation of the solution that was not possible earlier, thereby giving engineers new insight into problems and solutions. Only using analysis software can however easily cause dissociation from real-world physics and prevent early identification of flawed solutions. To correctly interpret simulation results it is important to first understand how the practical model behaves.

The aim of this thesis is to show that one device, the ribbon microphone, can be used as a laboratory tool for students to make the link between theory, computer simulation and the physical world over a wide range of physics areas. This is attempted through the proposal of a number of experiments and simulations, all centred around the ribbon microphone, which can be performed to visualize a specific or combinations of physics areas. Four physics domains are covered in the thesis through a selection of simulated and real-world experiments concerning the ribbon microphone. The physics domains are:

- Acoustics
- Mechanics
- Magnetics
- Low frequency, low energy electromagnetics

The acoustics domain is addressed by a simulation experiment to illustrate how an object with limited size and mass will behave compared to the theoretical displacement of an infinitely large object with zero mass. The experiment is also used to illustrate the challenges of extreme ratios and the importance of meshing during simulation.

The mechanics domain is addressed by a modelling and simulation experiment to illustrate how different ribbon designs will influence the deflection and resonance of the ribbon in a sound wave.

The experiment is concluded with an acoustic test with the ribbon microphone that validates the simulation results, showing that a ribbon with more corrugations has a better low frequency response.

The magnetics domain is addressed by a modelling and simulation experiment to illustrate the direction of magnetic field lines and the magnetic field strength inside and around the microphone. It also includes an experiment to illustrate how the magnetic field strength can be manipulated with an iron yoke. Two real-world experiments are used to confirm the validity of the simulated results.

The electromagnetics domain is addressed by adding transformers to the microphone system and conducting both simulation and physical experiments with the transformers to illustrate the concept of impedance matching. To conclude the chapter an experiment with an electronic amplifier is performed to illustrate the advantages and disadvantages of transformers vs. electronic amplifiers.

A paper based on chapters 6 to 8 of the thesis has been delivered at a conference [1] and a follow-up paper based on chapter 9 is currently scheduled for presentation.

1.1 Content Overview

The aim of this thesis is to present a selection of experiments to illustrate how students can learn about the aspects of four different physics domains through exercises that are concerned with the ribbon microphone. The experiments consist of computer simulations and real-world exercises. Theory is provided for each physics domain as an introduction to the experiments. The outline of the thesis therefore, departs from the typical research layout. The thesis is organised by physics topic, with each chapter showing how the ribbon microphone can be used to introduce a particular physics topic.

Chapter **one** is a short introduction to the thesis.

Chapter **two** supports the thesis with literature about engineering education and the importance of laboratory experiences in education.

Chapter **three** provides a brief history and background information on microphones in general and an introduction to the ribbon microphone in particular.

Chapter **four** expands on the history of the ribbon microphone with a series of patents to illustrate the progression of the ribbon microphone over eighty years.

Chapter **five** is used to describe the simulation software and hardware used in later chapters.

Chapter **six** to **nine** explores in detail the four physics domains of the ribbon microphone with theory of the physics, software modelling and simulation, laboratory tests and conclusions.

2 ENGINEERING EDUCATION

2.1 Engineering and Science

The connection between engineering, science and mathematics is described in [2].

The word engineer originates from the Latin verb *ingeniare* that means to design or devise. *Ingeniare* originates from another word *ingenium* (the Latin word for engine) that means clever invention. Engineering can therefore be summarised as the process of designing the human-made elements of our world.

The word science originates from the Latin noun *scientia* that means knowledge. Science can be seen as the study of the natural world.

While scientists are finding out how things work in the natural world around us, engineers are conceiving ways to modify the world according to people's needs and wants. Engineering and science do not work in isolation however, but complement each other. What scientists discover about the laws of nature is used by engineers to create new inventions. In turn, the tools that engineers design are used by scientists to make new discoveries that were not possible before. Science is such an integral part of engineering that engineering can be seen as the process of putting science to work.

Most systems are more than the sum of its parts. To fully understand a system it is not only necessary to understand each part, but also to understand the interaction amongst the parts. Engineering takes care of the finest details in addition to satisfying the bigger picture. Some engineers will prefer to work on the detail, while others will prefer to design the larger system. It still remains important however for engineers to be trained in grasping and appreciating the work on both sides of the picture.

Engineers use modelling to test concepts and better understand the functioning of a process or design. The model can take on the form of a drawing, mathematical equation, computer simulated representation or scaled physical model. By using these models engineers can predict the behaviour of different solutions before building it and testing it experimentally. This process of predictive analysis is an important aspect of engineering design. The importance of mathematical modelling and predictive analysis makes also mathematics an integral part of engineering.

The close relation between engineering, science and mathematics emphasises the importance of science, technology, engineering and mathematics (STEM) education at all student levels.

2.2 History of Engineering Education

The history of engineering education in the USA can be found in the background information to [3]. The chronicles of graduate engineering education belongs mostly to the post-World War II era. In

the USA for example, the number of graduate engineers before the war quadrupled by 1949 and by the 1970s master's degrees increased 15-fold and doctoral degrees 30-fold.

The technology explosion during World War II was the first event to have a major impact on graduate engineering education in the USA. Jet planes and atomic energy were developed during the war and prior problems with radar were overcome. Most of the problem solvers on radar were physicists and mathematicians. This fact and a realisation that solutions to post-war problems would increasingly depend on scientific knowledge led to the inclusion of more science and mathematics in the engineering curricula. Research at universities was largely supported by the armed services. This helped to stimulate a constant supply of new graduate engineers until the establishment of the National Science Foundation in 1950.

The academic move to include more science in the engineering curriculum was formalised in 1955 by the Report on Evaluation of Engineering Education, also known as the Grinter Report (named after the chairman of the steering committee). The Grinter Report recommended the integrated study of analysis, design and engineering systems to improve background knowledge of professionals. It also included recommendations on curricular flexibility, the strengthening of humanities and social sciences, and skills in written, graphical and verbal communication. Furthermore, it encouraged experimental engineering. A steady increase in the number of graduate engineering programs and graduating engineers was seen after this report. This was good news after a decline between 1950 and 1955.

Engineering education in the USA received another incentive in 1962 with the publication of the President's Science Advisory Committee's report entitled *Meeting Manpower Needs in Science and Technology*. This report emphasised the urgency of graduate training (especially at doctoral level) in engineering, sciences and mathematics in order to prevent a shortage of these skills in the American economy. This was of course in reaction the Russian success with the Sputnik satellite. The space-race, in part, ensured an increasing number of graduate engineers until late in the sixties.

The engineering profession experienced a number of economic setbacks after the aerospace cutback in 1969. By that time the swing towards science and maths was taken so far that even the engineers who advocated it started to protest. To worsen matters, the popularity of television around the same time caused children (potential future engineers) to stop tinkering and rather sit glued to their television sets. The pendulum swung so far towards science that hands-on skills had dropped tremendously by the eighties. The number of engineering graduates only started to increase again after frustration with the lack of skills encouraged a shift back to more laboratory time and design skills. By the nineties universities listened more to industry concerns and moved to less science with more hands-on and applied work.

In the past two decades hands-on experience was taken to a new level with the introduction of undergraduate research experiences (UREs) by many educational institutions. Many of the benefits of UREs are aligned with the three most important learning outcomes of the American Association of Colleges and Universities, namely (1) intellectual and practical skills, (2) personal and social responsibility, and (3) integrative and applied learning. Undergraduate research encourages the experiences that transform students' perceptions and understanding of what they are learning and how it is applied in real-world situations. It has personal benefits by increasing the self-confidence and independence of students while preparing them for the next level of challenges with an ability to tolerate obstacles. It also has professional benefits by enhancing critical thinking and providing experiences that can be beneficial to career opportunities. UREs provide opportunities for students to develop intellectual tools that continue building on their education by encouraging them to ask questions as they seek to understand [4].

Modelling, aided by increasingly more powerful computers, create new possibilities to solve problems and make discoveries that were not possible just a decade before because of the complexities or nonlinearities of those problems. Massive system problems that could not be solved before because of the large amounts of data to be processed are now computed daily, often in real time. Application-specific integrated circuits (ASICs) perform computational tasks orders of magnitude faster now than standard computer processors. The methods that are used for laboratory experimentation are changing because data processing happens while the experiment is run. Design and manufacturing processes are changing as more activities are automated. The way that business is conducted is also changed by technology as the pace of electronic communication is advancing. The advances in computer capabilities stimulated experimental research and in some cases the ability to model natural phenomena outpaced the scientists' knowledge of nature itself. Increasing computer power and experimental research move in parallel, one stimulated by the other. The technological challenge affects every field of engineering and raises the requirements for improved education models. The accelerating pace of technological developments is constantly posing new challenges to engineering education, even more so today in the twenty first century. To quote Klaus Schwab, founder of the World Economic Forum: "In the new world, it is not the big fish which eats the small fish; it's the fast fish which eats the slow fish."

2.3 Experimentation

The concept that undergraduate students should be experimenters is fundamental to engineering education. Undergraduate experimentation in the laboratory should provide students with the fundamental tools to perform experiments as practicing engineers just as the engineering sciences provide them with the basic tools for analysis. Like clinical training being essential to medical practitioners, engineers should apply their knowledge of science and mathematics in an interactive cycle of analysis, design and experimentation [5].

Ferri, at al. argues that real hands-on laboratory experiences are also very effective to improve learning and retention of knowledge [6]. The long-term memory effect of sight combined with touch is one of the components in learning that is underestimated. Memory improves when multiple senses (vision, touch, hearing and smell) are utilised. Each of the senses has its own processing channel in the brain. Multi-sensory input helps to reduce the cognitive load on the brain during a learning exercise. The tactile sensory channel for example, can transfer similar information than the visual or the auditory channels to lighten the load on a single channel, or it can transfer different but complementary information to construct more complete concepts in the brain. This may explain why concepts that are reinforced through hands-on experiments are retained much more effectively than concepts learned through non-practical learning methods. Consciously adding checks and balances between the different channels in the brain will further enhance understanding and recall. Hands-on experimentation provides a way to incorporate multi-sensory modes and it can be designed to trigger deeper mental processing by means of exploratory and reflective activities.

2.4 Consequences of Inadequate Laboratories

The lack of proper laboratory facilities in schools makes it difficult for schools to attract good science teachers and forces teachers to teach science based on the memorisation of facts rather than developing a fundamental understanding of scientific principles through hands-on experiments. This approach leads to learners losing interest in science courses. Consequently the enrolment numbers for engineering could drop and the students that do pursue an engineering degree start with a skills disadvantage [7].

Student opinions about the motivational factors that have an effect on higher education were captured in a study by Savage et al. at the University of Portsmouth. All of the students that were interviewed noted that reading from PowerPoint slides is not very motivating. The novelty of new technology had worn off in 2011 already. All but one student was of the opinion that practical work was one of the best ways to learn, especially when the lecturer uses examples from his own experience, i.e. explaining the theory in context with real world examples, and discussing how the students may use that knowledge in future when working in their field. One of the students phrased their experience as follow: “I think I get motivated by something more if I think that it is going to be meaningful and used in real life rather than something that is just there and you are just going to learn it for the sake of it and you are never going to use it in real life.” [8]

2.5 Purposeful Laboratory Experiences

For undergraduates to study and experience science and engineering as if they were working scientists and engineers, they will need access to laboratories at non-prescribed times to complete their research projects, instead of completing it in predetermined blocks of time. When large

groups of students are required to perform laboratory work in predetermined time blocks, it often happens that the laboratory experience evolves into the rote following of prescribed activities to arrive at some conclusion to a list of predetermined questions. There is no opportunity for discovery and deeper analysis in this method. Students that are taught in this way and do not progress beyond undergraduate studies, will never experience or fully appreciate how scientific investigations are conducted or how the concepts that they study were formulated [9].

Laboratories that are designed with the primary role to reinforce lecture material, do not always deepen the student's understanding of the concepts in the lecture. Traditional laboratory manuals do not reflect the scientific process to develop hypotheses, design experiments, conduct experiments, take into account the errors induced by the measurement equipment's sensitivity or its influences on the experiment, reach conclusions, and write a report on their findings.

Curricula that include laboratory experiences that are well aligned with professional practices allow students to develop explanations for their observations, test their explanations, then refine existing models or build their own models through experimentation. This kind of laboratory experience is more effective than traditional laboratories for development of student's abilities to design experiments, collect and analyse data and partake in meaningful scientific communication.

With deductive experiments students first learn about a concept and then perform experiments. With inductive experiments students first perform the experiments and then cover the applicable material afterwards in lectures. Students initially prefer deductive experiments, but later on they value inductive experiments more because it provides them with knowledge for deeper understanding of the subsequent lecture material. Carefully designed inductive experiments may also be used to uncover common misconceptions in a certain area before explaining the theory and the reasoning behind these concepts [10].

Experimentation and purposeful laboratory experiences should be designed to promote a process of higher order thinking to keep students engaged. There is no simple definition for higher order thinking, but it can be clearly recognised when the following qualities are present:

- Non-algorithmic, i.e. the path of thought or action is not specified in advance.
- Complex, i.e. the correct path is not visible from a single angle.
- Multiple solutions exist, i.e. there is more than one correct path, each with its own pro's and con's, rather than a single unique solution.
- It requires judgment and interpretation of subtle variations.
- It contains the application of multiple criteria that could be in conflict with each other.
- It involves a measure of uncertainty.

- Requires self-regulation (closing the feedback loop) in the thinking process.
- Imposes meaning, i.e. finding a form of structure in seemingly disorder or chaos.
- Effortful, i.e. there is a considerable amount of mental work required.

These qualities are in line with the Washington Accord exit-level-outcomes for engineers. The Washington Accord was signed in 1989 and the Engineering Council of South Africa (ECSA) became a signatory to the Accord in 1999. Therefore, these qualities also reflect the formal education requirements for South African universities to be accredited by ECSA. Engineers can earn qualifications with international recognition at accredited universities.

Experimentation and laboratory time should involve a fair amount of metacognitive behaviour, for example checking one's own understanding, trying to relate new material to prior knowledge and fundamental principles, monitoring for consistency, checking for common-sense, and making use of alternative resources [11].

Advances in technology have opened up new opportunities to enhance the science teaching experience. These "virtual" experiences however, can never be a substitute for direct laboratory exercises. The "virtual" activities and the hands-on laboratory interactions offer different experiences that should complement each other [12]. This statement is supported by evidence from Feisel and Rosa showing the important role that hands-on experimentation has in engineering education, and how performing computer simulation can never replace the experience gained through real experimentation [13].

In a study by Liu it was shown that computer modelling combined with hands-on laboratory work is more effective than any one of the two in isolation [14].

2.6 Portable Laboratory Hardware

The ratio of student numbers to the amount of laboratory equipment is usually high because of the high cost and physical size of the hardware. As a result, students have to use this equipment in groups and for a limited time only. Students do not get the opportunity to fully explore the equipment or understand the experiment in depth. While many universities relied completely on simulation-based activities and provided no hands-on laboratory teaching, one institution in particular showed dramatic improvement in student engagement when simulation-only exercises were replaced with laboratory kits that student could take home for further experimentation. Not only did the students' interest improve dramatically, but their test scores also improved. It was observed that many students doing the computer simulations without hands-on exercises lost interest and submitted partially completed projects. The students with hands-on laboratory experience on the other hand, strived to see the project through until it worked completely to their satisfaction [15].

Motivated by these studies, Taylor et al. developed a low-cost, hardware platform to improve the teaching experience for systems engineering students. The hardware was affordable enough for each student to loan the hardware for the duration of the course and to take it home or elsewhere on campus for further work. This encouraged students to explore the system in their own time, allowed them to take control of their own learning to best match their individual learning styles, and hence to promote independent learning. Use of the hardware as an educational aid was so successful in its purpose that the authors believed it could be used even as a marketing tool to attract future students into the department. The hardware was originally developed for an MSc course, but the experience was received so well by the MSc students that it was planned to extend its usefulness into a final year undergraduate course [16].

In contrast to complex, high cost laboratory equipment, Ferri et al. invented small experimental platforms to study the effect of hands-on laboratories on large enrolment classes. These platforms are portable and affordable enough for students to own. This hardware opened up new possibilities to teach students in non-traditional settings such as standard classrooms that have no laboratory infrastructure and asynchronous distance education. The requirements for their portable laboratory were to

- address concepts that are difficult to grasp by theory alone
- integrate with the theory that is taught in class
- require a low learning curve
- provide a skeleton for students who are new to the equipment
- necessitate students to draw relations between the theory and experiments
- include design, building, testing, troubleshooting, analysing, and exploration activities.

The study from Ferri et al. revealed that hands-on experimentation has a positive impact on both learning and the confidence of students. They found that student performance in the laboratory was also a good indicator of what could be expected in written tests later on. It was noticeable that the improvements in performance and in confidence level were only seen with middle and high achievers. The low achievers' test scores did not benefit from the laboratories. Unsurprisingly, their laboratory scores were also low. This phenomenon was ascribed to the fact that the lowest achievers skipped laboratories and only did the bare minimum to complete the measurements. They never engaged in the higher level thinking activities [6].

2.7 A Generation with Limited Technical Childhood Exposure

Practical demonstrations are important - especially now in South Africa where many new engineering students come from a background with limited technology exposure. They hardly ever

saw their parents working with new technology or repairing anything technical. On the other hand are students who grew up in a high-tech environment but whose only interaction with technology remains a screen and (maybe) a keyboard. Not only in South Africa but the world over institutions are witnessing an increasing lack of mechanics knowledge – so much that in 2006 already the Engineering Education journal published an article on the limited mechanics knowledge of students entering higher education in the United Kingdom [17].

2.8 Physics Education

All engineering disciplines should start with a broad selection of fundamental physics before specialising into specific domains during later years of study. Physics is an empirical study. Everything that we know about the principles that govern the behaviour of the physical world has been learned through observations of events in nature. The ultimate test for theory lays in its agreement with observations and measurements of the physical phenomena. Physics is therefore inherently a science of measurement. Lord Kelvin (1824-1907) said that “when you can measure what you are speaking about, and express it in numbers, you know something about it; but when you cannot express it in numbers, your knowledge is of a meagre and unsatisfactory kind; it may be the beginning of knowledge, but you have scarcely, in your thoughts, advanced to the stage of science, whatever the matter may be.” [18].

Physics is introduced at school in the order of most tangible to least tangible concepts. The simpler it is to measure something; the easier it is to explain the physics concerning it. The tuition of more difficult concepts can build on prior knowledge of simpler concepts. It is important however, that students understand the complexities that are added when moving to domains that are more difficult to measure. By the time that students start with undergraduate studies they should have been exposed at school level to a broad range of physics, but not necessarily with enough depth. Their knowledge should include, but not be limited to, the following:

- Physical and mechanical properties of matter
- Motion (including conservation of momentum)
- Waves (electromagnetic spectrum and sound)
- Work, energy and power (including conservation of energy)
- Fluid statics and fluid dynamics
- Electrostatics and electrodynamics
- Magnetism
- Electronics

- Electromagnetics

Students will understand some of the physics well because of personal interaction at school with tangible objects to test the theory. The rest however, they will only know in theory. More advanced laboratory experiences are required during undergraduate studies to give students a better understanding of the physics they could not test at school and, more importantly, the higher level of physics they will be taught at undergraduate level.

2.9 The Ribbon Microphone as Laboratory Aid

Many of the physics concepts listed in 2.8 can be addressed in one way or another with the ribbon microphone as a laboratory aid. Through simulation and/or physical experimentation it can be applied as follow:

- The construction of the ribbon can be used to demonstrate the physical and mechanical properties of thin metal and polymer foils.
- The movement of the ribbon demonstrates motion and inertia of an object in a sound wave. Sound waves in air can be modelled with the principles of fluid dynamics.
- The magnetics of the microphone is useful for many experiments with magnetism.
- The electromotive force (emf) generated by the microphone is a classic example of electrodynamics and because the emf is so small, it provides a good challenge to harness very low levels of power and energy.
- The inclusion of a transformer in the system provides a good illustration of low frequency electromagnetics.
- The inclusion of an electronic amplifier in the system provides exposure to electronics in more than one way.

While the physics in 2.8 can be shown through numerous other examples, having one experimental vehicle which allows experiments on acoustics, mechanics, electromagnetism and electrical circuits and noise, is invaluable. Also, because of the extreme bandwidth (20 - 20 000 Hz) required, the large dynamic range (≈ 90 dB), and the very small signal levels developed, the microphone can illustrate a wide range of non-ideal effects. The ribbon microphone provides students with a simple signal source in the microwatt/nanowatt range to learn about the challenges of small signal processing.

The ribbon microphone is practical as a laboratory aid for working both in the laboratory and away from campus. Most of the experiments in this thesis can be conducted in a study room with only the aid of a personal computer with sound card, a multimeter and a piece of breadboard. Only a limited number of tests require professional test equipment in a conventional electronics laboratory.

3 THE MICROPHONE

3.1 General Information

The carbon microphone was developed by Thomas Edison as early as 1877. Low-cost variations of this type of microphone can still be found in the handsets of older telephones. After the carbon microphone, the greatest step forward was the invention of the condenser (capacitor) microphone by Edward Wente in 1917 [19]. Condenser microphones have no magnetics. Movement of the diaphragm causes a change in capacitance. It was the beginning of what would become a great instrument for many decades. The human ear can perceive a multitude of sounds, ranging in intensity (or rather sound pressure level) from 20 µPa to more than 1 Pa and ranging in frequency from 20 Hz up to 20 kHz. For more than a century, various inventors have attempted to design a microphone that possesses the same characteristics as the human ear. Yet, no single microphone exists that matches all the qualities of the human ear. Various microphones are available today, each with advantages and limitations. They can be grouped either by their construction (dynamic, condenser or ribbon) or by their sound pattern characteristics (unidirectional (or cardioid), bidirectional (or figure-of-eight) or omnidirectional) or by the physics behind the design (pressure or velocity) [20] [21] [22].

The diaphragm of a pressure microphone is exposed to sound waves on one side of the transducer only. Its output changes in accordance to the instantaneous pressure of a sound wave. Dynamic and condenser microphones are examples of pressure microphones. A dynamic microphone resembles the moving coil construction of a speaker; it is only much smaller and operates in reverse. Velocity microphones are exposed to sound waves on all sides. The difference in sound pressure (the gradient of the sound wave) between the front and the rear of the diaphragm causes the displacement of the diaphragm. They are also known as pressure gradient microphones. Its electrical output changes according to the instantaneous velocity of the air particles in the sound wave. The ribbon microphone is an example of a velocity type microphone.

3.2 The Ribbon Microphone

The ribbon microphone was patented in 1932 by Harry F. Olson [23]. It consists of an extremely thin aluminium foil ribbon suspended in a magnetic field. Pressure gradients in the air cause the ribbon to move. The movement of the ribbon in the magnetic field generates a small electromotive force (emf) which can be amplified and recorded. The ribbon microphone quickly gained popularity with audio engineers for its uniform frequency response and figure-8 directivity pattern.

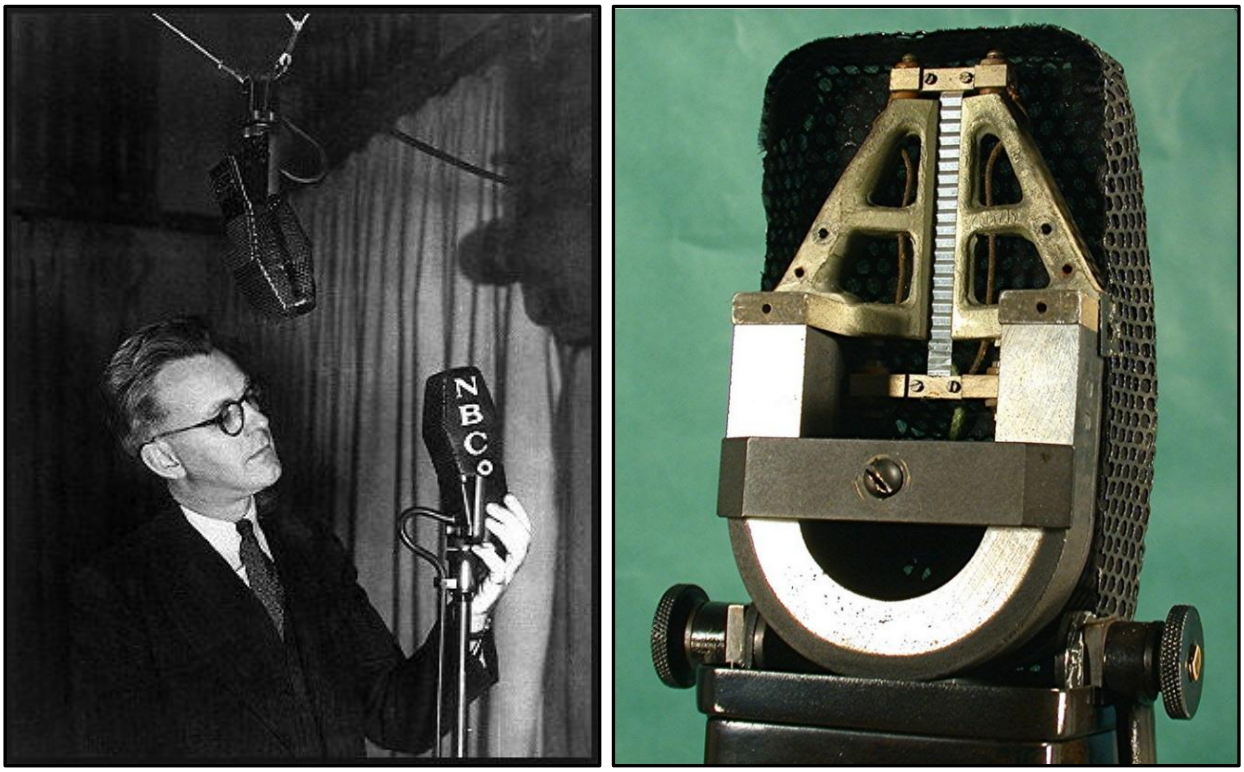

Figure 1: RCA 44A ribbon microphone circa 1931 **[24]** (Silvia Classics)

When magnetic tape became the dominant recording media, ribbon microphones became less popular and condenser microphones took over. With recordings and sound mixing processes making use of magnetic media there is always a slight loss of high frequencies. This problem could be remedied by large capsule condenser microphones. These microphones have a number of resonances in the 8 kHz to 12 kHz range that enhances the high frequencies before recording. The capsules of condenser microphones are tensioned tightly, causing the high-frequency resonances [25].

The aluminium foil element of the ribbon microphone is only lightly tensioned, causing resonance at very low frequencies. When digital recording became the order of the day, ribbon microphones made a major comeback because high-frequency transfer loss was no longer an issue. Its ability to record fast transients accurately without adding upper-range resonances became again a very positive attribute [25]. See [26] and [27] for more detail about the fall and the rise of the ribbon microphone throughout history.

4 TECHNICAL DEVELOPMENT OF THE RIBBON MICROPHONE

Articles about the ribbon microphone dates back as far as 1931. Most of the early publications were authored by Harry F. Olson who patented the ribbon microphone. Few publications besides those by Olson can be found about the ribbon microphone, but plenty of patents relating to the ribbon microphone are freely available. A selection of those patents is discussed in the paragraphs to follow.

4.1 Patents

4.1.1 Olson 1932

Harry Olson filed the first patent for the ribbon microphone in 1931 and the patent was awarded on 25 October 1932 with the title “Apparatus for converting sound vibrations into electrical variations” [28]. The patent illustrations are of very sturdy mechanical designs as illustrated in Figure 2.

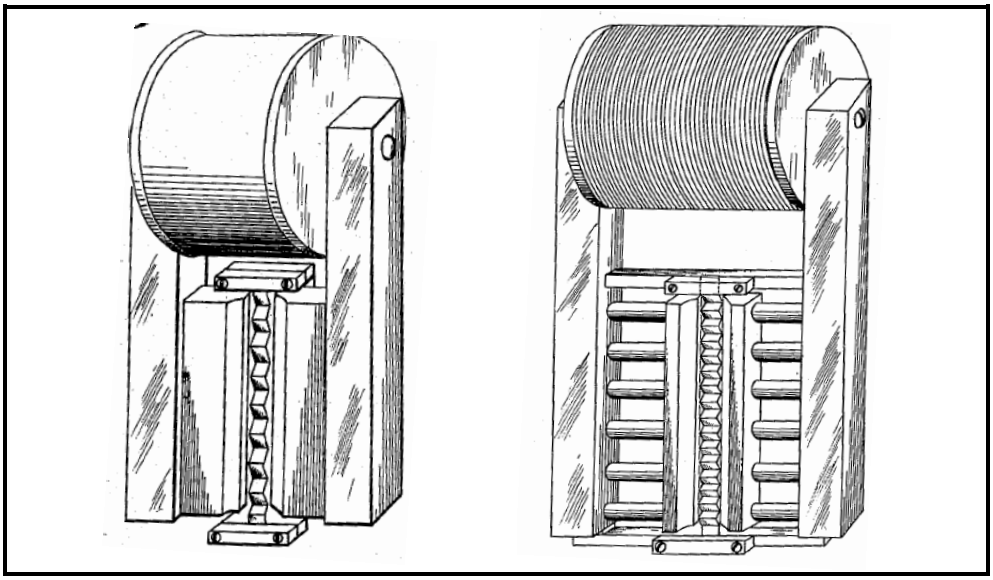

Figure 2: Sketches of two ribbon microphone models **[28]**

It describes the ribbon as a relatively small item that is supported in such a way that it resembles the motion of a particle in free air. A device of this nature is classified as a velocity microphone. The combination of mechanical parts surrounding the ribbon is called a baffle. The size of the baffle around the ribbon is calculated according to the highest frequency that the microphone is designed for. The baffle should be designed so that the path length from the front of the ribbon to the rear of the ribbon is half the wavelength of the required frequency. Figure 3 provides a graph from the patent to illustrate the effect of the baffle size on the frequency response of the microphone.

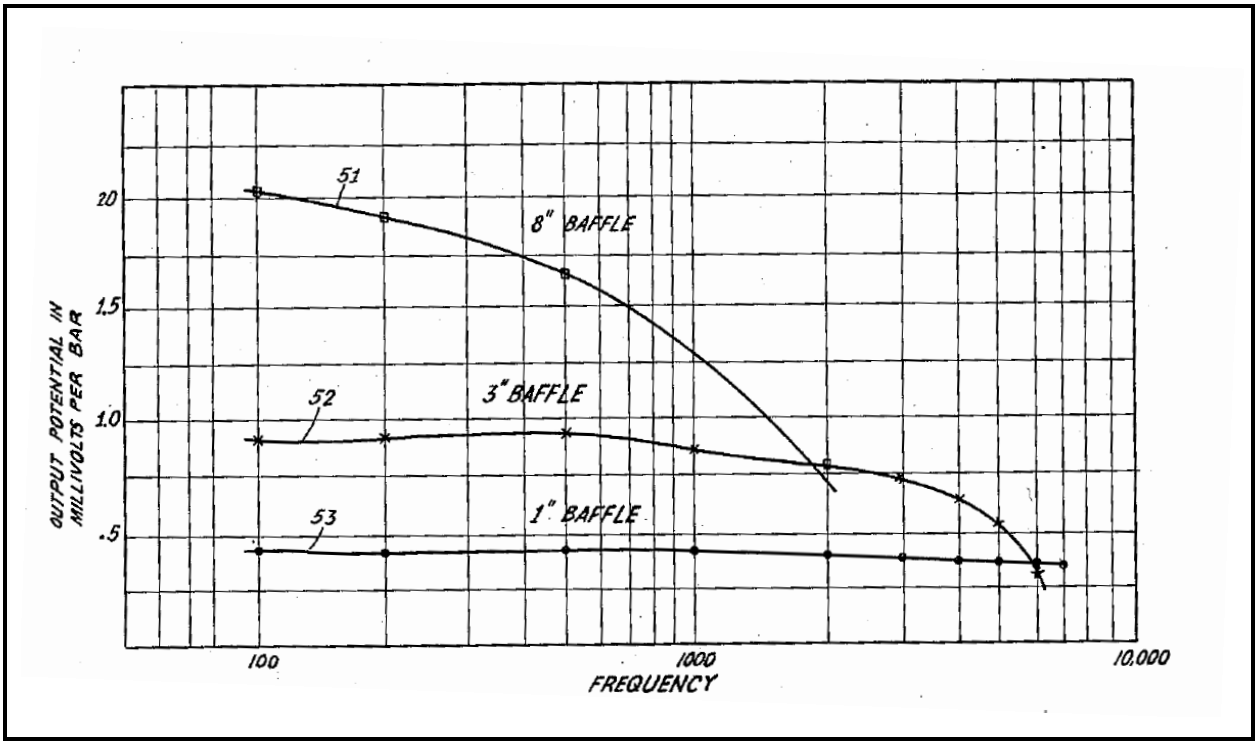

Figure 3: Frequency response vs. baffle size **[28]**

The ribbon is made of conducting material that is light in weight and that has low elasticity, for example aluminium foil. The ribbon must not be stretched tightly between its supports. It is crimped in order to suspend it rather loosely between its supports to promote flexibility along its whole length. The supports are made of non-ferro-magnetic conducting material, but it is electrically isolated from the ribbon by non-conductive material. The two signal wire leads are electrically connected to the two ends of the ribbon. The light weight and small restoring force of the ribbon causes its natural vibration frequency to be below the audible range. Tests that were done before the patent submission had shown that a natural vibration frequency of approximately 10Hz produced the most desirable results. The patent states that “When a diaphragm of small mass is suspended in this manner its mechanical reactance is small compared to the impedance of the air. In other words its mass reactance is negligible over a large frequency range compared to the acoustic resistance of the air which it displaces.”

The ribbon is suspended in the air gap between two poles of a magnet in such an orientation that its surfaces are parallel with the magnetic force lines. The magnet can be a permanent magnet or an electromagnet. The gap between the ribbon and the magnet poles are kept to a minimum to prevent the leakage of air around the ribbon, but the gaps must still be sufficient to prevent frictional contact between the ribbon and the magnet. The patent suggests an air gap of 5.6mm with the ribbon slightly narrower. The ribbon cuts the magnetic field lines while moving in the air gap between the poles because of the sound pressure variations across it. This causes an

electromotive force that is proportional to its movement. The electromotive force can be amplified with suitable electronic equipment.

The magnetic pole pieces with its supporting structure forms the baffle. The baffle increases the path length from the front to the back of the ribbon. The length of this path has an influence on the response of the microphone. The paths around the top and bottom supports of the ribbon are shorter than the paths around the baffle, but its effect is relatively small because it influences only a small part of the ribbon. The clamping structure that secures each end of the ribbon is made of non-magnetic material (ex. copper or brass if it is made from metal). Although it is desirable to make the ribbon as light as possible, it is sometimes necessary to vary its thickness in order to increase its efficiency within the particular baffle setup. The movement of the ribbon is caused by the phase difference of the sound wave between the front and back of the ribbon. The phase difference is determined by the distance that the sound wave has to travel around the baffle from the front to the back of the ribbon. The greatest phase difference occurs when the path length around the baffle is half a wavelength of the sound wave under question. Olson provides a helpful visual representation of this effect in his patent. Figure 4 shows a horizontal cut through the microphone and a sinusoidal representation of a sound wave. If the path length A-B around the baffle is plotted as E-F on the axis of the sound wave, then the pressure difference between points A and B on the ribbon will be equal to the sum of C-E plus D-F.

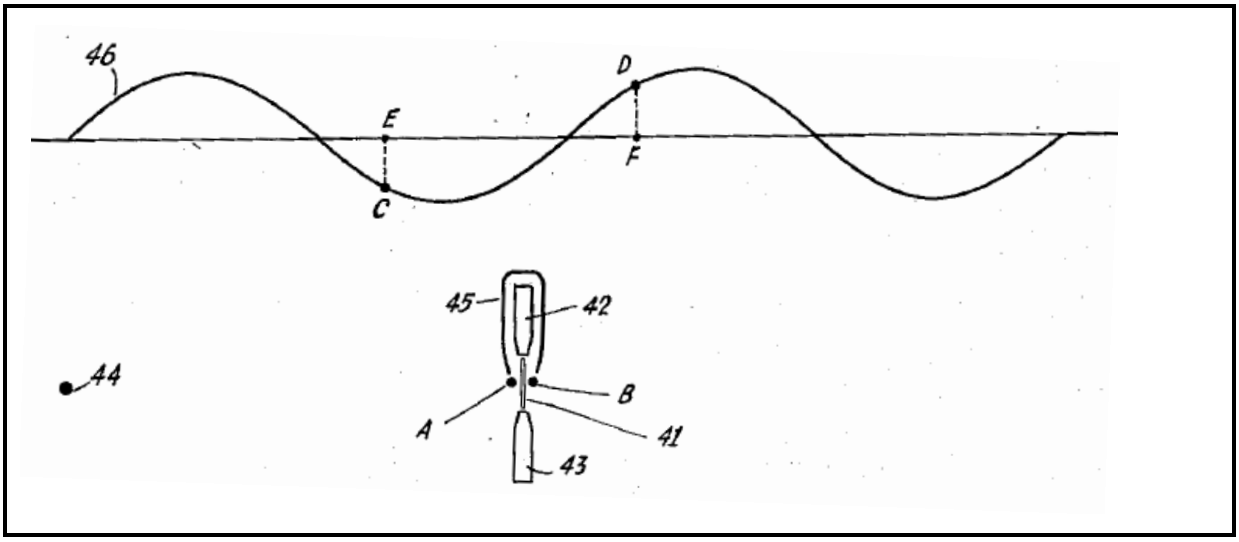

Figure 4: Path length around the baffle **[28]**

The sound intensity at the opposite sides of the baffle is virtually the same for all wavelengths that are longer than twice the distance around the baffle. At wavelengths shorter than this, the intensity on the approaching side of the ribbon increases and the intensity at the retreating side decreases. The reasoning follows that the pressure difference across the ribbon is proportional to the frequency as long as the distance around the baffle is less than half the wave length. Due to the nature of the design the ribbon microphone exhibits very directional characteristics. Sound waves

coming from an angle will produce less of a pressure difference across the ribbon. A sound wave directly from the side will produce virtually zero pressure difference. The pressure difference can be calculated with simple trigonometry rules.

An alternative design is also provided in the patent. The alternative design does not make use of a ribbon, but of a lightweight diaphragm. This design is however overly complicated and will not be discussed further.

4.1.2 Olson & Weinberger 1933

In 1933 Olson, in cooperation with Julius Weinberger, filed a patent that made use of a combination of the pressure gradient (velocity) ribbon microphone and a pressure component microphone to achieve unidirectional operation [29]. Unidirectional operation is desirable in order to improve the ratio of the sound source relative to the sound reflections in the room. The patent achieved its purpose through the use of a normal ribbon (as in the 1931 patent) assembled in series with a modified ribbon. The modified ribbon was adapted to act as a pressure microphone by enclosing the back of the ribbon. The normal and modified ribbons are working in phase for sounds generated in front of the microphone, but are out of phase for sounds originating from the rear side of the microphone. This patent illustrates the influence of the baffle in the extreme case of making the baffle infinitely large by enclosing the rear side of the ribbon completely.

4.1.3 Anderson 1937

Leslie Anderson added electronics to Olson and Weinberger's unidirectional microphone to file a patent in 1937 [30]. The electronics made it possible to adjust the phase differences between the two ribbons, thereby making it possible to adjust the directionality of the microphone from the mixing desk.

4.1.4 Ruttenberg 1938

In 1938 Samuel Ruttenberg filed a patent to address one of the imperfections of the ribbon microphone [31]. When speaking close to the microphone, the low frequencies are over emphasised because the higher frequencies are attenuated. The high frequency attenuation happens because different sections of the ribbon move out of phase. Thus one section cancels out the electrical current that is generated during vibration of another section. The sections move out of phase due to the fact that the ribbon is longer than the wavelength of the higher frequency sound waves. Ruttenberg addressed this problem by designing a special housing for the microphone which closes up the rear of the microphone with an adjustable shutter. When closing up the rear of the microphone, its characteristics are changed from that of a velocity microphone to that of a pressure microphone because the sound wave does not have access to the rear of the ribbon. This idea clearly borrows from the same principles than Olson and Weinberger's patent on the

unidirectional microphone. The microphone's operation in pressure mode tends to minimise the effect of high frequencies being attenuated. This patent clearly illustrates that tampering with the physical surroundings of the ribbon microphone, does have a distinct influence on its operation.

4.1.5 Bostwick 1938

Telephone conferencing has been around for longer than one would expect. In 1938 Lee Bostwick already addressed the problem of feedback between speaker and microphone during teleconferencing. He filed a patent for a device making use of two ribbon microphones and a loudspeaker [32]. The device is constructed with a loudspeaker facing downwards onto a deflector underneath that reflects the sound waves in a horizontal direction toward the conference attendees. Two ribbon microphones are fitted perpendicular on top of each other, both on top of the loudspeaker. Because of its directionality, the ribbon microphones are insensitive to the sound waves emanating from below it, but are sensitive to the voices of the conference attendees around the table.

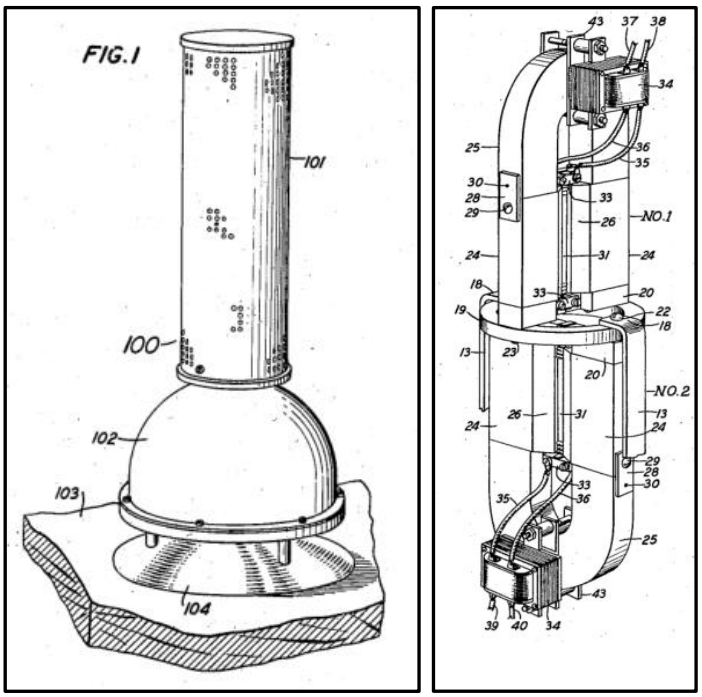

Figure 5: Bostwick's teleconference solution **[32]**

4.1.6 Olson 1940

In 1940, Harry Olson filed a patent for an improved version of the 1933 unidirectional microphone [33]. Olson discovered that he can design a unidirectional microphone with a single ribbon instead of the dual-ribbon method used previously. Furthermore, this microphone could be easily changed from unidirectional to bidirectional, to non-directional operation. The method of achieving this was to place a pipe structure (resemblance of a smoking pipe) behind a single ribbon. The pipe ends in a labyrinth that is filled with a soft fabric acting as acoustic resistance. The pipe has shutters that

can be opened or closed to achieve the desired results, i.e. shutters open allows bidirectional operation, shutters partly closed enables unidirectional operation and shutters completely closed constrains it to non-directional operation. This patent illustrates once again the influence of the surroundings of the ribbon on its operation.

4.1.7 Anderson 1942

Leslie Anderson built upon Olson's 1933 patent by filing a patent in 1942 about the magnetic equalization of sensitivity in a unidirectional microphone [34]. It is fundamentally an improvement on Olson and Weinberger's design by adding a mechanism to adjust the magnetic fields for the two ribbons and by changing the shape of the pole pieces in such a way that it is possible to vary the flux density of one air gap relative to the other. This patent indicates support for Olson and Weinberger's idea of modifying the baffle in order to change the operation of the microphone for a specific purpose.

4.1.8 Rogers 1942

Ernest Rogers filed a patent in 1942 for a microphone with selective discrimination between sound sources [35]. He claimed that the microphone can be used to determine the direction of a sound source. The microphone receives sound waves approaching the microphone straight-on, but attenuates sound waves approaching the microphone from an angular displaced direction. The construction of the microphone is basically four ribbon microphones assembled in an X-pattern. The ribbons are connected to a mixing circuit in such a way that the phase relationship between the ribbons can be adjusted. By adjusting the phase relationship, the microphone can be tuned so that the phases of sound waves from a certain direction cancel each other out, while the phases of sounds waves from another direction will add to each other.

4.1.9 Olson 1946

The ribbon microphone inherently has a figure-8 directivity pattern. Olson filed a patent in 1946 to combine two ribbon microphones in a perpendicularly fashion in order to get a microphone that has a 360° pattern on the horizontal plane [36]. This microphone would be ideal for use in orchestras for example, recording all the instruments around it, but attenuating sound waves reflecting from the ceiling and from the floor. Part of the idea is borrowed from Bostwick's teleconferencing microphone discussed earlier [32].

4.1.10 Anderson 1947

Anderson's patent application in 1947 was filed as an improvement on Olson's 1931 design [37]. According to Anderson, Olson's design displayed a considerable drop in output when the distance around baffle approaches one fourth of the sound wave's wavelength. Anderson's design claimed to have a more uniform response over the operating range of the microphone and also to have an

enhanced high frequency response compared to the conventional design. This was accomplished by mounting one or more semi-circular bands behind the ribbon. The bands provide cavities that are resonant at the frequencies where the enhancements are deemed necessary.

4.1.11 Olson 1950

Olson and Preston applied for a patent in 1950 that introduced a new magnet design for the ribbon microphone [38]. The new design brought the magnet closer to the ribbon by doing away with the pole pieces and using a magnet structure consisting of two large magnets, one on each side of the ribbon, with an oval hole in each magnet. The holes in the magnets are there to reduce the path length from the front to the back of the ribbon, thereby extending its upper frequency response. Olson's motivation for the design is that the efficiency of the magnetic structure increases as the magnetic source is placed closer to the air gap because the amount of leakage flux decreases. It is also an attempt to minimise the effect of the pole pieces on the difference in sound pressure between the front and the back of the ribbon.

4.1.12 Anderson 1954

In 1954 Anderson filed a patent concerning the magnetic circuit of the ribbon microphone [39]. This patent addressed the problem of the air gap between the ribbon and the magnetic structure. If the gap is too small, the ribbon might touch the structure as it moves. If the gap is made larger, then the sensitivity of the microphone is adversely affected. Therefore the gap must be adjusted to a very specific distance. The patent provides no recommendations about the optimum size of the air gap or anything about the magnetics itself. It is purely an assembly method to mount the magnetic yoke pieces accurately and reliably in a repeatable manner.

4.1.13 Fisher 1965

Charles Fisher addressed the upper frequency limit of the ribbon microphone in his 1965 patent [40]. The patent illustrates the design of a ribbon microphone with an exceptionally large horseshoe magnet at the base with conical pole pieces attached to the magnet. The conical pole pieces are constructed such that it does not only taper off to the top, but also makes the opening for the ribbon narrower as it protrudes away from the magnet. The pole pieces and the ribbon are thus broad at the end closest to the magnet and narrow at the end furthest from the magnet. The front to rear path around the baffle at the furthest end is thus much shorter than that of the conventional design. The patent claims good response and directivity up to 20 kHz, but no frequency response graphs are provided to support the claim.

4.1.14 Royer 1999

For three and a half decades (mainly the period that the condenser microphone dominated) the US patent office did not receive any submissions concerning the ribbon microphone. David Royer and

Richard Perrotta broke the silence in 1999 with their patent to modify the original ribbon microphone [41]. The digital conversion of sound recordings was the motivation behind their invention. Non-ribbon microphones produce large frequency dips and phase distortions that get falsely interpreted by the digital equipment as valid data. Ribbon microphones do not have this problem. Royer and Perrotta deemed it necessary to modify the ribbon microphone so that it could be used at higher volume levels. To achieve the desired effect they designed a ribbon microphone with magnetic pole pieces which are much wider from front to back and with the ribbon positioned not in the centre, but one quarter of the pole width from the front of the microphone. In the original ribbon microphone the pole pieces are tapered to become narrower towards the ribbon. In Royer and Perrotta's design the pole pieces are purposely not tapered. The frequency response graph in the patent application shows a very flat response from 40 Hz up to 15 kHz. Frequencies lower than 40 Hz are attenuated by as much as 5 dB (at 20 Hz) and frequencies above 15 kHz are attenuated by as much as 7 dB (at 19 kHz). No graph is provided to compare the volume levels of the original (prior art) with the new design. This design increases the baffle size slightly with the increased thickness of the magnetic poles. Olson's 1931 patent only shows the frequency response between 100 Hz and 7 kHz, so no direct comparison can be made between the original and the new designs concerning the effect of the baffle size on the frequency response.

4.1.15 Royer 2004

In 2004 Royer and Perrotta filed two more patents [26] [42]. They filed two patents for the same microphone on the same day, but each application emphasised a different aspect of their invention; thereby slightly changing the classification of each patent. One patent emphasises an angled magnet structure to improve the sensitivity and frequency response of the microphone. The other patent emphasises the specially designed transformer for said microphone. The applicants incorporated some of the principals of their previous patent, but this microphone was designed with pole pieces that taper narrower towards the ribbon (unlike the thicker magnetic poles of the 1999 patent). The angled magnet design effectively reduces the front-to-rear distance around the baffle. This is in accordance with Olson's rule that a shorter distance around the baffle will produce a higher frequency range. The angled magnet design aids in the sensitivity of the microphone because it maximises the amount of magnetic flux lines running perpendicular to the ribbon. Totally perpendicular magnets would have the highest impact on the sensitivity, but that would increase the path length around the baffle. The patent's design with magnets at an angle less than 80º, provides a good compromise between the baffle length and flux direction in order to get good sensitivity while also improving the frequency response. Royer and Perrotta made use of Neodymium magnets in this design. The Neodymium magnets are much more powerful than the magnets used in previous designs. The alloy for the pole pieces in this patent is Permendur or Hyperco 90 which has a much higher magnetic permeability than iron. The magnetic structure has

thus been improved in more than one way. Detailed dimensions for the air gap and the ribbon are provided in the patent. This particular design also helped to reduce the size and weight of the microphone. Much other detail is also provided, but no graphs are provided to support the claims of the improved sensitivity and frequency response.

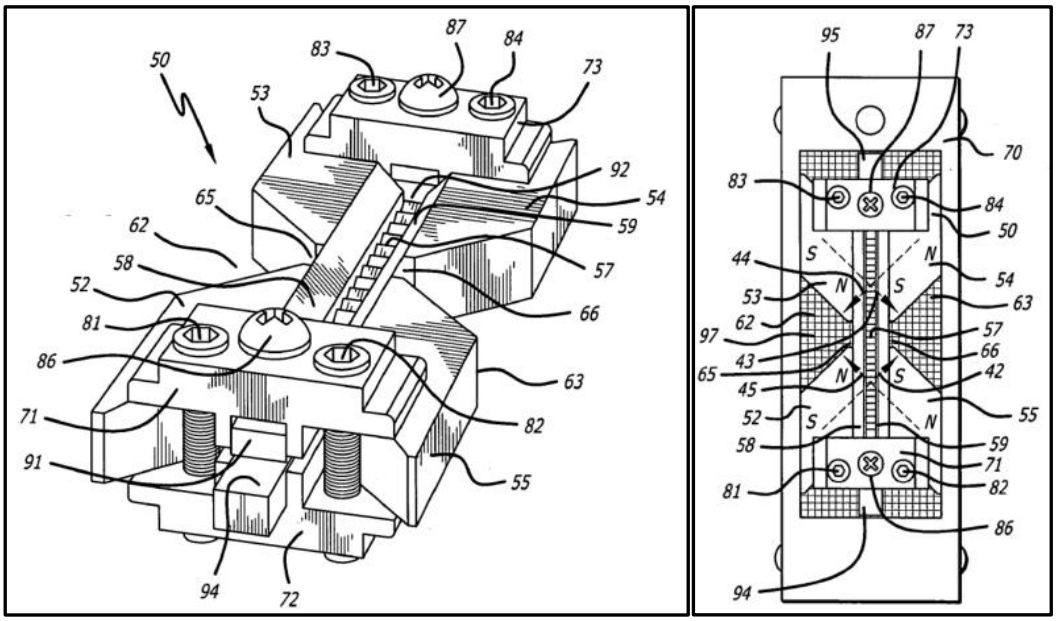

Figure 6: Royer's modern version of the ribbon microphone **[26]**

The special purpose transformer is a complex toroidal transformer design. It has four primary coils, is a tape-wound-core transformer, has turn ratios of 100:1 and 200:1, includes at least three interleaved secondary coils, and/or includes at least three interleaved primary coils. The primary and secondary windings are also interleaved with each other. A buffer circuit is also enclosed within the outer casing and is electrically coupled to one of the secondary coils. The input impedance of the buffer circuit is at least 10 MΩ including a field-effect transistor. The core of the transformer consists of a "tape wound" configuration instead of compressed ferrite or composite materials. The "tape wound" core is constructed from thin M-6 nickel iron strips that are rolled up very tightly into the shape of a doughnut.

These two patents are both noted for their thorough description of the workings of a ribbon microphone and its illustration of the improvements that are possible with modern technology.

4.1.16 Akino 2005

Hiroshi Akino addressed the design of the ribbon (not the microphone motor) in his patent application of 2005 [43]. He patented the idea of depositing a thin layer of gold over the traditional aluminium ribbon. Gold is also deposited to the ends of the electrode plates. The reason for the gold plating onto the aluminium ribbon is to prevent oxidation of the ribbon. The electrode plates are also gold plated to prevent corrosion due to intermetallic electrolytic reactions. Preventing

corrosion at the ribbon-electrode-junction ensures that the impedance of the junction remains as low as possible, thereby preventing the loss in sensitivity that would usually occur over time.

4.1.17 Crowley 2005

During the same year Robert Crowley filed a lengthy patent with twenty different claims [44]. The patent aims to enhance quality and repeatability during the manufacturing process of the ribbon microphone. Crowley stresses the importance of the ribbon in his patent. He addresses the trade-off between mass and resistance of the ribbon by using composite materials. The ribbon in this patent is claimed to consist of carbon fibre nanotube filaments attached to a layer of conductive material.

4.1.18 Tripp 2007

With the main focus still on the ribbon, Tripp and Crowley filed a patent in 2007 for the invention of a polymer ribbon [45]. Their patent makes us of a polymer ribbon that exhibits high toughness, high conductivity and good shape-memory. The ribbon's corrugated structure is formed by compressing the ribbon between two dies and then heating and cooling it to set it permanently into this shape. The polymer ribbon is coated with a conductive coating. The polyethylene terephthalate (PET) that it consists of does not become brittle with age because it contains no plasticisers. The invention claims that the ribbon will not be damaged by phantom power (48VDC applied by mixing boards) because the PET that is used is about eight times stronger than a normal aluminium ribbon. Another advantage of the high strength of the PET is the fact that the ribbon can be made much thinner and thus lighter, making it more responsive to low intensity sound waves.

4.1.19 Akino 2009

In 2009 Akino patented another ribbon design [46]. In any ribbon microphone design the ribbon must be set to a resonance frequency that is below the lowest frequency to be recorded. To achieve this, the tension on the ribbon must be very low. The corrugated form of the ribbon helps to realise this low tension. The corrugated ribbon is manufactured by feeding the ribbon through a set of spur gears. According to the patent the flat areas between the corrugations cause a high mechanical resonance within the required frequency range to be recorded. To solve this problem a ribbon was invented onto which a special pattern is transferred by means of a roller with a transfer mould. The selective embossing of the ribbon produces a more rigid ribbon that suppresses the sharp resonances. On the frequency response graphs in the patent it can be seen that the specially formed ribbon suffers less from high frequency resonances (noticeably in the region above 10 kHz), but it suffers from lower sensitivity above 5kHz.

4.1.20 Horng 2009

The National Chung-Hsing University in Taiwan recognised an opportunity to address the design of the ribbon with the aid of micro electro-mechanical systems (MEMS) technology [47]. The patent claims that the frequency response of the microphone will be better if its sensitivity is improved and that the sensitivity can be improved by using a lighter ribbon. The weight and the size of the ribbon are however restricted by conventional manufacturing processes. According to this patent it is the size and weight restrictions of the ribbon that causes the attenuation of low and high frequencies. By applying the techniques that are used in semiconductor fabrication and in MEMS, the patent describes the manufacturing of a smaller diaphragm and voice coil. No dimensions are provided in the patent to judge the reduction in size and no frequency response characteristics are given to illustrate any improvements.

4.1.21 Cloud 2010

With new designs for the ribbon itself being thoroughly covered since 2005, Cloud and Sank's patent focussed on other aspects of the ribbon microphone, namely the magnet motor assembly, a back-wave chamber and electronics [27]. The patent introduces round magnet poles to the design. The rounded poles cause sound waves to reflect of it in a diverging pattern, thereby diffusing the reflected sound waves. Therefore the ribbon reacts to the sound with minimal interference from sound waves reflecting off the pole pieces. The result is a flatter frequency response compared to conventional flat magnets. No frequency response graphs are provided in the patent to support this claim. Another part of the patent illustrates a different design with a horizontal ribbon and a blast filter in front of the ribbon to protect it against high pressure sound waves. The same configuration also has a chamber at the back of the ribbon which prevents reflected sounds from entering the microphone from the rear. This design is completely different form the normal upright configuration of the ribbon microphone, looking more like the ice-cream cone design of an ordinary condenser microphone. The design is complemented by the addition of a differential cascade JFET amplifier that is powered by phantom power from the recording desk. The patent claims a signal boost of +20 dB with its JFET amplifier.

4.1.22 Akino 2012

In his 2012 patent, Akino claims that the ribbon can be protected against impact by short-circuiting the ribbon's electric circuit when it is not in use [48]. He claims that the back-emf generated in the ribbon will suppress its movement significantly due to electromagnetic damping. No calculations or data is provided to quantify his claim. Although the back-emf effect is a scientific fact, the author is of the opinion that the electromagnetic damping will not be significant enough to qualify the patent as anything more than a marketing exercise. This patent presents a good simulation challenge for students to determine how substantial Akino's claim is.

4.2 Other Publications

Most literature that can be found on the ribbon microphone is merely concerned with patents and advertising. The few publications that could be found with academic content on the ribbon microphone are summarised below.

4.2.1 Ke 2009

Ke, et al. designed a symmetrical voice coil using MEMS technology [49]. The aim of the MEMS design was to increase the effective length of the coil while reducing its physical dimensions. They succeeded to manufacture a voice coil with a 77.5 mm effective length while limiting the overall length of the ribbon to 17 mm. Compared to a standard 50 mm ribbon, it is a gain of 55% in effective length with a 66% size reduction. Figure 7 provides a drawing from Ke's paper to illustrate the design. The voice coil is designed in such a way that half of the windings run through the magnetic field (all in the same direction) while the returning half of the windings run outside of the magnetic field (in the opposite direction). If the returning conductors were also inside the magnetic field, they would have generated an emf in the opposite direction. By having the return path outside of the magnetic field, the total length of the electric conductor in the magnetic field is increased without the returning conductors cancelling the emf. The paper includes an overview of the design and a COMSOL® simulation of the magnetic flux density between the magnets. No frequency response information is provided. The frequency repose of this novel design would provide valuable information since the voice coil is fixed to the magnets and not allowed to move freely in the magnetic field like a conventional ribbon.

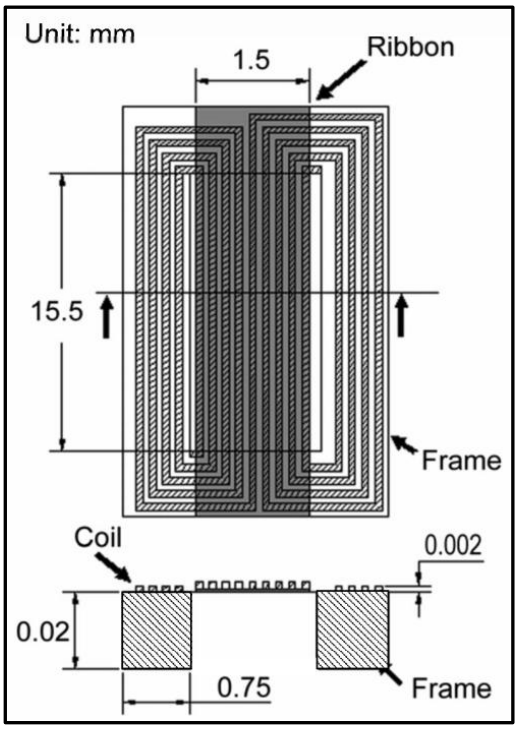

Figure 7: MEMS ribbon **[49]**

4.2.2 Horng 2011

Horng presented a conference paper in 2011 after further study on the miniature ribbon microphone design that Ke published in 2009 under Horng's guidance [50]. The conference paper expands on the previous publication by illustrating more detail on the MEMS manufacturing process and providing test results on the displacement of the voice coil, the velocity of the diaphragm, and the microphone's frequency response. It was shown that the displacement of the bare diaphragm (without coil) is slightly larger than the displacement of the diaphragm after printing of the coil. The reason is the additional weight of the coil. The displacement of the voice coil is almost linear with increasing sound pressure over the measurement range of 10 Pa to 100 Pa. It is not clear what equipment was used for the displacement measurements. The velocity measurements were done with a laser Doppler vibration system. Although the displacement tests showed a minor difference, the velocity tests showed a more prominent difference between the bare diaphragm and the diaphragm with coil. The measurement results of displacement and velocity cannot be directly compared since the displacement measurements were performed from 10 Pa upwards and the velocity measurements were done at a sound pressure level of 1 Pa. A displacement of 0.5 µm was measured for the diaphragm (including coil) at 10 Pa. At a pressure of 100 Pa a displacement of 6.0 um was measured. The velocity at 1 kHz with a sound pressure of 1 Pa is only 1.3 µm/s. This provides the reader with an understanding of just how small these measurements are (and thus prone to measurement errors). Horng's frequency response measurements show an increasing sensitivity from 100 Hz (-64 dBV/Pa) up to 20 kHz (-50 dBV/Pa). It is worth noting that the microphone's sensitivity is not dropping at high frequencies (> 10 kHz) as one would expect from a closed baffle design.

4.2.3 Kwon 2016

Kwon and Honorato performed out of the ordinary tests with a ribbon microphone at the Naval Postgraduate School in Monterey, California. They tested the ribbon microphone as an underwater transducer. They observed that its directional characteristics approach that of an ideal dipole with its two lobes becoming narrower with increasing frequency [51].

4.3 Educational Benefit of Technical Histories

From an educational perspective, the progress of patents and history itself is a powerful learning tool, showing progress from the original basic idea to an advanced model. It also illustrates how faults and shortcomings are identified; how opportunities for improvement are discovered and how new technology can be applied to solve old problems.

This thesis does not explore any improvements to the ribbon microphone. It rather illustrates how different fields of physics can be explored by students with the aid of a ribbon microphone as a multi-physics laboratory aid.

5 MODELLING AND TESTING

This chapter introduces the different software solutions that are available for modelling and simulation. It provides a brief overview of a number of identified commercial software packages and indicates the software packages that were chosen for the simulations in this thesis. A summary of the author's experience with two simulation packages is included. The ribbon microphone and the test equipment that was used for the experiments in the thesis are introduced in this chapter. Information on the ribbons that were used and an experiment with vapour deposition on the ribbon are presented.

5.1 Modelling and Simulation

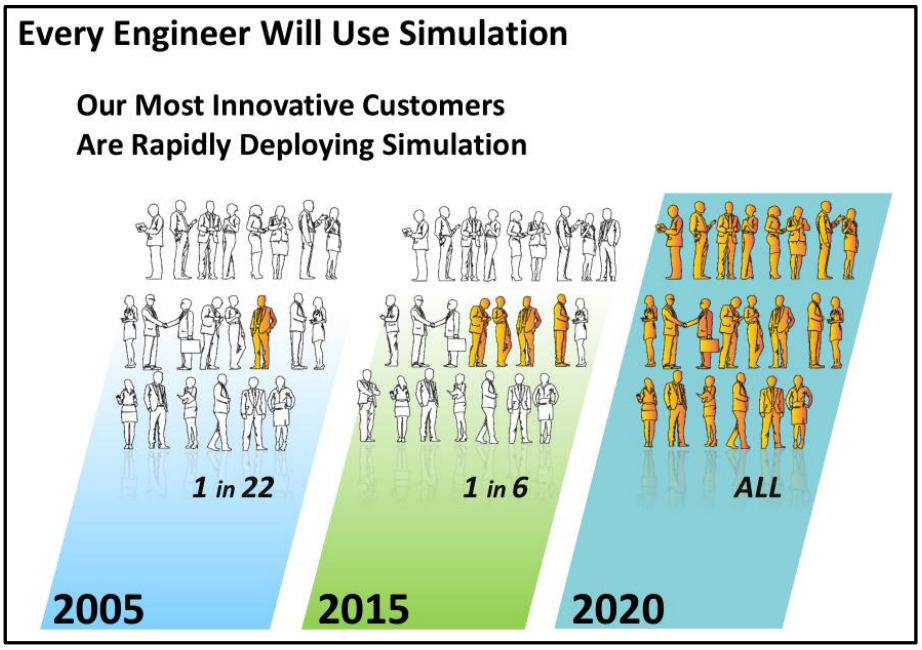

Figure 8: Marketing view of the future **[52]**

There is a major marketing drive from companies that provide modelling and simulation software to expand the use of simulation tools. Figure 8 indicates how one of these companies sees the future. Adopting simulation early in the development of a product has time, cost and reliability benefits. Therefore it is important for students to be exposed to the use of simulation software.

The acoustic-mechanic-magneto-electrical physics of the microphone model can be simulated by means of any of the following options or a combination of these:

- Completely self-written software.
- Mathematical software.
- Finite Element Method (FEM) modelling software.

Writing one's own software requires extensive programming experience that falls beyond the scope of this thesis. Therefore only mathematical and modelling software were considered. Creating a model with mathematical software still requires a good measure of programming on the user's side though.

In each of these categories both open source and commercial software are available. There is a myriad of software packages available to choose from. Only a few of the more familiar ones or those stumbled upon during the work on this thesis are covered here. The following table lists a few available products that were considered for the simulation of the microphone models.

Table 1: Modelling and simulation products

	Open Source	**Commercial**
Mathematical	GNU Octave (www.gnu.org) Scilab (www.scilab.org)	MathWorks MATLAB® (www.mathworks.com) WOLFRAM Mathematica® (www.wolfram.com/mathematica)
FEM	Clawpack (www.clawpack.org) Finite Element Method Magnetics (www.femm.info)	Altair HyperWorks® (www.altairhyperworks.com) COMSOL Multiphysics® (www.comsol.com) QuickField (www.quickfield.com) ANSYS® (www.ansys.com)

The open source software requires a much steeper learning curve than the commercial software and was therefore put aside. The commercial software is discussed below.

5.1.1 Website Calculators

To calculate the force between two magnets or between a magnet and a steel plate the following online calculator can be used: http://www.kjmagnetics.com/calculator.asp

5.1.2 MathWorks MATLAB® & Simulink®

MATLAB® is the abbreviation for MATrix LABoratory. It is a high-level language used for numeric computations and visualisation of the results. MATLAB® can be used either to analyse data or to create models and develop algorithms.

Simulink® is an environment using block diagrams to create multi-domain simulations and model-based designs. It also provides automatic generation of software code for embedded systems. Simulink® is integrated with MATLAB® so that the algorithms in MATLAB® can be imported into Simulink® models and the simulation results can be exported back to MATLAB® for analysis.

5.1.3 WOLFRAM Mathematica®

Mathematica® uses the Wolfram symbolic language for programming. Equations, code, graphics and data are all represented as symbolic expressions. It can be used for mathematical computation, numerical analysis, visualisation of results, algebraic manipulation, number theory, data analysis, graph computation, image computation, geometric computation and interactive computation.

5.1.4 Altair Hyperworks®

Altair HyperWorks® is a computer-aided engineering (CAE) and simulation platform used for modelling and analysis of mostly mechanical designs. It addresses computational fluid dynamics (CFD) problems in particular, but also offers multi-physics and multi-disciplinary analysis. HyperWorks® is mainly geared towards the transportation industry for simulation, analysis and optimization of structural designs, the aerodynamics thereof and impact tests, to name a few. Since 2014 the South African developed FEKO® electromagnetic analysis software suite is also falling under the umbrella of Altair®.

5.1.5 COMSOL Multiphysics®

COMSOL Multiphysics® uses finite element analysis (FEA) for physics-based modelling and simulation. It is a general purpose platform for modelling and simulation of various disciplines, including electrical, mechanical, chemical and fluid flow for example. COMSOL's capability to model magnetism and electromagnetism with its AC/DC module together with the dedicated acoustics module makes it the first choice for the topic of a ribbon microphone. COMSOL® makes it possible to couple the phenomena in these physics domains with one another. COMSOL's LiveLink application interfaces seamlessly with Microsoft Excel, Inventor and MATLAB®. The interface with Microsoft Excel is handy for loading variables and parameters from lists that can be generated outside of COMSOL®. The interface with MATLAB® is useful for further analysis of simulation results. 2D and 3D models can be constructed within COMSOL® with its own geometry tools. The interface with Inventor is essential for mechanical models that are difficult or impossible to construct with COMSOL's own design module. The application builder feature of COMSOL® makes it possible to create a user friendly application that hides the complexity of the model while providing access to selected parameters. These parameters can be manipulated by a user at another location who needs to observe the model's behaviour without necessarily understanding

the underlying complexities of the model. Horng and Ke [47] [49] used COMSOL® during their work on the miniaturisation of the ribbon microphone.

5.1.6 ANSYS®

ANSYS® offers engineering simulation software for a wide range of physics including fluids, structures, electronics, semiconductors, embedded software, and even short duration severe loadings due to explosions. The ANSYS® simulation software is extremely powerful, but the drawing tool in ANSYS® is very limited. For best results models have to be created in a CAD package outside of ANSYS® and then be imported for simulation. ANSYS® is the other simulation software package that was used for simulations in this thesis.

5.1.7 Software choice

The author identified COMSOL® and ANSYS® as preferred simulation packages because of the fact that it provides modules for all aspects of the ribbon microphone, i.e. acoustics, mechanics, magnetics and electromagnetics.

The author's experience with these two simulation packages throughout the work for this thesis is summarised as follow:

- COMSOL® is a relatively new product with all the physics modules seamlessly integrated into a single user interface. Excellent examples for each physics domain are easily found on the COMSOL® website. The user interface is very intuitive and can be mastered in a short time by following the step-by-step tutorials and the videos that are freely available from the COMSOL® website. Local support for the product is very limited however.
- ANSYS® consists of a wide suite of mature products that are well integrated to share information and results amongst each other, but each product still has its own unique user interface. ANSYS® is in the process of creating a central user interface, but at the time of this thesis it still had a long way to go. Tutorials are freely available from the ANSYS® website, but needs a lot of searching to find it inside the huge amount of user support data. It is difficult to master the ANSYS® user interface if one needs to learn more than one of the products to perform a multi-physics simulation. This package is for well-seasoned simulation experts and does not come intuitively. The local support for ANSYS® is however outstanding. With regular hands-on workshops ANSYS® more than compensates for the learning barriers.

5.2 Test Equipment

The following hardware and the software were used to perform the experiments described in the rest of the thesis.

5.2.1 Ribbon Microphone

Ribbon microphones are amongst the most expensive microphones on the market today. It is not cost effective to buy an off-the-shelf ribbon microphone for the laboratory work described here. A simple do-it-yourself (DIY) ribbon microphone is constructed from commercially available materials for this purpose. It should be noted that the process can be repeated by school children with virtually no special equipment. The microphone design is dependent on the dimensions of the magnets that can be sourced and on the width of the ribbon.

5.2.1.1 Magnet Motor Construction

Neodymium magnets with dimensions of 10x10x50 mm are of practical size for this design. A mild steel frame is designed to fit the two magnets as well as two nylon clamps for the ribbon. The frame is designed to keep the magnets 6 mm apart. The 6 mm gap makes provision for a 5 mm wide ribbon with 0.5 mm clearance on both sides.

Extreme care must be taken when handling the magnets because of the strong magnetic forces between the magnets. These forces are powerful enough to break the magnets if they are allowed to snap together from a short distance. Plastic or wooden spacers must be used between the two magnets when inserting it into the mild steel frame. Without the spacers it is impossible to hold the magnets 6 mm apart by hand. Once the magnets are inside the frame, the frame provides a magnetic field path from the north pole on the outside of one magnet to the south pole on the outside of the other magnet. As long as the magnets remain in contact with the inside of the frame the magnetic field flowing through the frame is strong enough to overcome the magnetic force between the two magnets and the magnets remains “stuck” to the inside of the frame apart from each other. Nylon clamps secure the ribbon in the centre of the gap between the two magnets. Electrical connection is made between the ribbon and the wires by means of copper tape that is stuck from the inside to the outside of the nylon clamps. The complete frame is fastened onto a piece of wood inside the lid of a glass jar. Two lids are mounted back-to-back so that the jar can either act as a stand for the ribbon microphone or as a container to keep the microphone safe from the environment and make it easy to transport. Two views of the laboratory version ribbon microphone are shown in Figure 9.

Figure 9: DIY ribbon microphone

5.2.1.2 The Ribbon

Information on a commercial ribbon (Shure Roswellite™) that is the ideal ribbon for laboratory tests because of its durability is discussed in this paragraph. An attempt to reproduce a similar ribbon in the laboratory is documented. All the experiments can be performed however, with DIY ribbons manufactured at home or in the laboratory from inexpensive materials.

The first DIY ribbon is made from light aluminium foil commonly found in a kitchen. Heavy-duty foil is 20 µm thick and light-duty foil is 10 µm thick. Even the light-duty foil is 5 times thicker than the ideal ribbon thickness of 2 µm, but for the purposes of this thesis 10 µm is adequate. To obtain a 60 mm long by 5 mm wide ribbon, a 90 mm strip of 5 mm wide aluminium foil can be cut and then corrugated with the gears from a Lego set.

The second DIY ribbon is manufactured from a piece of thermal space blanket. The thermal blanket consists of a Polyethylene Terephthalate (PET) film with a thin aluminium deposit on one side. It is the ability of the aluminium layer to reflect radiated heat that gives the blanket its thermal properties. Strips of the thermal blanket cannot be corrugated with the Lego gears because it immediately returns to its original flat form after going through the gears. The only way to corrugate the PET strips is to form it in a jig and then bake it in the jig at 90º C for an hour. In this process

special care must be taken not to damage the thin aluminium coating. The product of the baking process is a corrugated ribbon with the ability to return to its corrugated form after being stretched out to its original length.

Shure Incorporated owns the intellectual property for a shape-memory ribbon material called Roswellite™. It was developed by Soundwave Research but Shure got the rights to it when they acquired Crowley and Tripp Ribbon Microphones from Soundwave Research Laboratories in 2009 [53]. Roswellite™ is a replacement for the aluminium foils that are normally used in ribbon microphones. Shure claims it to be a “nano-enabled ribbon material” that is much more durable than metal foils [54]. The claim that it is more durable is true, but it has nothing to do with nanotube technology. Unless Shure has deviated substantially from their patent application [45], these ribbons are simply made from a thin polymer (e.g. 2.5 µm PET) that is coated with a layer of conductive material like aluminium or gold.

The ribbon of a ribbon microphone can be easily damaged during experimentation. To replace a 2 µm aluminium foil ribbon is a very delicate process that would rather be avoided. Therefore it is desirable to conduct all experiments by using a custom made ribbon that has similar properties to Roswellite™. An attempt was made to manufacture a Roswellite™-like ribbon by depositing 1 µm (10 000 Ångstrom) of aluminium onto pieces of Mylar™, Polypropylene and PET film. Mylar™ would make an excellent ribbon. It is used in certain dynamic microphones for its unique qualities. Mylar™ is a polyester film manufactured by DuPont. It is extremely durable, has high tensile strength, can withstand extreme temperatures (-40ºC to +170ºC) and has half the weight of aluminium [22]. It also has a long lasting flex life. When formed under high temperature and pressure its molecular structure changes permanently. The shape memory will cause it to return to its shaped form even after large temporary deformations. Mylar™ will therefore produce a gust proof ribbon. It only has to be coated with a thin layer of conductive material to add the required electromagnetic properties.

The engineering department of the university has vapour deposition equipment that can be used to deposit various metals onto other substrates. Aluminium was deposited at an evaporation rate of 5 Å/s for a duration of 33 minutes to deposit a 10 kÅ thin layer. The Mylar™ and Polypropylene were visibly affected by the heat of the vapour deposition process. The PET showed little adverse effects to the heat (Figure 10). The resistance of the ribbon can be calculated as:

$$R = \rho L / A \qquad (1)$$

where R is the resistance in ohm, ρ the resistivity constant of the material in Ω/m, L the length in m and A the cross-sectional area in m^2. The resistivity of aluminium is 2.82 x 10^{-8} Ω/m.

The resistance of this ribbon should be 0.325 Ω for a ribbon length of 50 mm, width of 4 mm and thickness of 1.0 µm. After the vapour deposition however, the resistance of the aluminium layers

on all the polymers were measured to be in the kilo-ohm range, which is much too high for 1 µm of aluminium. The colour of the aluminium layer was not bright and shiny like a mirror, but brownish. The aluminium layer also allowed much light through. The high resistance, brownish colour and transparency of the aluminium led the author to believe that impurities were present in the evaporation chamber during the evaporation process. The impurities will lead to poor cohesion of the aluminium molecules and poor adhesion to the substrate. The impurity molecules that are also deposited along with the aluminium will cause electrical insulation between the aluminium molecules. On close inspection an oily substance was found on the sensor arm of the vapour deposition system. This oily substance may explain the impurities that were present in the chamber. After further investigation it turned out that the vapour deposition equipment was faulty and it would take a considerable amount of time before the equipment would be repaired. No further attempts were made at vapour deposition. Photos of the vapour deposition equipment are shown in Figure 11.

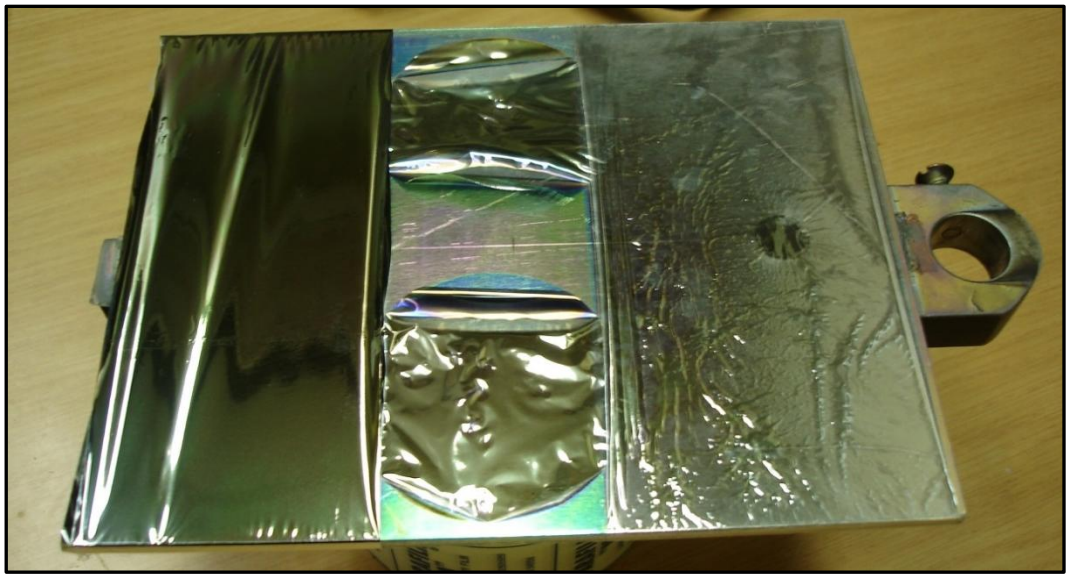

Figure 10: Vapour deposition of aluminium onto PET (left), Mylar™ (centre) and Polypropylene (right)

The upper frequency range of the ribbon microphone is limited by the length of the path from the front to the back of the ribbon and not by the ribbon thickness (up to a reasonable point). According to Artur Fisher the reason why thinner ribbons tends to sound better is because of the transient response of the ribbon [55]. In musical definition it affects the attack of the sound. In other words, it produces a brighter sound. These transients are especially important in the reproduction of the sounds of percussion instruments, symbols and acoustic guitars. In this thesis the subtleties of these transients are not investigated. Therefore the 10 µm aluminium and the space blanket ribbons are sufficient.

Figure 11: Vapour deposition equipment setup

5.2.2 Laboratory Equipment and Software

The following laboratory equipment is used for the experiments in the thesis:

- A Wavetek 11MHz Stabilised Function Generator model 21 is used to generate the sinusoidal voltage signals for the transformer experiment.
- An Agilent DSO5012A oscilloscope is used to view the sinusoidal signals throughout the circuits to confirm that no clipping or deformation of the signals occurs.
- A Fluke 189 True RMS Multimeter is used to measure the voltages in the circuits. The Fluke 189 can measure alternating current from 45 Hz up to 100 kHz.
- A 5Hz-13MHz Hewlett Packard 4192A LF Impedance Analyser is used to take impedance measurements. A limited number of measurements can be performed manually at specific frequencies, but with the aid of software it is possible to take automated measurements at many points over a wide range of frequencies in a short time. The HP 4192A dates from the era when the General Purpose Interface Bus (GPIB) was the latest standard in test equipment control and automation. To connect a modern computer to the GPIB interface a USB to GBIP adapter is required. A GPIB-USB-HS+ from National Instruments can be used for this purpose. The software that is used is the HP 4192A Sweep Utility Software that Michael Kelzenberg wrote in LabVIEW® for his PhD thesis [56]. Good contact between the

analyser adapter and the item under test is very important. To obtain the best possible contact, short pieces of silver wire is soldered onto the transformer wires before performing the measurements.

- A set of low cost Logitech S-220 speakers is used for the acoustic tests. The set consists of an active subwoofer with built-in amplifier and a pair of stereo speakers.
- Many of the tests are performed with the aid of John Mulcahy's Room EQ Wizard (REW). The software is intended for acoustic analysis of room and loudspeaker response, but it works equally well for turning a personal computer (PC) or laptop with soundcard into a laboratory tool. REW may be downloaded free of charge from www.roomeqwizard.com to be used within the (very lenient) restrictions of its licensing agreement.

5.2.3 Acoustic Environment

Ideally all acoustic tests should be performed in a room with sound absorbing and damping material that prevents reflected sound waves from influencing the test results. For the thesis however no special arrangements were made to the acoustic environment. The idea is to have an acoustic environment that students can quite easily arrange themselves. All acoustic tests were performed with a speaker relatively close to the microphone so that any reflected sound waves would be small compared to the intensity of the sound waves from the speaker itself.

6 ACOUSTICS

The first of the physics areas for which the ribbon microphone can be used eminently as demonstration tool, is that of acoustics. The propagation of a wave in space, phenomena such as reflection and interference caused by the physical structure of the microphone, the behaviour of the wave as a function of frequency, and concepts like phase differences in space can be coupled seamlessly with the working and properties of the microphone, especially when using modelling software for complex analysis and graphical visualization. While a sound wave in an obstructionless, ideal environment can be modelled by a simple mathematical formula, the movement of an object due to such a wave is much more sophisticated, as size, weight, elasticity and orientation all play a role. As this problem is at the heart of the ribbon microphone operation, analysis of such a structure serves well to illustrate behaviour of acoustic waves in the vicinity of obstacles, and its effect on a small obstacle. This is normally far beyond what can be illustrated with simple mathematical models, and provides significant additional insight.

In addition, modelling aspects such as meshing, computer limitations, etc. is well illustrated by this problem. This area of engineering education (i.e. use of modelling software) has become extremely important, and the extreme ranges required for the analysis of microphones forms a perfect vehicle for illustrating this.

This chapter presents 8 experiments which can be performed using a basic ribbon microphone as simulation model.

- A set of simulation experiments modelling objects of varying size, weight and elasticity in an acoustic wave. Here the focus is on the movement and deformation of the object, with the object constituting a small section of a ribbon. The aim here is to illustrate mainly the dynamic movement of solids in waves.
- Experiments showing the effects of meshing on solutions. These are of a more advanced nature, and it is presented here since computer simulation is currently introduced into engineering courses from a very early stage, and problems with meshing can create completely false results.
- Experiments showing the influence of a solid object on an acoustic wave. Here, the focus is on the wave, and how it is affected by obstacles over the very wide frequency range of 1:1000.

No physical experiments are done in this chapter since its main purpose is to demonstrate the power of modelling and simulation and to highlight a number of challenges in simulation.

6.1 Theory

Sound waves are longitudinal waves, but for illustration purposes it is often drawn as transverse waves as illustrated in Figure 12. The crests on the transverse wave represent the high pressure sections of the longitudinal wave (dense, compression of particles) and the troughs represent the low pressure sections (sparse, rarefaction of particles).

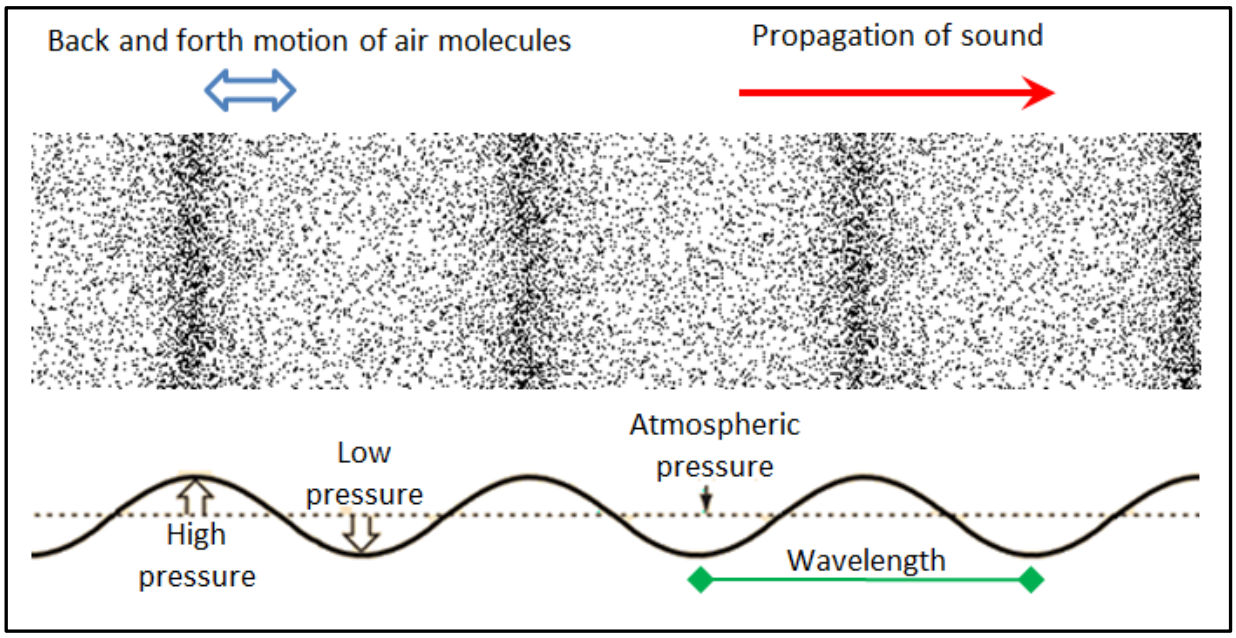

Figure 12: Transverse wave representation of a longitudinal sound wave

A simple periodic sound wave in an elastic medium can be described by the wave function

$$y = Asin(\omega t - kx) \tag{2}$$

where y is the displacement from equilibrium of a particle in position x at a moment t in time. A is the maximum displacement and k the propagation constant. The angular frequency ω equals $2\pi f$ (where f is the frequency). The value of A may be large when illustrating wave motion by means of a string or a coil, but for a sound wave in air the value of A is in the nanometre range.

The theoretical maximum distance (s_{max}) that a weightless particle will be displaced in a sound wave can be calculated as

$$s_{max} = \frac{\Delta P_{max}}{\rho v \omega} \tag{3}$$

where ρ is the density of the medium, v the speed of sound, ω the angular frequency ($2\pi f$) and

$$\Delta P_{max} = \sqrt{2\rho v I} \tag{4}$$

with I the intensity level of the sound wave in W/m^2 [57].

From (3) it can be seen that the particle's displacement is directly proportional to the pressure difference and inversely proportional to the frequency.

Combining (3) and (4) into one equation gives

$$s_{max} = \sqrt{\frac{2I}{\rho v \omega^2}} \tag{5}$$

To illustrate the tiny magnitudes that are involved when air particles are displaced in a sound wave, the displacement is calculated for two extreme scenarios:

- The threshold of hearing ($1x10^{-12}$ W/m^2, i.e. 20 µPa or 0 dB), i.e. the intensity of the faintest 1 kHz pure tone that can be detected by the human ear, and
- The threshold of pain (1 W/m^2, i.e. 20 Pa or 120 dB), i.e. the upper limit for human hearing.

With the speed of sound equal to 343 m/s in air (at 20ºC), the density of air equal to 1.2 kg/m^3 and a frequency of 1 kHz, (5) yields a displacement of $\mathbf{11.1 \times 10^{-12} m}$ at the threshold of hearing and a displacement of $\mathbf{11.1 \times 10^{-6} m}$ at the threshold of pain.

Comprehending that the displacement of an air particle at 120dB is one million times larger than the displacement at the lower threshold of hearing, it is no wonder that sound this loud hurts the inner ear regardless of all the damping mechanisms inside the ear.

The relationship between the displacement, velocity and acceleration of a particle in a sound wave is shown in Figure 13 [22].

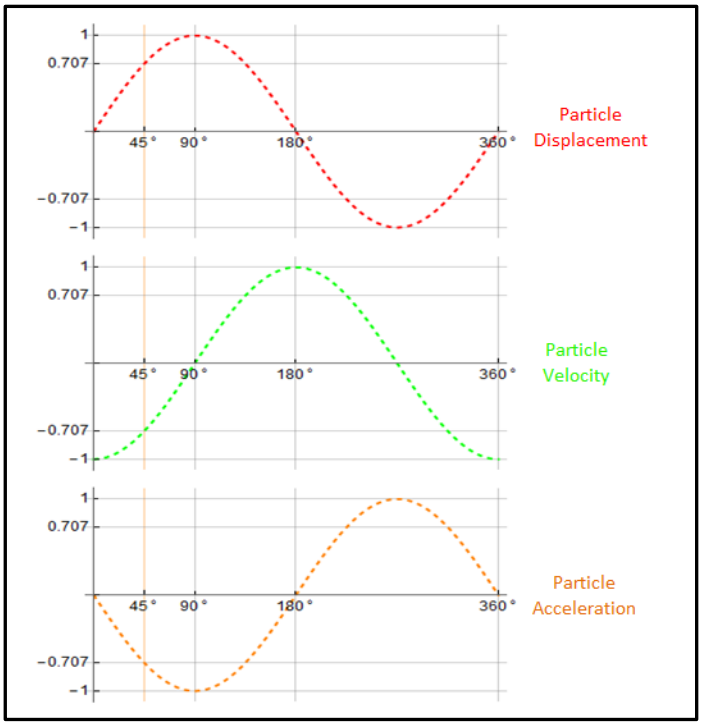

Figure 13: Relationship between particle displacement, velocity and acceleration **[22]**

From Figure 13 it is notable that the electrical output of the ribbon microphone is at its peak amplitude when the movement of the ribbon is at its highest velocity. It can thus be seen that the electrical signal lags the displacement of the air particles by 90 degrees.

6.1.1 Magnitude of a Sound Wave

The magnitude of a sound wave is expressed in various terms throughout literature. One way to express it is in terms of its energy and it is called *sound intensity* or *acoustic intensity*. Otherwise the term *sound pressure* is used to express it as a function of its force.

Sound Intensity

Sound intensity is the energy transmitted per unit of time (i.e. power), in a specific direction, through a unit area that is positioned perpendicular to the direction of propagation [58].

Sound intensity is expressed in watts per square metre (**W/m^2**) [59].

Sound Pressure

Sound pressure is the force that a sound wave exerts per unit area. Although force is a vector, pressure is a scalar quantity.

Pressure is expressed either in Newton per square metre (**N/m^2**), or in Pascal (**Pa**) [57].

Due to the fact that the dynamic range of human hearing stretches over such a wide range (typically 1x10^{-12} W/m^2 to 1 W/m^2), sound pressure and sound intensity are not commonly expressed in W/m^2 or N/m^2, but rather as a ratio relative to a certain reference level. The reference level that has been chosen in both cases is the lower threshold of human hearing, i.e. the faintest sound of a 1 kHz pure tone that can be distinguished by a healthy young adult. In terms of intensity this level is 1x10^{-12} W/m^2 and in terms of pressure it is 20x10^{-6} Pa. Because the ratios are so large, it is expressed on a logarithmic scale. The unit that is used is the decibel (dB). The decibel is not a measuring unit in a physical sense but only a reference to the logarithmic ratio definition.

The sound *intensity* level in dB is defined as

$$I = 10log_{10}\left(\frac{I}{I_0}\right)\ dB \tag{6}$$

where I_0 = 1x10^{-12} W/m^2.

The sound *pressure* level in dB is defined as

$$SPL = 20log_{10}\left(\frac{p}{p_0}\right)\ dB \tag{7}$$

where p is the root mean square pressure and p_0 equals 20 µPa [60].

The sound *pressure* level is defined differently from sound *intensity* because the pressure ratio equals the square root of its corresponding power ratio [58].

The outputs of microphones produce voltage outputs that are proportional to the *pressure* of the sound waves. Therefore in practice, sound *pressure* levels (SPL) are more widely used than sound *intensity* levels [59].

6.1.2 Mathematical Models for Acoustic Analysis

In this paragraph an overview is provided of the acoustic theory that is required for the simulation of acoustic models. This information was obtained from [61].

6.1.2.1 Frequency Domain Studies

In standard acoustic problems the small variations in the acoustic pressure p on top of a stationary background pressure p_0 must be solved. The following two equations form the basis for a lossless (i.e. no thermal conduction and no viscosity) compressible fluid flow problem:

1. The momentum equation (Euler):

$$\frac{\partial \boldsymbol{u}}{\partial t} + (\boldsymbol{u} \cdot \nabla)\boldsymbol{u} = -\frac{1}{\rho}\nabla p \tag{8}$$

2. The continuation equation:

$$\frac{\partial \rho}{\partial t} + \nabla \cdot (\rho \boldsymbol{u}) = 0 \tag{9}$$

where ρ is the total density, p total pressure, $\boldsymbol{u}$ velocity field.

The thermodynamic processes are assumed to be adiabatic and reversible, i.e. isentropic processes. The small parameter expansion is performed at a pressure p_0 (in Pascal) on a stationary fluid with density of ρ_0 (in kilogram per cubic metre) in a way that the following apply:

$$p = p_0 + p'$$
$$\rho = \rho_0 + \rho'$$
$$\boldsymbol{u} = \boldsymbol{0} + \boldsymbol{u}'$$

where $p' \ll p_0$ and $\rho' \ll \rho_0$ (the primed variables indicate the small acoustic variations).

Inserting these expressions into the base equations and keeping only the terms that are linear in the primed variables lead to the following:

$$\frac{\partial \boldsymbol{u}'}{\partial t} = -\frac{1}{\rho}\nabla p' \tag{10}$$

$$\frac{\partial \rho'}{\partial t} + \rho_0(\nabla \cdot \boldsymbol{u}') = 0 \tag{11}$$

Density is a dependent variable and can therefore be eliminated by expressing it through linearization (1st order Taylor expansion):

$$\rho' = \frac{\partial \rho'}{\partial p}|_s \, p' = \frac{1}{c_S^2} p' \tag{12}$$

where c_S is the speed of sound at constant entropy s.

Rearranging the equations and dropping the primes lead to the following equation for sound waves in a lossless medium:

$$\frac{1}{\rho c^2}\frac{\partial^2 p}{\partial t^2} + \nabla \cdot \left(-\frac{1}{\rho}(\nabla p - \boldsymbol{q_d}) \right) = Q_m \tag{13}$$

where ρc^2 is the bulk modulus (N/m^2) of the medium, $\boldsymbol{q}_d$ the dipole source (N/m^3) and Q_m the monopole source (1/s^2), showing that the speed of sound in a fluid is related to its compressibility.

A wave for which the pressure changes over time (time-harmonic wave) can be expressed as:

$$p(\boldsymbol{x}, t) = Re(p(\boldsymbol{x}) e^{i\omega t}) \tag{14}$$

where $\omega = 2\pi f$ (rad/s) with f the frequency in Hertz.

Taking this time-harmonic wave and assuming the same time dependence for its source, the wave equation can be reduced to an inhomogeneous Helmholtz equation:

$$\nabla \cdot \left(-\frac{1}{\rho}(\nabla p - \boldsymbol{q}_d) \right) - \frac{\omega^2 p}{\rho c^2} = Q_m \tag{15}$$

This is the equation that COMSOL® solves for frequency domain studies of 3D geometries.

6.1.2.2 Eigen Frequency Study

The solutions of the wave equation will be limited to a series of discrete functions (Eigen functions) when boundary conditions are applied to the system. Eigen functions are also known as the normal modes of the system. A unique frequency is associated with the solution of each mode. This frequency is known as the Eigen frequency or natural frequency. The normal mode with the lowest Eigen frequency is known as the fundamental mode. The frequency associated with this mode is called the fundamental (first) harmonic. The rest of the Eigen frequencies (second, third, fourth, etc. harmonics) are called overtones [59].

One or more of the following boundary conditions may be applied to the wave equation or the Helmholtz equation:

- Sound hard boundary or wall, where the acceleration of the normal component is zero

$$-\boldsymbol{n}\cdot\left(-\frac{1}{\rho_c}(\nabla p_t-\boldsymbol{q_d})\right)=0 \tag{16}$$

- Sound soft boundary, where the acoustic pressure disappears ($p=0$).
- Impedance boundary, where Z_i represents the impedance somewhere between a hard boundary ($Z_i\to\infty$) and a soft boundary ($Z_i\to 0$)

$$-\boldsymbol{n}\cdot\left(-\frac{1}{\rho_c}(\nabla p_t-\boldsymbol{q_d})\right)=-\frac{i\omega p_t}{Z_i} \tag{17}$$

- Radiation boundary or perfectly matched layer, with minimal reflections to the model (an unbounded open domain).

The attenuation of sound waves in a medium where losses occur is modelled by adding a first order time derivative with a damping coefficient d_a

$$\frac{1}{pc^2}\frac{\partial^2 p}{\partial t^2}-d_a\frac{\partial p}{\partial t}+\nabla\cdot\left(-\frac{1}{\rho}(\nabla p-\boldsymbol{q}_d)\right)=Q_m \tag{18}$$

(15) can be used to solve the Eigen modes and Eigen frequencies of the acoustic problem by removing the two source terms, yielding the equation:

$$\nabla\cdot\left(-\frac{1}{\rho_c}\nabla p\right)+\frac{\lambda^2 p}{\rho_c c^2}=0 \tag{19}$$

where $\lambda=i2\pi f=i\omega$. In other words, the eigenvalue λ is related to the Eigen frequency f and the angular frequency ω.

6.2 Modelling and Simulation

Sound waves are useful for an introduction to wave theory, as points of low and high pressure can be heard by the human ear. Also, the behaviour of sound wave particles is easier to visualise than for instance electromagnetic waves.

To get an idea of the maximum distance a ribbon may travel in sound waves of different frequencies and to see how it compares to the theoretical displacement of a weightless particle, a small element of extremely low mass is placed freely inside a modelling sphere.

The model consists of a small flat disk (10 µm thin, with 25 mm radius) suspended freely in the path of a sound wave. The modelling domain is enclosed in a sphere with 40 mm radius. The disk is positioned on the x-z plane with its thickness in the direction of the y-axis. The model is shown in Figure 14.

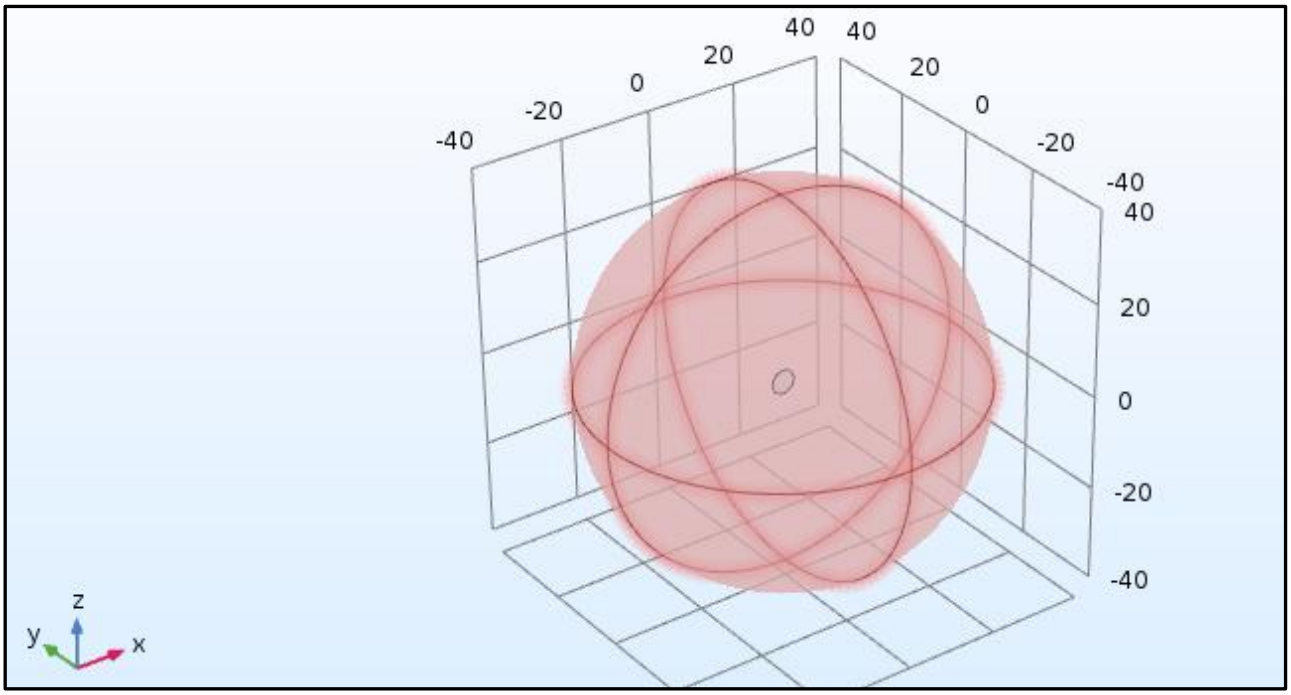

Figure 14: Model of free floating disk inside a sphere (the modelling domain)

During the simulation a number of obstacles and challenges were encountered that will be discussed in the paragraphs to follow.

6.2.1 Selecting the Sound Level

The incident sound wave is modelled as a plane wave travelling in the positive y-direction. The pressure of the sound wave is 1 Pa (≈ 94 dB).

$$L_p = 20log_{10}\left(\frac{p}{p_0}\right) dB \tag{20}$$

where L_p is the sound pressure level in dB, p is the pressure of the sound in Pascal and p_0 is the reference pressure equal to 20 μPa.

A sound level of 94 dB is very loud, but realistic compared to the voice intensity of an opera singer at a distance of 30 cm from the microphone [62]. Although the dynamic range of a singer's voice at this level is only between 300 Hz and 1.2 kHz, the same pressure will be used for modelling all frequencies up to 20 kHz. At lower intensities the dynamic range of a singer's voice is much wider.

Human perception of frequency is dominated by hearing. To put audible frequencies into perspective: The frequency of middle-C on a piano is tuned to 261.63 Hz and the frequency of the C-key two octaves higher is 1 046.52 Hz. The fundamental frequency of the notes on a standard 88-key piano ranges from 27.5 Hz on the low end to 4 186 Hz on the high end [63].

6.2.2 Narrow Faces

This experiment illustrates the importance of handling extreme ratios in simulations.

Generating a mesh for the model becomes troublesome when extreme differences in dimensions exist within the model. A particle of only 2 um thick in a sphere with a 40 mm radius presents such a dilemma with its one-to-twenty-thousand ratio between small and large dimensions. A method is provided to deal with these extremities by deleting narrow faces from the model. To test the effect of deleting the narrow faces, a model that is on the edge of the large ratio dilemma is chosen and simulated with narrow faces and without narrow faces. The model chosen consists of a 10 um thick disk, with a radius of 2.5 mm, hit by a plane wave with a sound pressure level of 1 Pa (94dB). The simulation is performed over a frequency range of 500 Hz to 1 kHz. Figure 15 and Figure 16 provide a comparison between the two simulations. The coloured lines in the figures represent a cut along the z-axis through the centre of the free floating disk in Figure 14, showing the displacement of the disk at different frequencies.

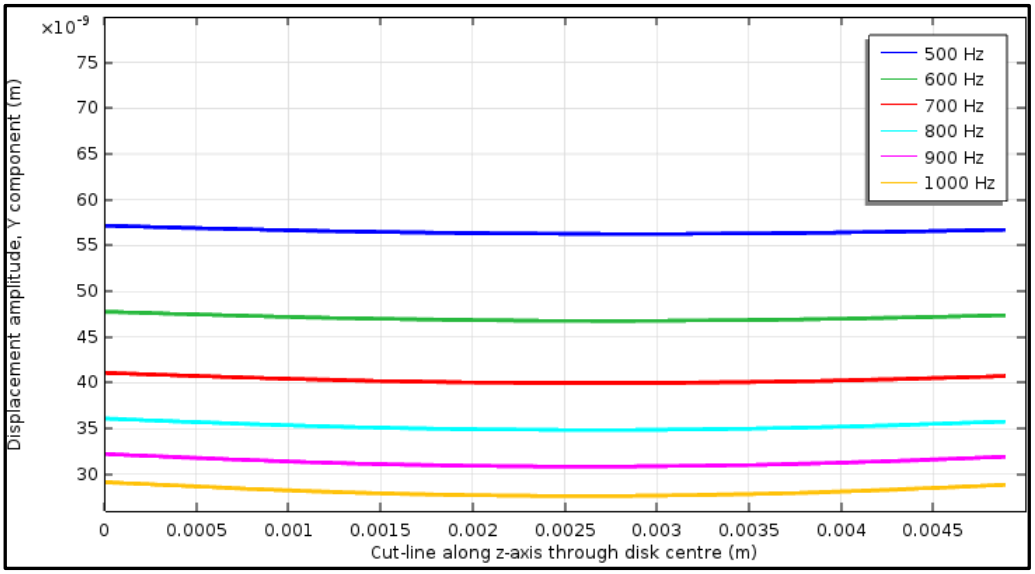

Figure 15: Free floating disk with narrow faces, 500 Hz to 1 kHz

From the displacement plots in the two figures it is clear that there is a considerable difference between the simulation results of the two models (30% at 700 Hz). The model without narrow faces gives a mean displacement value of 52×10^{-9} m at 700 Hz and the model that includes the narrow faces is only displaced by 40×10^{-9} m. The equation in (5) yields a displacement value of 794×10^{-9} m at 700 Hz for a weightless particle in a 94 dB sound wave (i.e. sound *intensity* of 2.512×10^{-3} W/m^2). The results from both simulations are so far below the theoretical maximum displacement that the theoretical value cannot be used to deduce which of the two simulation models is the better. The large difference between the theoretical and the simulated values can be ascribed to the inertia of the disk. The influence of the disk's weight is further analysed in 6.2.4.

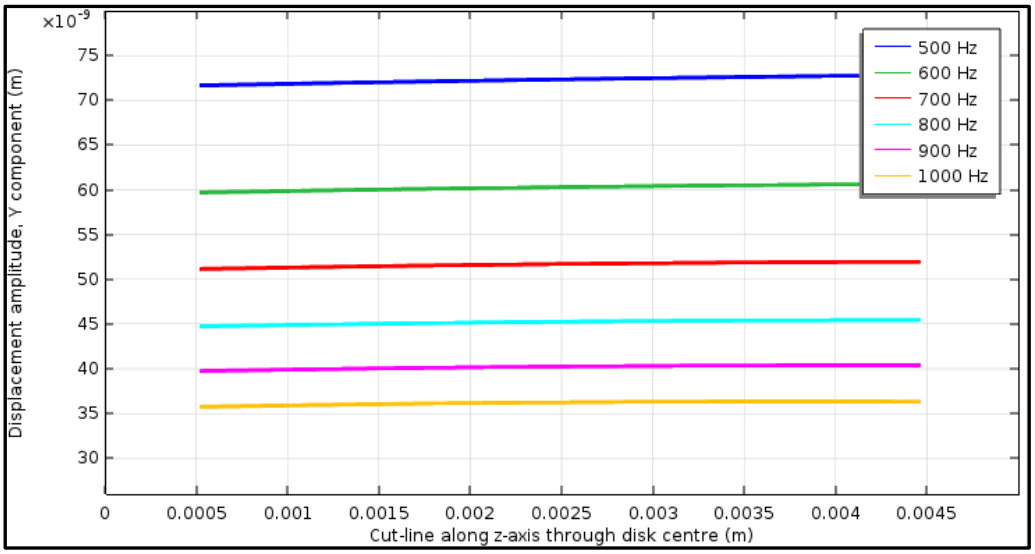

Figure 16: Free floating disk without narrow faces, 500 Hz to 1 kHz

In the 500 Hz to 1 kHz range there is no resonance of the disk – at least not on any of the 100 Hz steps. When the simulations are repeated in the 3 kHz to 4 kHz range, the difference between the model with narrow faces and the one without narrow faces becomes more noticeable. In the model with narrow faces (Figure 17) there is resonance at 3.5 kHz. The cut-line graphs clearly show how specific parts of the disk barely move while other parts of the disk display a large displacement. When the narrow faces are removed there is no resonance (Figure 18). Resonance is an important factor that cannot be ignored in experiments with microphones. A further drawback of deleting the narrow faces is that the relative tolerance of the simulation has to be relaxed a hundredfold (from 0.01 to 1.0) for the solution to converge. Clearly the narrow faces are an integral part of the model for a ribbon simulation. From here on forward all narrow faces will remain part of the models. Figure 19 provides a visual image of the simulated disk to illustrate how the disk is bending in its resonant state.

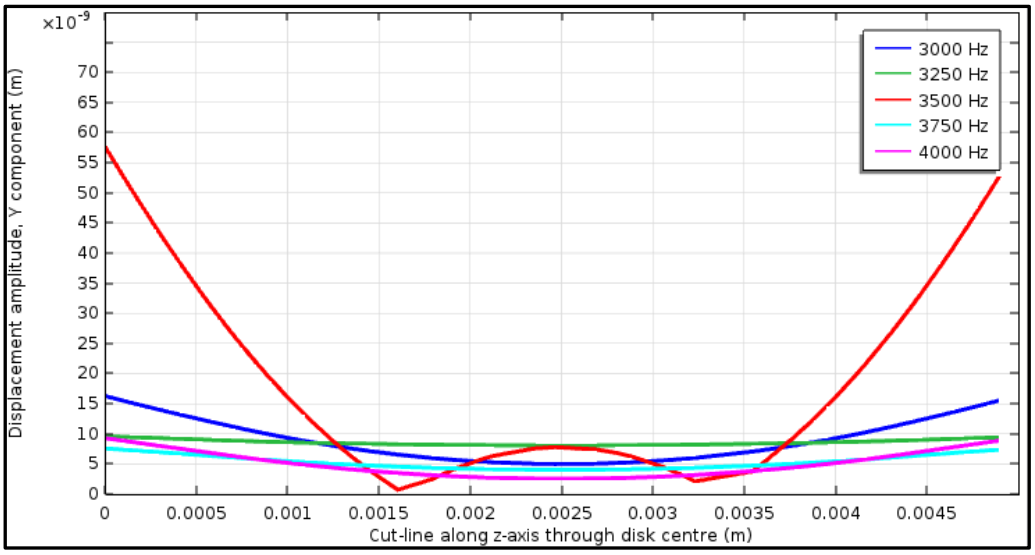

Figure 17: Free floating disk with narrow faces, 3 kHz to 4 kHz

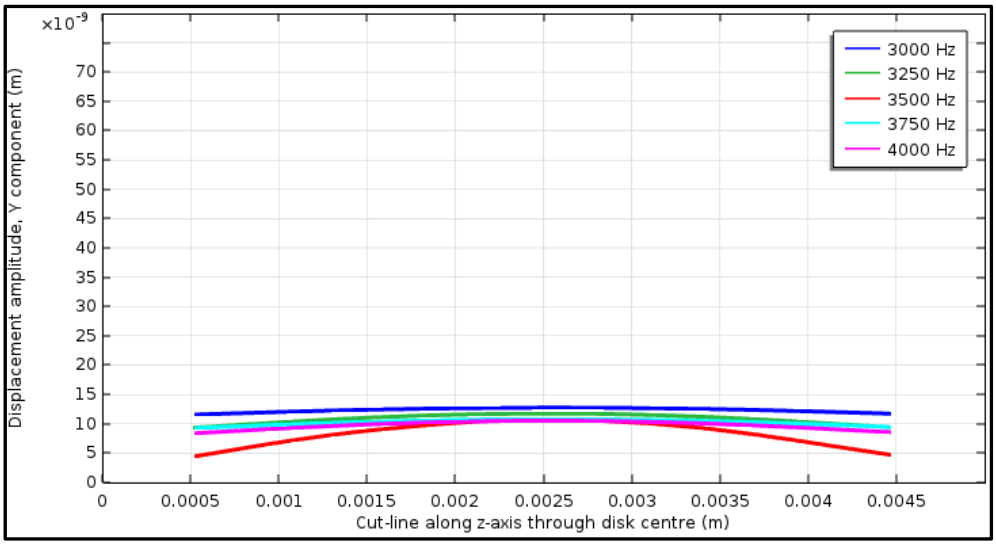

Figure 18: Free floating disk without narrow faces, 3 kHz to 4 kHz

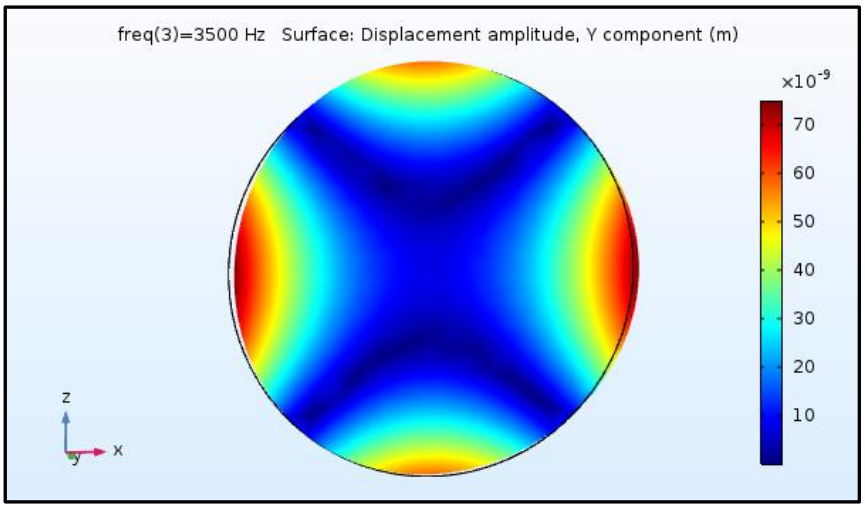

Figure 19: Disk resonance illustrated at 3.5 kHz (simulated with narrow faces)

6.2.3 Mesh Density

This experiment illustrates the importance of choosing the best mesh in simulations.

For this experiment the model of Figure 17 is used and the mesh density is halved in the y-direction. See Figure 20 for a visual comparison of the two meshes and Figure 21 for the displacement results of the simulation. It is noticeable that the resonant frequency becomes less dominant. The mesh resolution and the element quality are important considerations. When the mesh resolution is low in comparison to variations in the geometry or the solution, it will lead to inaccurate results. A low mesh element quality may lead to inverted mesh elements with misleading results. It may also prevent the solution from converging. Thus, the mesh must be as fine as reasonably possible, subject to the processing capabilities of the computer that is used to run the simulation and also time permitting since the simulation with a finer mesh takes much longer to compute. See Figure 23 in the next experiment for an additional example of the influence that different mesh settings have on the simulation results.

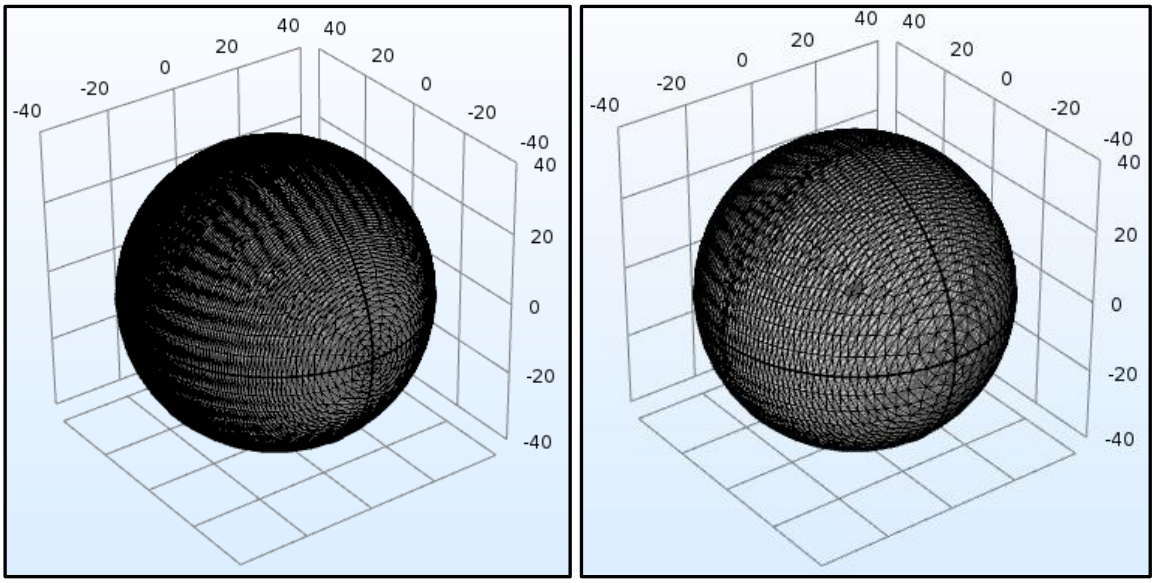

Figure 20: Mesh illustration (grid dimensions in mm)

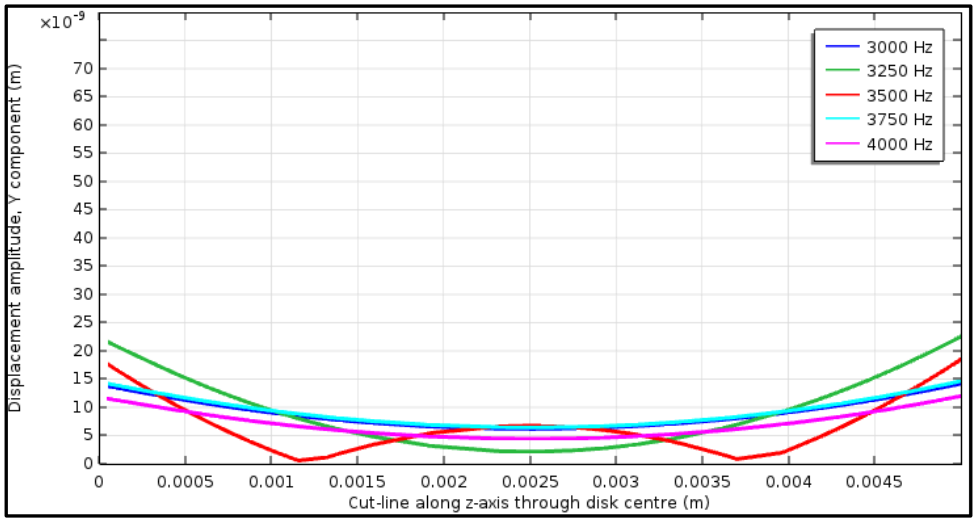

Figure 21: Free floating disk, simulated with poor mesh

6.2.4 Modelling Domain Size

This experiment illustrates the importance of choosing an appropriate size for the modelling domain – in this case the sphere that encloses the disk.

To illustrate the influence of the modelling sphere on the simulation results the radius of the sphere that surrounds the modelling domain is decreased from 40 mm to 20 mm. The result is a minor increase in the number of mesh elements, but these elements fit into one eighth of the original volume. The mesh of the sphere becomes in effect much denser.

- Mesh with sphere radius of 40 mm: Complete mesh consists of 179 816 domain elements, 10 168 boundary elements, and 652 edge elements, 253 567 degrees of freedom to solve.
- Mesh with sphere radius of 20 mm: Complete mesh consists of 181 221 domain elements, 10 542 boundary elements, and 668 edge elements, 258 370 degrees of freedom to solve.

The results in Figure 22 show that the displacement amplitude of the disk increases when the modelling domain is made smaller without changing the other parameters. Resonance of the disk becomes more noticeable and the resonance frequency also changes. These changes are caused by the mesh that becomes denser when the size of the modelling sphere shrinks. This response is supported by the results of Figure 21 where the density of the mesh was manipulated deliberately.

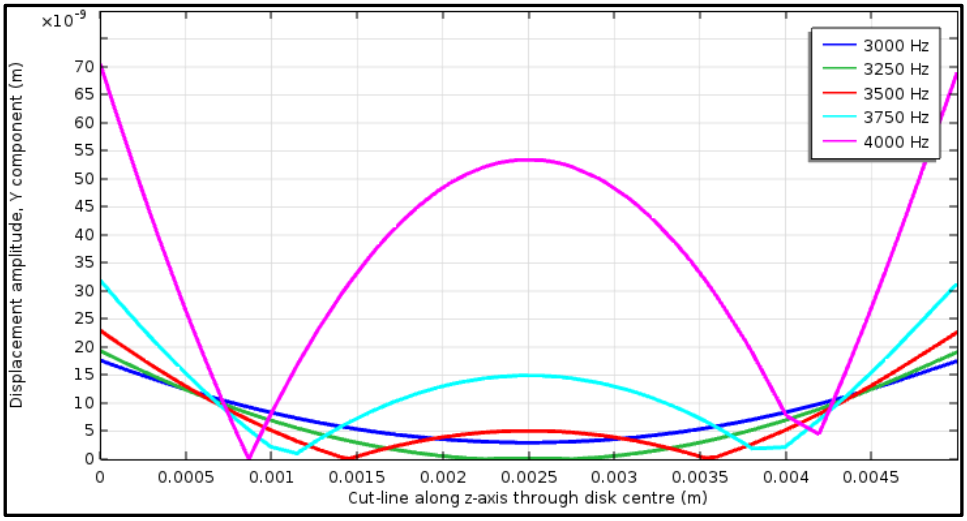

Figure 22: Free floating disk, modelling sphere radius halved

The improvement of the denser mesh is realised when viewing the surface displacement in the three-dimensional simulation (Figure 23). With the denser mesh it can be seen how the whole disk flexes. In the less dense mesh only two of the outer edges of the disk are bending. This illustration clearly shows the importance of knowing what to expect from the simulation before making any conclusions from the results. A denser mesh produces more accurate results, but at the cost of computation time. By reducing the volume of the modelling sphere, the problem of high computation time can be addressed because the effective mesh density is increased with only a slight change in the number of mesh elements. The difference in computation time between the two simulations in Figure 23 is only 3%.

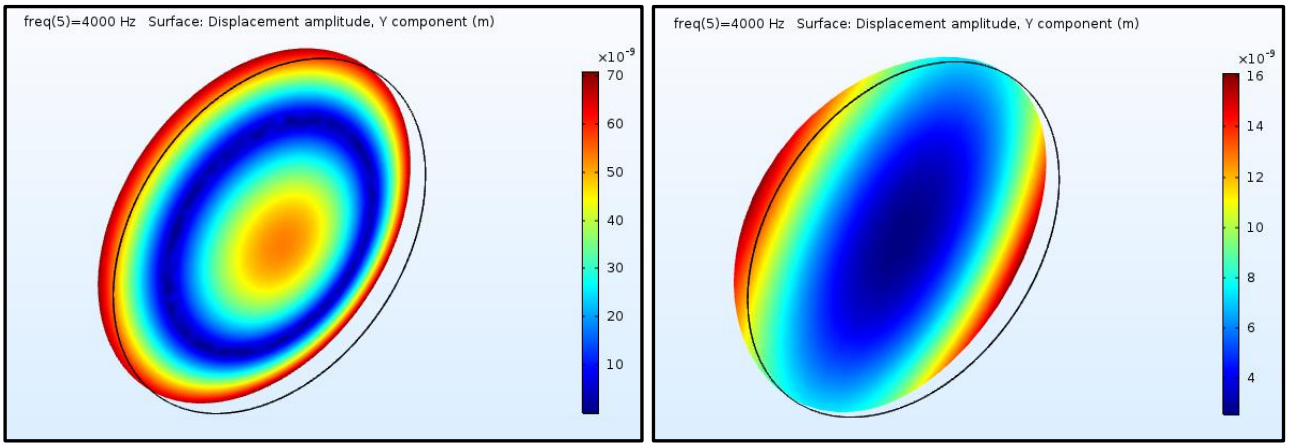

Figure 23: Simulation with denser mesh inside 20 mm boundary (left) and less dense mesh inside 40 mm boundary (right)

With the mesh and the model volume both having an influence on the results, no results can be interpreted as exact figures. Results should rather be interpreted as the reaction of the model relative to another simulation with the same settings, except for a single change, to test the influence of that change.

This experiment concludes the illustration of effects that the user controlled environment of the modelling and simulation software has on the results.

In contrast to the disk that is used in the simulation, the imaginary particle in (5) has no weight. The equation does not make provision for weight or size, or any other mechanical properties of the particle. The next four experiments will demonstrate by means of simulation how the weight, thickness, elasticity and size of the disk influence its displacement in a sound wave. The radius of the modelling domain for these tests remains the same as for Figure 22.

6.2.5 Disk Weight

This experiment illustrates the influence of inertia on the resonance and displacement of the disk.

The weight of the disk is doubled by changing the density of the material in the material properties of the disk model. All other parameters remain as before.

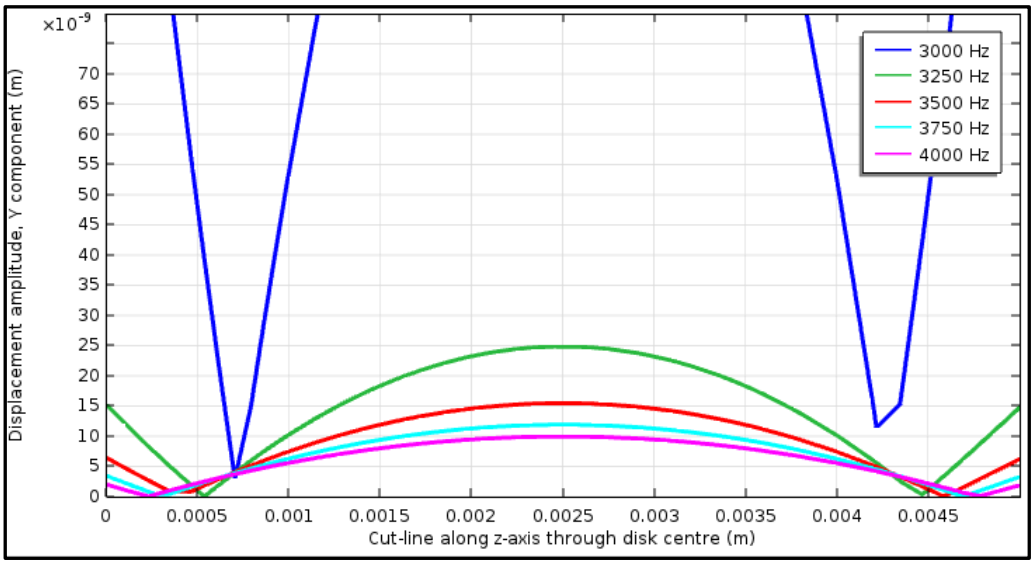

Figure 24: Free floating disk with twice the weight

The average displacement differences between Figure 24 and Figure 22 are much larger at the resonance frequencies than at the other frequencies. The resonance frequency shifted with 25% from 4 kHz to 3 kHz. Because the displacement changes are overshadowed by the change in resonance frequency, an extreme change is made next to confirm the influence of the weight on the displacement. Figure 25 shows the result when the material density is increased by a factor of 10. This change shows clearly that the displacement of the disk is inversely affected by its weight. The inertia of the disk is thus a limiting factor in its displacement.

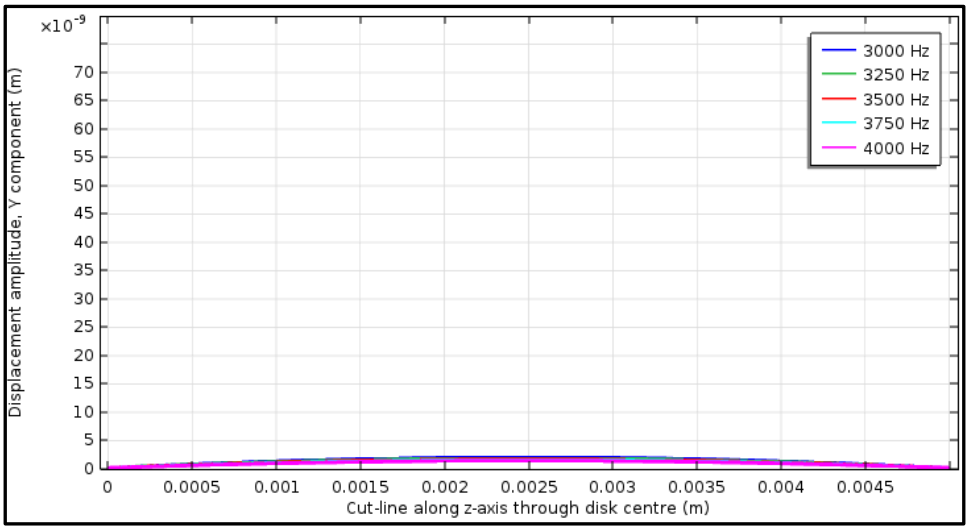

Figure 25: Free floating disk, 10 times the weight

6.2.6 Disk Thickness

This experiment illustrates the influence of geometry on the resonance and displacement of the disk.

Figure 26 shows the simulation results for a disk that is double as thick as the original disk. A comparison with Figure 22 indicates that the displacement is now less than half of what it was. The reason is two-fold: the thicker disk is heavier and it is also more rigid. Although the thicker disk is the same weight than the disk that was used in Figure 24, the displacement is not the same. The thicker disk displays no resonance in this frequency band because it is more rigid than the original disk. It illustrates that the displacement of an object is much lower when it does not resonate.

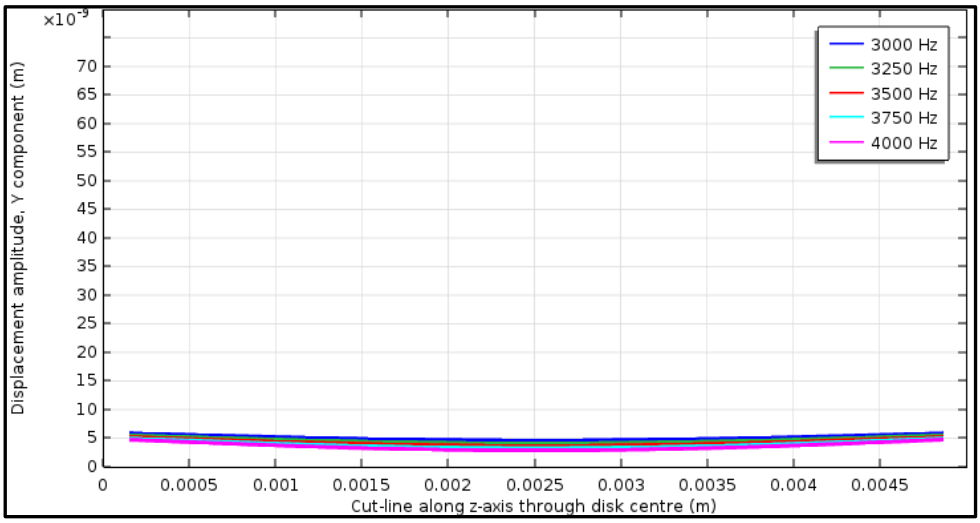

Figure 26: Free floating disk twice as thick, original density

To isolate the disk thickness as the only change in the model, the weight of the disk is reduced to its original weight by halving the material density. The result of a thicker disk with the same weight than the original disk is shown in Figure 27. This result confirms that the thicker disk does not

resonate in the frequency band between 3 kHz and 4 kHz. The displacement of the disk in Figure 27 is double the displacement of the disk in Figure 26. This supports the conclusion of the previous experiment about the inertia of the disk.

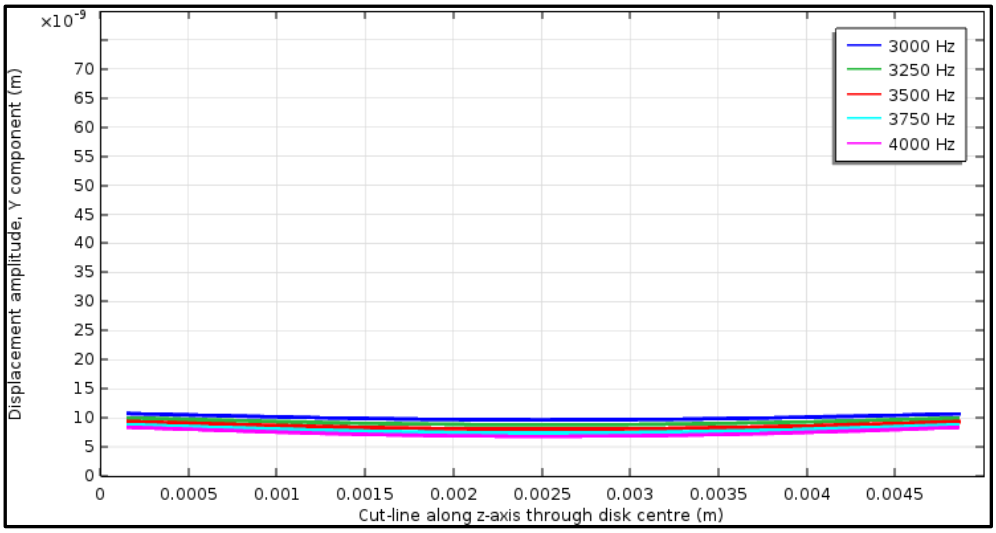

Figure 27: Free floating disk twice as thick, original weight

6.2.7 Disk Elasticity

This experiment illustrates the influence of elasticity on the resonance frequency and the displacement of the disk. The disk is not perfectly rigid and can therefore be used to illustrate how an object deforms when subjected to stimuli at its natural resonance modes.

The elasticity of the disk can be manipulated by changing the Young's modulus of the material that the disk is made of. When the Young's modulus of the disk is doubled, the disk becomes more rigid and the model behaves as in Figure 28.

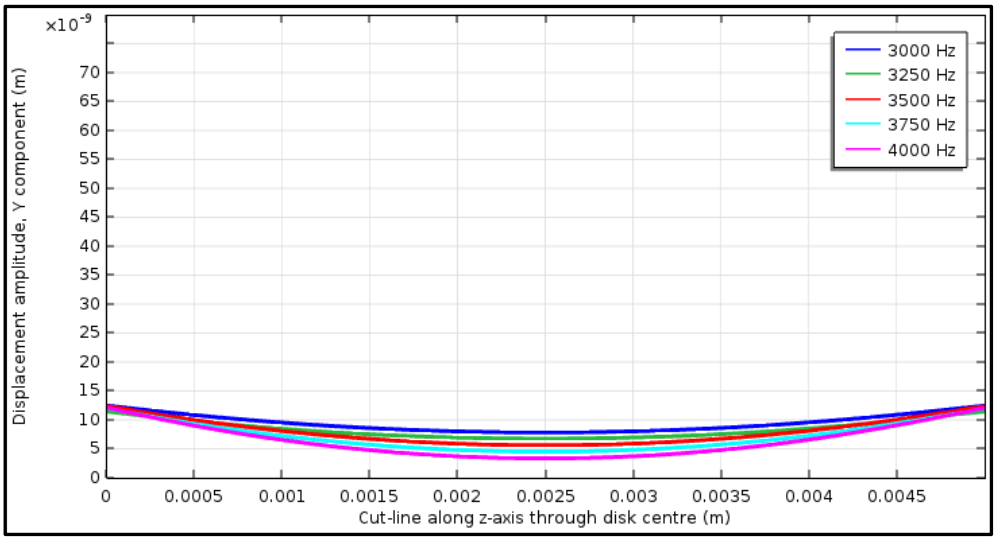

Figure 28: Free floating disk, less elastic

Comparing to Figure 27 the mean magnitude of the displacement is the same, but the disk is bending slightly more. The disk is not as rigid as a disk that is twice the thickness, but it is rigid

enough to shift the resonance frequency out of this band. Making the disk more elastic, has the opposite effect, as illustrated in Figure 29. The material properties that influence a material's resistance to deformation are listed here for reference [57]:

- Young's modulus: A measure of a material's resistance to change in its length.
- Shear modulus: A measure of a material's resistance to movement of parallel planes within the material.
- Bulk modulus: A measure of a material's resistance to change in its volume when a force of uniform magnitude is applied perpendicular over the total surface of the object.

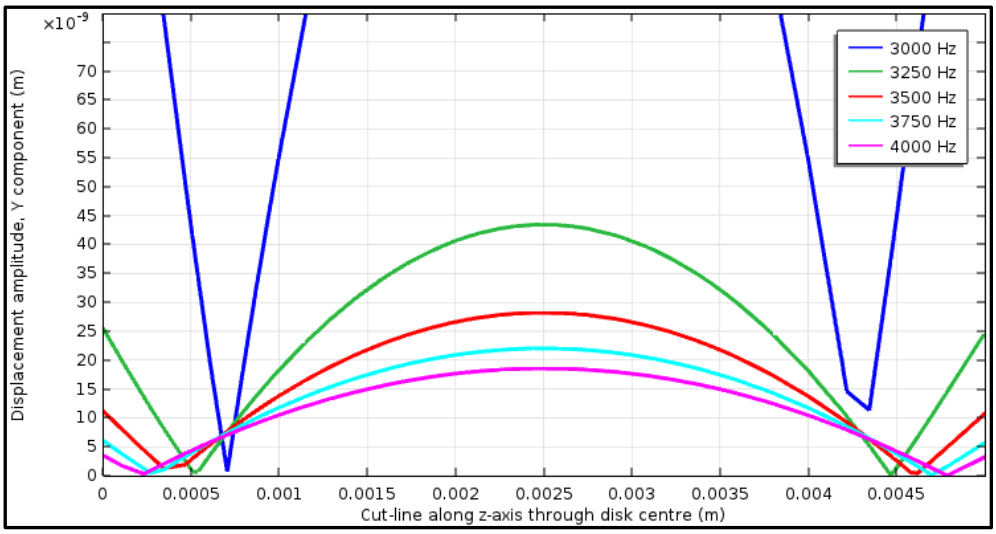

Figure 29: Free floating disk, more elastic

6.2.8 Disk Radius

This experiment illustrates the influence that the total area of the disk has on its resonance frequency and the displacement of the disk.

For Figure 30 the disk's radius is increased to double the original radius. The result with the larger radius is higher displacement amplitude – double the mean amplitude compared to Figure 22. The reason for this behaviour is that the wave front now has an impact on a surface area that is four times larger. The larger surface area of the disk has a greater positive impact on its response than the negative effect of the increased inertia.

To isolate the disk radius as the only change in the model, the weight of the disk is reduced to its original weight. Figure 31 clearly illustrates how the displacement of the disk increases with the increased area. The overall rigidity of the disk is lower because of the increased area. Therefore the disk is bending much more in the sound wave.

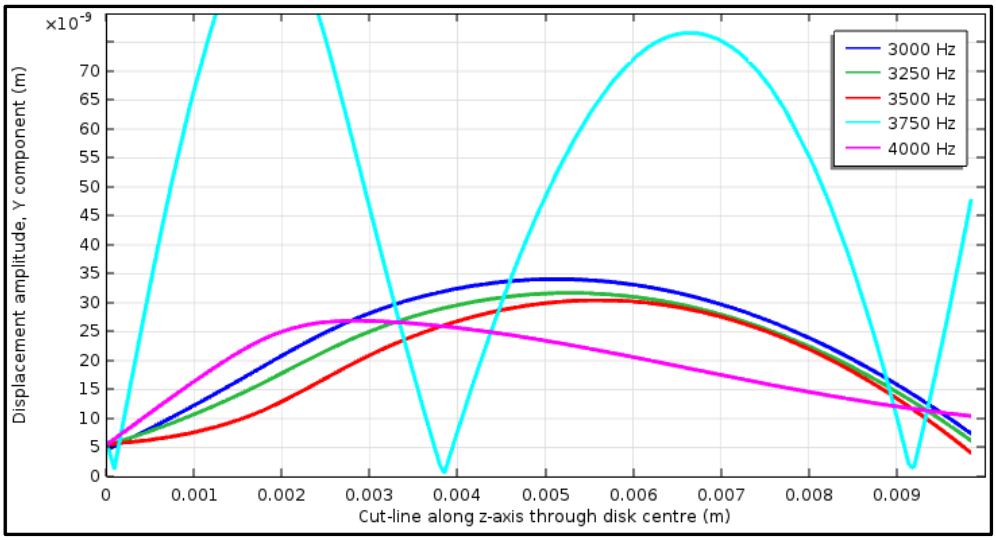

Figure 30: Free floating disk of double the radius, original density

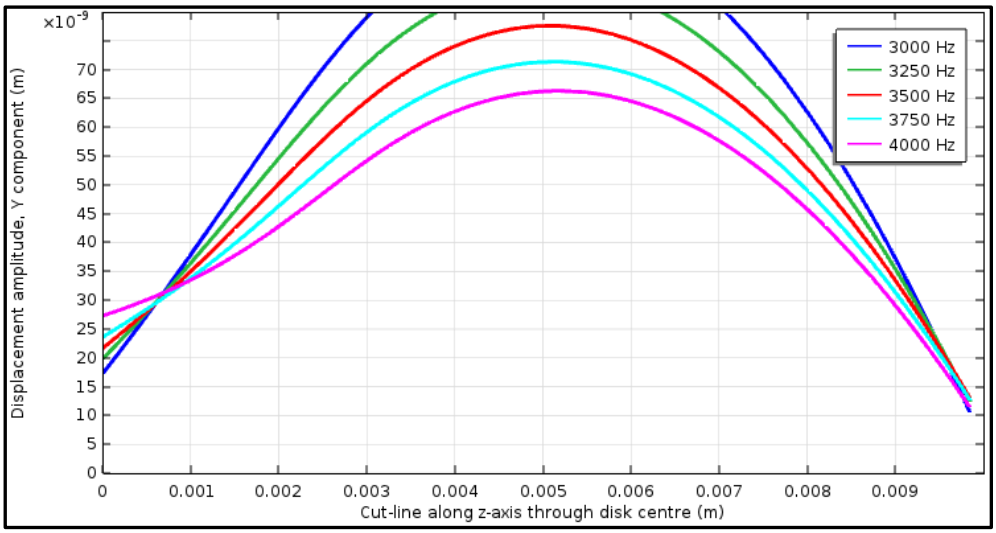

Figure 31: Free floating disk of double the radius, original weight

6.2.9 Final Model for the Free Floating Disk

For the final disc illustration a model is created with a disk that is the thickness of the ideal ribbon. The radius is kept at 2.5 mm because a diameter of 5 mm corresponds to the width of most commercial ribbons. The ideal thickness of a microphone ribbon is 2 µm according to literature. This is only 20% of the thickness of the disk in the preceding simulations. So there has to be a change in the model to get the mesh right and to get the simulation to converge to a solution. Reducing the radius of the modelling sphere to 10 mm provides a mesh that accommodates the 2 µm thin disk. The simulation result is presented in Figure 32.

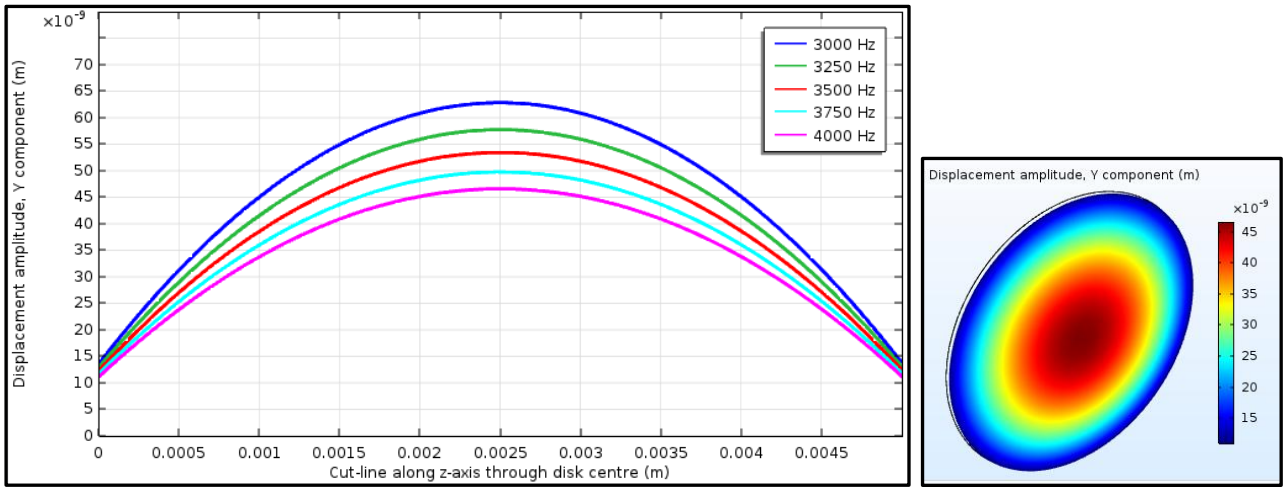

Figure 32: Free floating disk, 2 µm aluminium, modelling sphere radius 10 mm

The final assembly of the microphone will however not fit in a sphere this small, so another solution needs to be found to accommodate a 2 µm ribbon. The mesh densities of the disk and the modelling sphere can be manipulated individually. The disk is positioned with its thickness in the direction of the y-axis. Consequently, the mesh density is increased in the y-direction only. By increasing the y-direction mesh scale of the disk from 10 to 50 and the mesh scale of the sphere from 10 to 20 a combination is found that produces a mesh without errors for the 40 mm sphere. The result of the 40 mm sphere with 2 µm disk that is simulated with this mesh combination is presented in Figure 33. The consequence of the compromise that is made with the mesh can be seen in the surface plot along the cut-line of the disk. It is clear in the 3D representation of Figure 32 that the displacement of the disk is perfectly concentric as would be expected, but the 3D displacement in Figure 33 is not perfect. Because of the denser mesh in such a large volume the simulation has to be solved for more degrees of freedom. In this example it takes 50% longer to compute the results for the model in Figure 33 than to solve the model for Figure 32.

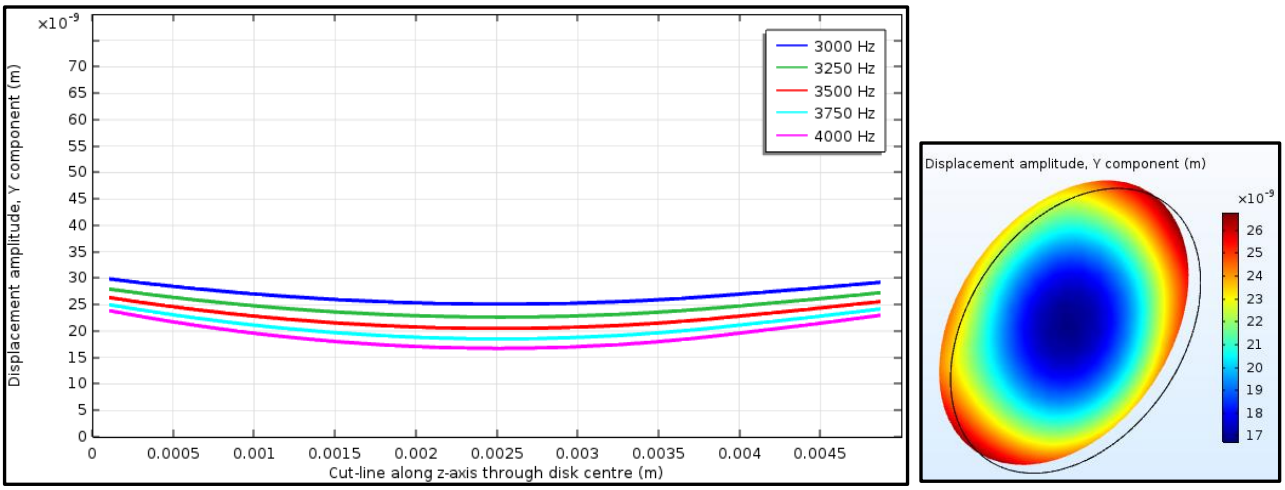

Figure 33: Free floating disk, 2 µm thin, modelling sphere radius 40 mm

6.2.10 Impact of the Microphone Baffle on a Sound Wave

The microphone magnets are modelled by two rectangular bars inside a sphere. The purpose of the sphere is to limit the size of the model to the area of interest. The simulation software makes use of artificial boundaries to mimic an open field within the limited size model. In this case a *Spherical Wave Radiation* node is used to add a radiation boundary condition which allows outgoing spherical waves to leave the model with minimal reflections. Therefore the microphone baffle (mechanical structure and magnets) is modelled as if it exists in an open field with almost no reflection from any surroundings. The magnets are completely solid compared to the density of air. Therefore the baffle parts are modelled as *Interior Sound Hard Boundary (Wall)* entities. No deformation of the baffle is taken into account.

Olson stated that the upper frequency of the ribbon microphone is limited by the path length around the baffle of the microphone [28]. In the simulation model, the neodymium magnets themselves are forming the baffle. To visualise the influence of the baffle on an incoming sound wave, the microphone with ribbon is modelled and a simulation is done to illustrate the sound pressure on the x-y plane through the centre of the microphone. A frequency of 20 kHz is chosen for the simulation because it is the upper frequency of human hearing and the wavelength (17.15 mm) fits well inside the modelling sphere for visualisation purposes. In Figure 34 it is clearly shown how the sound wave bends around the magnets and that the path length around the magnets are longer than the wavelength of the 20 kHz sound wave. The displacement of the ribbon is also visible and will be covered in more detail in paragraph 7. Figure 35 provides more views for the same model. In this model the sound wave is travelling in the positive x-direction.

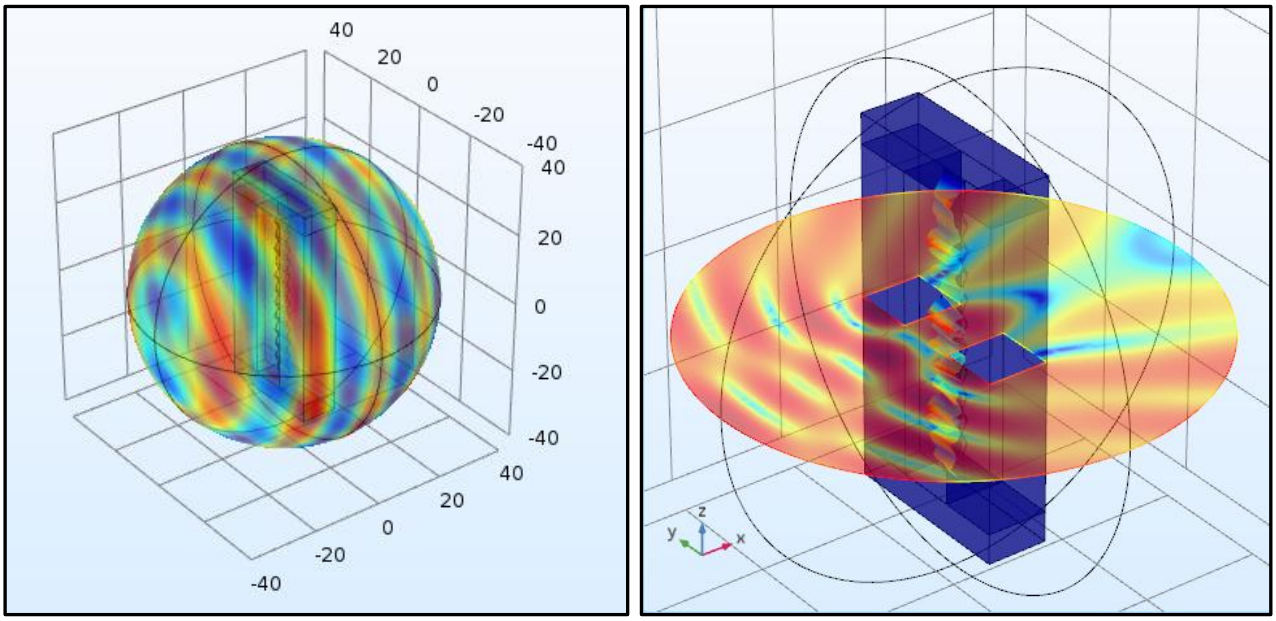

Figure 34: Ribbon microphone in a 20 kHz sound wave **[1]** © 2016 IEEE

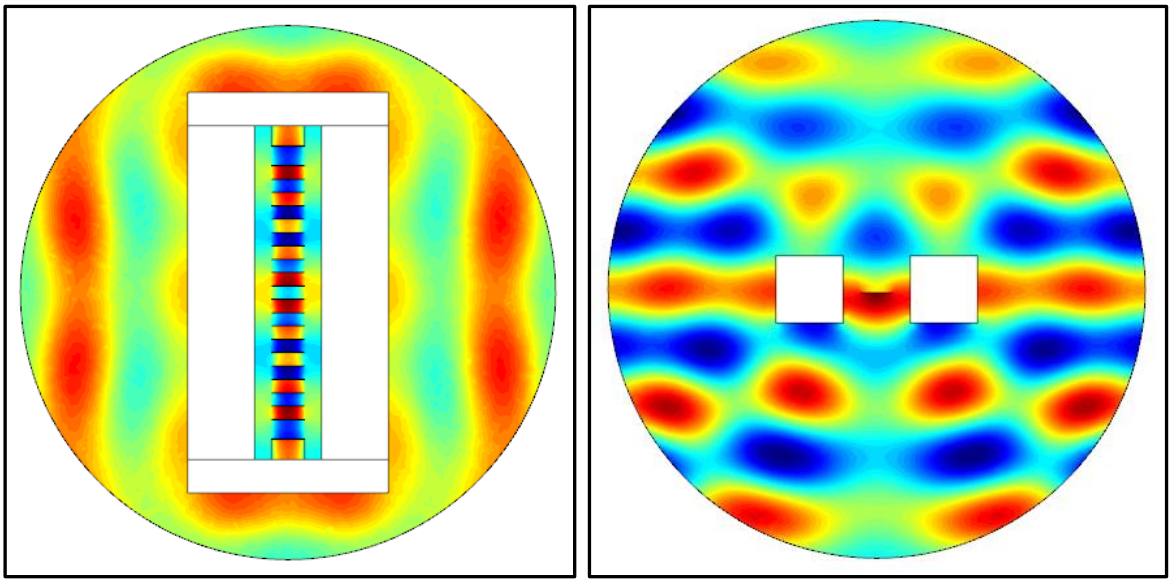

Figure 35: Total acoustic pressure field on the y-z plane (left) and the x-y plane (right)

An experiment is done to illustrate the influence of the baffle on a sound wave and therefore its influence on the movement of the ribbon.

To examine the difference that the size of the baffle makes to the sound wave, the diameter of the magnets in the model are changed from 10x10 mm to 5x5 mm. The simulation in Figure 36(left) is the top-view of the same slice that is made through the centre of the microphone with the 10x10 mm magnets as illustrated in Figure 34 (right). Figure 36 (right) illustrates the results with the 5x5 mm magnets. In the side by side comparisons of Figure 36 it is clearly visible that the smaller baffle has less of an effect on the sound wave than the large baffle. Therefore, as explained by Olson, the ribbon will respond well to the sound wave when a baffle is used of which the circumference is smaller than the wavelength of the sound wave.

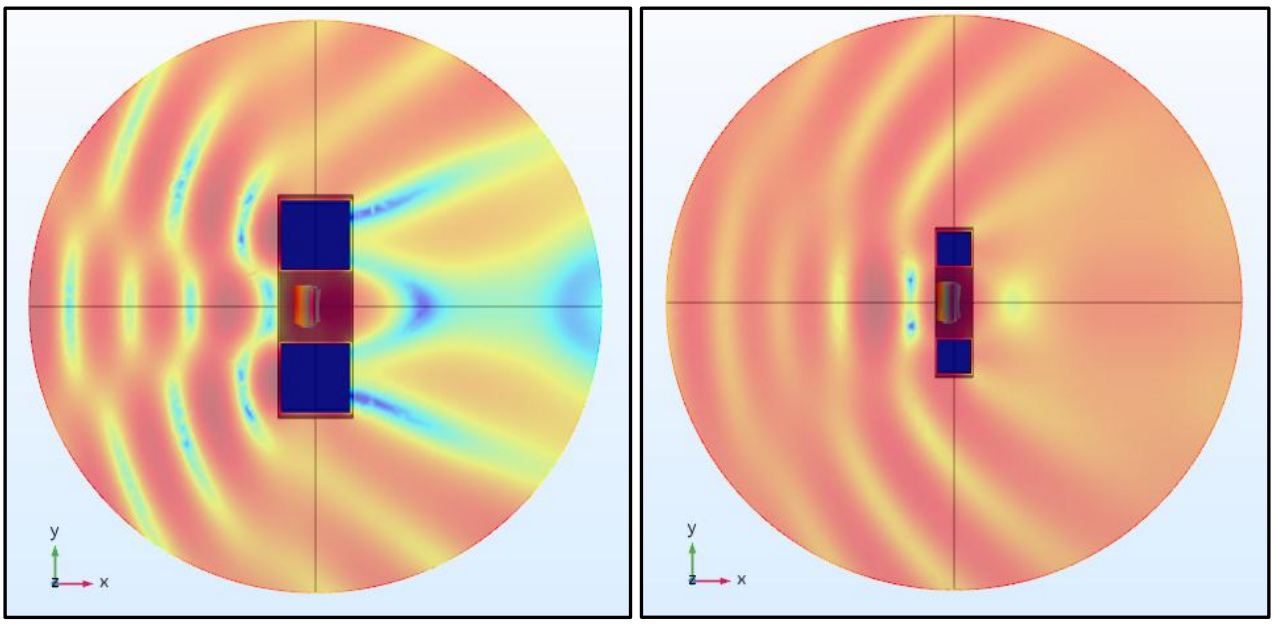

Figure 36: Sound pressure level with 10x10 mm magnets (left) and 5x5 mm magnets (right)

6.2.11 Impact of the Microphone Baffle on the Pressure Gradient

The ribbon microphone is a sound velocity microphone, also commonly known as pressure gradient microphone. Figure 37 illustrates the pressure gradient across the ribbon of a microphone on the x-z plane through the centre of the ribbon. It can be seen that the pressure gradient across the ribbon of the microphone with 10x10 mm magnets is different from the pressure gradient across the ribbon of the microphone with 5x5 mm magnets. This confirms once more that the size of the baffle plays an important role at the upper frequencies where the wavelength of the sound becomes comparable with the path length around the baffle.

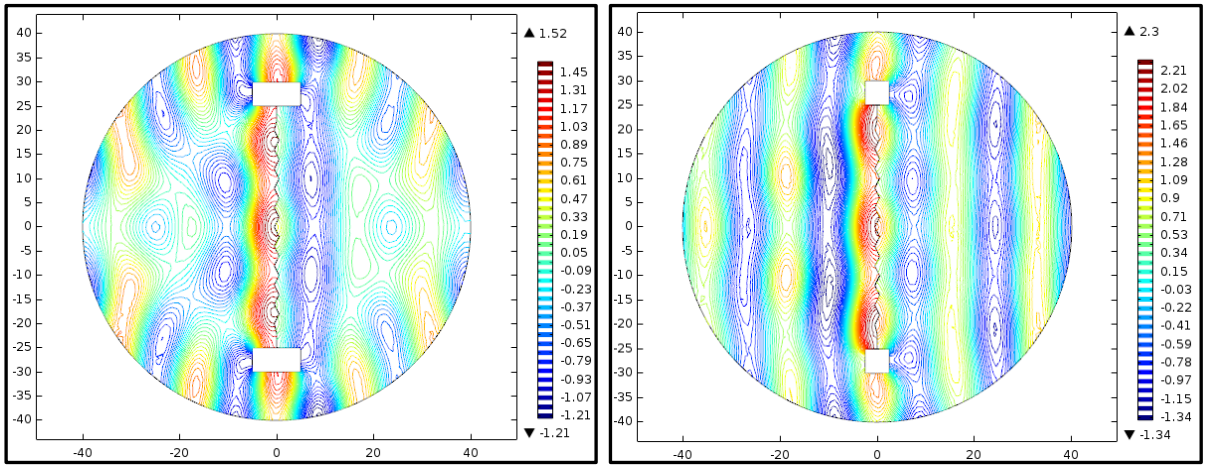

Figure 37: Pressure gradient across the ribbon: 10x10 mm magnets (left) and 5x5 mm magnets (right)

6.3 Testing

No tests were conducted to illustrate the effects that are discussed in the modelling and simulation paragraphs of the acoustics section, but the following test is advised for students that wish to put the simulations into practice: Perform a test with the exact same setup (same sound equipment, same acoustic environment, same microphone), but with two different thickness ribbons - 10um and 20um. The test results will verify that the thicker (heavier) ribbon will have a lower amplitude output signal and that resonance of the thicker ribbon is at a lower frequency.

6.4 Conclusion

Through modelling and simulation of the ribbon microphone and its acoustic environment, it can be illustrated how physics concepts that are not included in the simple mathematical form will influence its behaviour. Modelling and simulation can give students much more insight about physics problems and its solutions than what can be accomplished by numerical methods alone. Through simulation, the experiments in this section illustrate physics concepts like inertia, mechanical structure, elasticity, pressure and waves. It also illustrates how statements in literature can be verified through simulation; for instance that the path length around the microphone baffle plays an important role in the frequency response of the microphone, as stated by Olson in his patent for the first ribbon microphone.

7 MECHANICS

The second physics area for which the ribbon microphone can be used as demonstration tool, is that of mechanics. The mechanical response of a ribbon that is subjected to the effects of a sound wave effectively illustrates the concept of resonance and deformation of mechanical structures. The model may even be scaled to simulate the destructive results of resonance on large mechanical structures like bridges.

This chapter presents 2 experiments which can be performed using a basic ribbon microphone.

- A set of simulation experiments modelling different ribbon designs. The focus is on the movement and deformation of the ribbon itself, with the object constituting the whole ribbon in isolation from the microphone structure. The aim here is to illustrate how mechanical design affects the dynamic movement and deformation of a thin foil in a wave and the design impact on natural resonance.
- A microphone experiment showing the effect of two ribbon designs. This real-world experiment is presented here to demonstrate the credibility of simulations, but at the same time to show the variances that can be expected when simulation models are incomplete.

7.1 Theory

Deformation of a ribbon in a sound wave will be illustrated by experiments in this chapter.

A random particle that is initially located at coordinate $\boldsymbol{X}$ will follow a path during deformation that can be described by

$$\mathbf{x} = \mathbf{X} + \mathbf{u}(\mathbf{X}, \mathrm{t}) \tag{21}$$

where $\boldsymbol{x}$ is the spatial coordinate, $\boldsymbol{X}$ is the material coordinate, and $\boldsymbol{u}$ is the displacement.

The gradient of the displacement in a 3D system is

$$\nabla \boldsymbol{u} = \begin{bmatrix} \frac{\partial u}{\partial X} & \frac{\partial u}{\partial Y} & \frac{\partial u}{\partial Z} \\ \frac{\partial u}{\partial X} & \frac{\partial u}{\partial Y} & \frac{\partial u}{\partial Z} \\ \frac{\partial u}{\partial X} & \frac{\partial u}{\partial Y} & \frac{\partial u}{\partial Z} \end{bmatrix} \tag{22}$$

An infinitesimal line, $d\boldsymbol{X}$ can be mapped against its corresponding deformed line to give the deformation gradient tensor $\boldsymbol{F}$

$$d\boldsymbol{x} = \frac{\partial \boldsymbol{x}}{\partial \boldsymbol{X}} d\boldsymbol{X} = F d\boldsymbol{X} \tag{23}$$

$\boldsymbol{F}$ can be written in terms of the displacement gradient $\nabla \boldsymbol{u}$ as

$$\boldsymbol{F} = \frac{\partial \boldsymbol{x}}{\partial \boldsymbol{X}} = \boldsymbol{I} + \nabla \boldsymbol{u} \tag{24}$$

where $\boldsymbol{I}$ is the identity tensor.

Deformation of the material will cause a change in the material's density. The ratio between the initial density and the density after deformation is expressed as

$$\frac{\partial V}{\partial V_0} = \frac{\rho_0}{\rho} = \det(F) = J \tag{25}$$

where ρ_0 is the initial density and ρ is the density after deformation.

$J < 1$ indicates compression, while $J > 1$ indicates expansion.

The right stretch tensor $\boldsymbol{U}$ is defined as

$$\boldsymbol{U} = \begin{bmatrix} \lambda_1 & 0 & 0 \\ 0 & \lambda_2 & 0 \\ 0 & 0 & \lambda_3 \end{bmatrix} \tag{26}$$

$$\lambda = \frac{L}{L_0} = 1 + \varepsilon_{eng} \tag{27}$$

where ε_{eng} is the engineering strain, L_0 the initial length and L the length after stretching.

Further detail for the student who requires a deeper understanding of the computations for deformation analysis, damping, stresses, and so forth, is available in the Structural Mechanics Theory section of [64].

7.1.1 Numerical Model of a Ribbon

Meiring developed a 1st order numerical model for the ribbon of the ribbon microphone. A summary of his work is presented here as part of the mechanics theory [65].

The time response of a corrugated ribbon can be determined by breaking the ribbon down into smaller elements of which each element represents the straight sections between corrugations of the ribbon (Figure 38).

Meiring modelled the movement of the ribbon by means of a spring-mass-damper system as illustrated in Figure 39, where each $\boldsymbol{k} - \boldsymbol{c} - \boldsymbol{m}$ group represents one of the elements in Figure 38. Only movement in the x-axis was considered since the movement in the y-axis is negligibly small in comparison and would overcomplicate the model. The model further ignores any influence that the elements may have on each other and it ignores the influence of the ribbon on the sound wave.

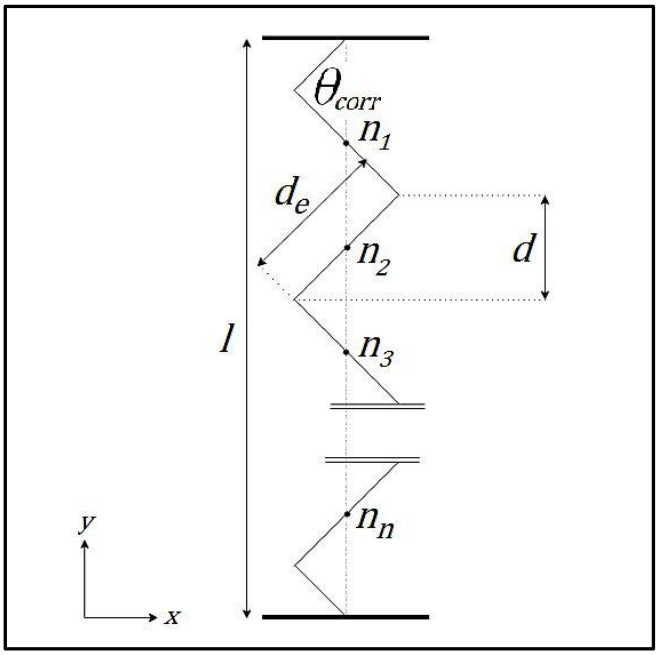

Figure 38: Ribbon geometry for numeric model **[65]**

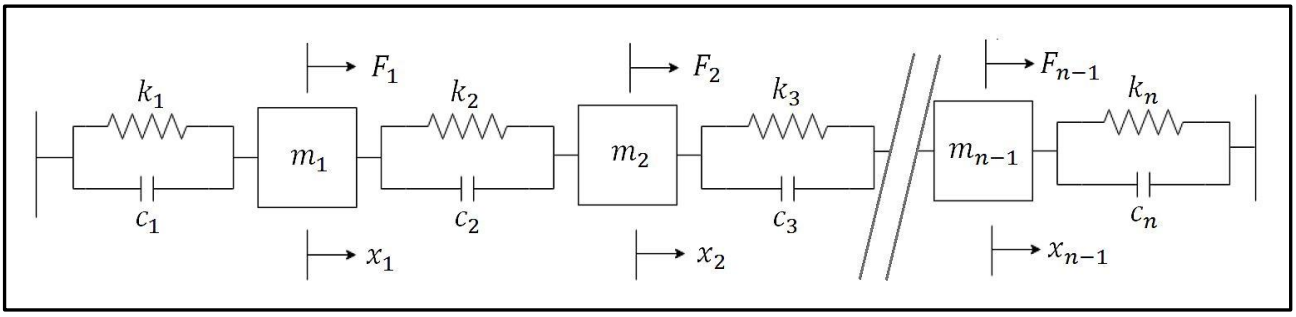

Figure 39: Spring-mass-damper model of a ribbon **[65]**

The basic form of a linear damped system is

$$M\ddot{\boldsymbol{x}} + C\dot{\boldsymbol{x}} + K\boldsymbol{x} = B\boldsymbol{F}(t) \tag{28}$$

where M is the mass matrix, C the damping matrix, K the stiffness matrix and $\boldsymbol{x}$ the vector of displacement. B is the matrix that contains the amplitude of the input force and $\boldsymbol{F}$ the vector that contains the trigonometric part of the input force as a function of time t in seconds.

If $\boldsymbol{y}_1(t) = \boldsymbol{x}(t)$ and $\boldsymbol{y}_2(t) = \dot{\boldsymbol{x}}(t)$ then (28) can be rewritten in terms of its displacement vector ($\boldsymbol{y}_1$) and velocity vector ($\boldsymbol{y}_2$) as

$$\dot{\boldsymbol{y}}_1(t) = \boldsymbol{y}_2 \tag{29}$$

$$\dot{\boldsymbol{y}}_2(t) = \frac{-K\boldsymbol{y}_2(t) - C\boldsymbol{y}_2(t) - B\boldsymbol{F}(t)}{M} \tag{30}$$

Rewriting it as a single first-order equation yields

$$\dot{\boldsymbol{y}}(t) = A\boldsymbol{y}(t) + \boldsymbol{f}(\boldsymbol{t}) \tag{31}$$

where

$$\boldsymbol{y}(t) = \begin{bmatrix} \boldsymbol{y}_1(t) \\ \boldsymbol{y}_2(t) \end{bmatrix} \tag{32}$$

$$A = \begin{bmatrix} 0 & I \\ -K/M & -C/M \end{bmatrix} \tag{33}$$

$$\boldsymbol{f}(t) = \begin{bmatrix} 0 \\ B\boldsymbol{F}(t)/M \end{bmatrix} \tag{34}$$

with I an $n \times n$ identity matrix and 0 an $n \times n$ matrix of zeros.

The mass, damping and stiffness matrices in (28) represents

$$M = \begin{bmatrix} m_1 & 0 & \cdots & 0 \\ 0 & m_2 & \cdots & 0 \\ \vdots & \vdots & \ddots & \vdots \\ 0 & 0 & \cdots & m_{n-1} \end{bmatrix} \tag{35}$$

$$C = \begin{bmatrix} c_1 + c_2 & -c_2 & 0 & \cdots & \cdots & 0 \\ -c_2 & c_2 + c_3 & -c_3 & 0 & \cdots & 0 \\ 0 & -c_3 & c_3 + c_4 & & \cdots & 0 \\ \vdots & 0 & & \ddots & \cdots & \vdots \\ \vdots & \vdots & & & c_{n-2} + c_{n-1} & -c_{n-1} \\ 0 & 0 & 0 & \cdots & -c_{n-1} & c_{n-1} + c_n \end{bmatrix} \tag{36}$$

$$K = \begin{bmatrix} k_1 + k_2 & -k_2 & 0 & \cdots & \cdots & 0 \\ -k_2 & k_2 + k_3 & -k_3 & 0 & \cdots & 0 \\ 0 & -k_3 & k_3 + k_4 & & & 0 \\ \vdots & 0 & & \ddots & & \vdots \\ \vdots & \vdots & & & k_{n-2} + k_{n-1} & -k_{n-1} \\ 0 & 0 & 0 & \cdots & -k_{n-1} & k_{n-1} + k_n \end{bmatrix} \tag{37}$$

where m is the mass of an element, c the damping coefficient acting on an element and k the stiffness coefficient acting on an element, with n the number of elements in the ribbon.

The stiffness coefficient is

$$k = 3EI/l_b^3 \tag{38}$$

where E is the modulus of elasticity, I the moment of inertia and l_b the length of the beam (length of ribbon corrugation element in this case).

Damping occurs due to internal viscous damping of the ribbon material and also because of air resistance. The internal viscous damping is calculated as

$$c_{eq} = k\psi/2\pi\omega_{in} \tag{39}$$

where ψ is a material property that is read from a table and ω_{in} is the input radial frequency.

The damping effect of air resistance is calculated as

$$C^{Hosaka} = 3\pi\left(\mu_a + \frac{b_r\sqrt{2\mu_a\rho_a\omega}}{4}\right) \tag{40}$$

where μ_a is the viscosity of air,b_r the breadth of the beam, ρ_a the density of air and ω the frequency at which the beam is vibrating.

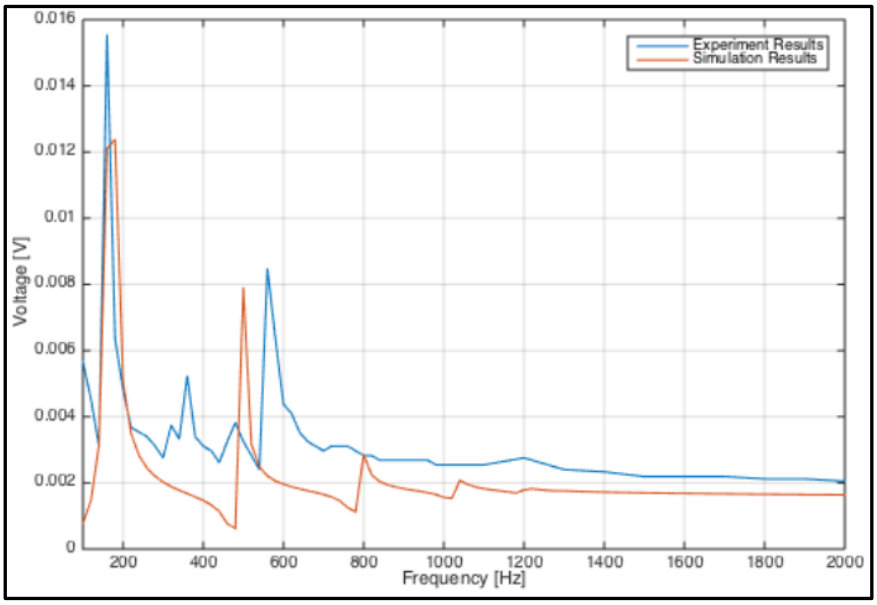

Figure 40: Numerical model of ribbon vs. experimental results **[65]**

The equation for the pressure difference across the ribbon (front to back) is

$$\Delta P = 2P_0 sin(\omega t - \omega\Delta t/2) - P_0 sin(-\omega t/2) \tag{41}$$

where P_0 is the amplitude of the pressure wave, ω the frequency, time t.

The phase lag Δt between the front and the back of the ribbon is determined by

$$\Delta t = \Delta L / c \tag{42}$$

where ΔL is the path length around the microphone poles and c is the speed of sound.

Meiring implemented all the equations in MATLAB® and determined the time response of the system with the aid of the Runge-Kutta integration functions in MATLAB®.

From the velocity Meiring calculated the emf that is generated by the ribbon by means of Faraday's law.

$$\frac{d\phi}{dt} = -BL\frac{dx}{dt} = -BLu \tag{43}$$

$$e = -\frac{d\phi}{dt} \tag{44}$$

where e is the emf, $d\phi$ the change in magnetic flux, B the magnetic flux density, L the length of the ribbon, dx the displacement and dt the time in which the displacement occurs.

The calculated emf was then verified experimentally. The results of the numerical model and the experimental results by Meiring are shown in Figure 40.

7.2 Modelling and Simulation

After investigating the behaviour of a free floating disk in chapter 6 the model can now be expanded to experiment with the ribbon itself. The next step is to simulate a ribbon without the surrounding structure of the microphone baffle.

The ribbon model consists of a 40 mm long corrugated aluminium ribbon with a thickness of 10 µm, suspended in a three-dimensional volume. The ends of the ribbon are kept stationary by adding a small element with extremely high mass at each end. The ribbon is placed inside a sphere of limited dimension to keep the volume of the model small enough to compute a solution within a reasonable time. The boundaries of the sphere are modelled in such a way that the sound source outside of the sphere will enter the sphere without any reflections. Similarly, all sound waves travelling inside the sphere are allowed to leave the sphere with minimal reflections from the inside boundary of the sphere. The incident sound wave is modelled as a plane wave striking the ribbon face-on, straight from the front.

7.2.1 Deformation and Resonance of the Ribbon

This experiment illustrates through simulation how the ribbon's mechanical structure influences its resonance and how the ribbon deforms.

Figure 41 illustrates the action of a fully corrugated ribbon in sound fields of 300 Hz and 3 kHz. At 3 kHz the largest section of the ribbon moves in unison, but at 300 Hz a standing wave is formed along the ribbon. From the units on the colour scale it can be seen that the displacement of the ribbon at 300 Hz is 100 times higher than the displacement at 3 kHz. Purely based on the wavelengths of the two sound waves, the difference in displacement should be a factor of 10 only. The difference by a factor of 100 indicates that the fully corrugated ribbon has a resonant frequency at 300Hz.

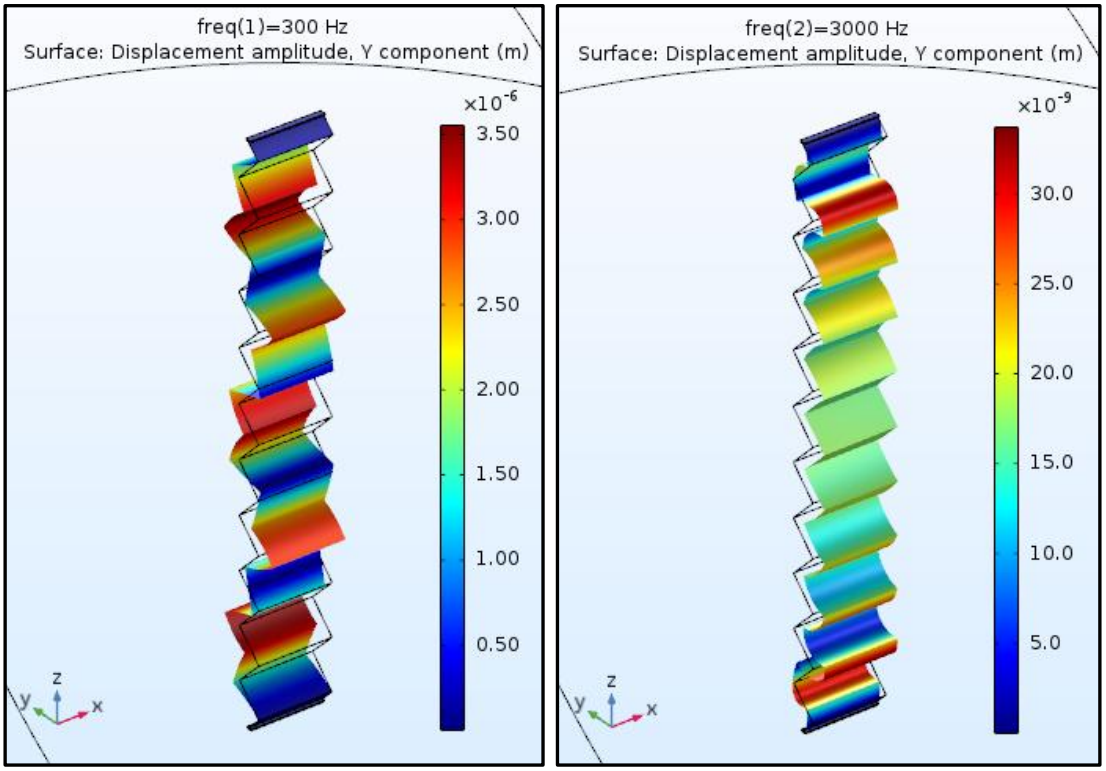

Figure 41: Ribbon action in 300 Hz and 3 kHz sound waves

The displacement of a zigzag ribbon can be clearly displayed in a 3D model, but the displacement amplitude cannot be easily plotted on a y-z graph for further analysis. It is possible to draw a cut-line through the centre of the ribbon along the z-axis and plot various properties along the cut-line on a graph. With the corrugations however, a straight line intersects the ribbon only at the points where it pierces the ribbon. Therefore only a few dots are displayed on the graph. A projection of the zigzag ribbon onto a flat surface will be a good option but such a solution is not available with the simulation software. The displacement of the ribbon at 3 kHz is only a few hundred nanometres, so there is no need for the ribbon to be corrugated along its whole length to provide sufficient flexibility for this experiment. In an effort to circumvent the graphing problem the ribbon design is changed from a completely corrugated ribbon to a flat ribbon with only two sections of corrugation (one on each end) to give the ribbon enough flexibility, but with a long flat section that can be plotted on a graph.

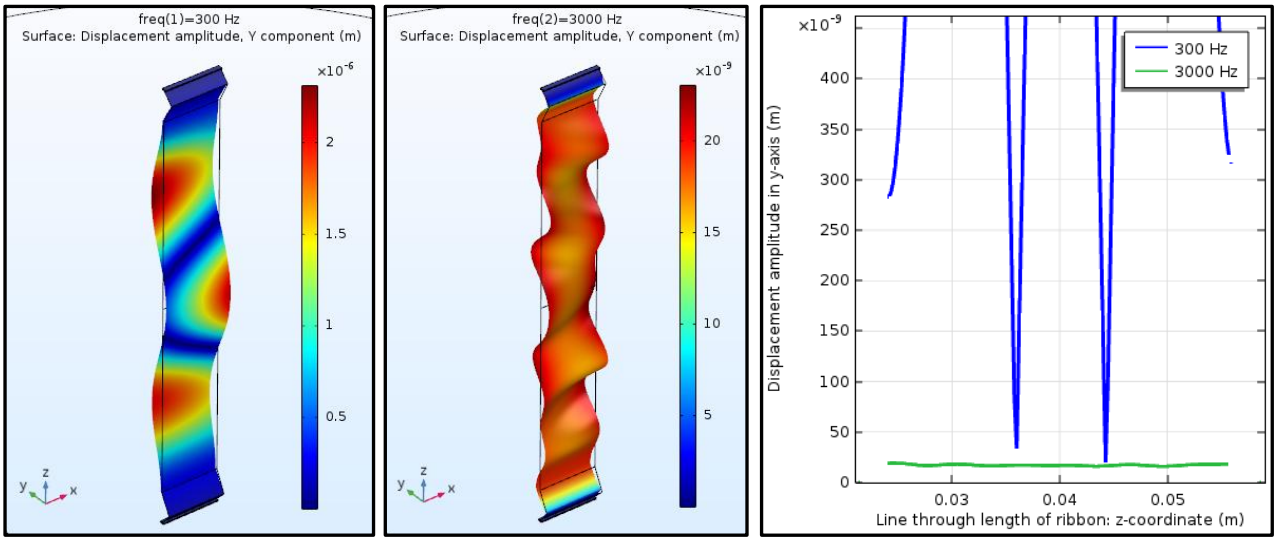

Figure 42: Action of ribbon with two corrugations in 300 Hz and 3 kHz sound waves

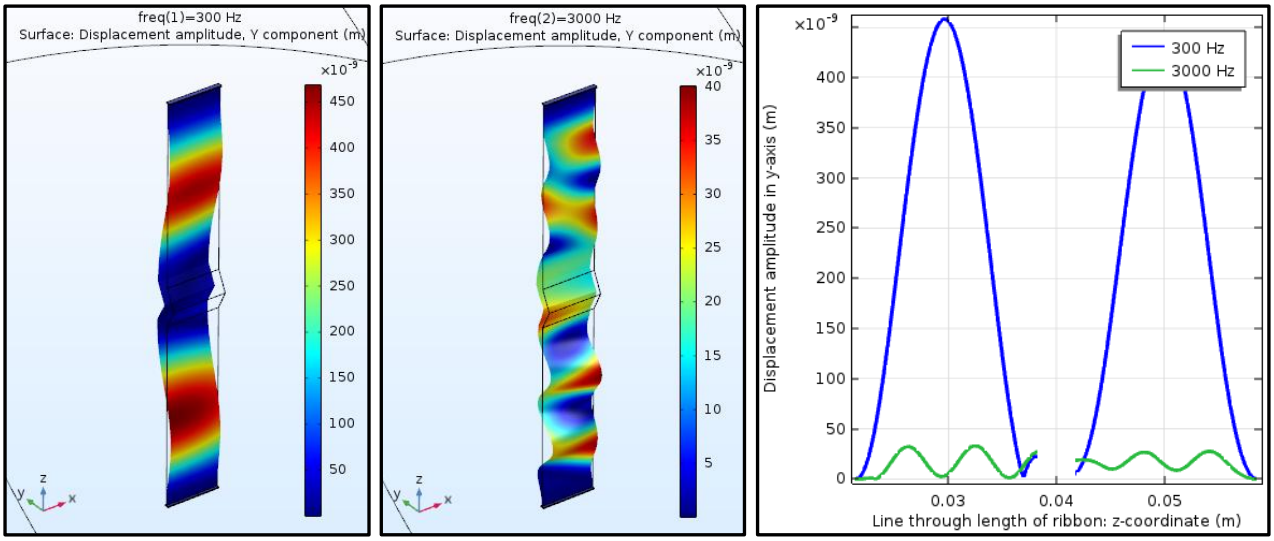

Figure 43: Action of ribbon with one corrugation in 300 Hz and 3 kHz sound waves

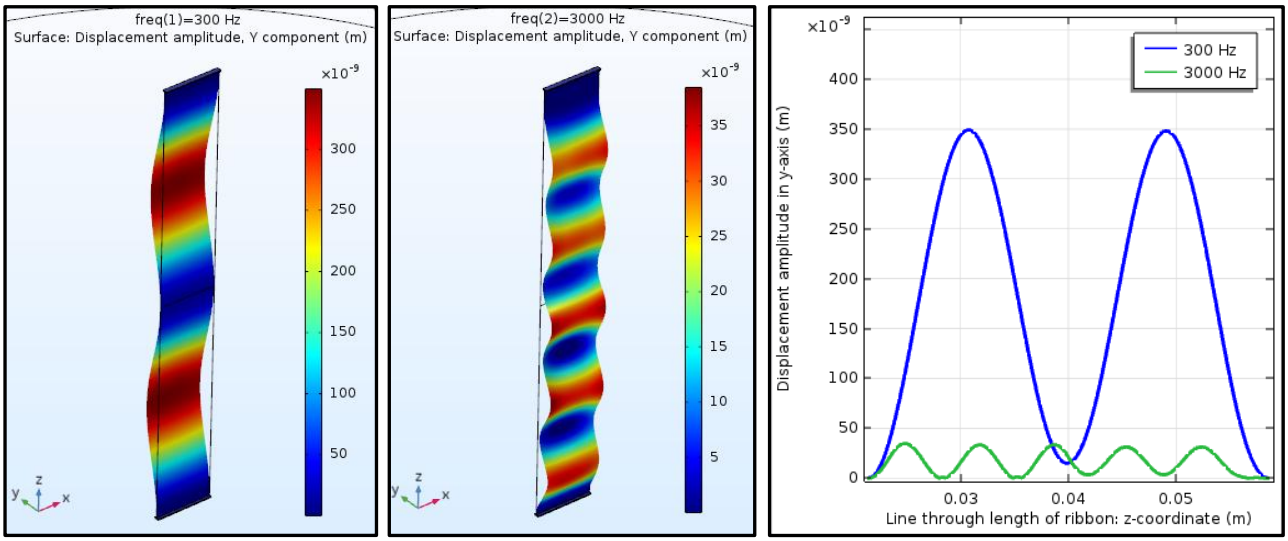

Figure 44: Action of ribbon with no corrugation in 300 Hz and 3 kHz sound waves

To evaluate the influence of the change in ribbon design, two other models are also introduced: one with a single corrugation in the middle of the ribbon and another with no corrugations at all. Figure 42 to Figure 44 illustrate how the shape of the ribbon influences its behaviour under the stresses of sound waves at 300 Hz and 3 kHz. The graphs of the displacement along the cut-lines are placed alongside the 3D results. The empty space that can be seen in the middle of the x-y graph of Figure 43 is the corrugated piece of ribbon that does not fall on the cut-line. In Figure 42 the empty sections are not as noticeable because the corrugations are at the ends of the ribbon. Only the ribbon with no corrugations (Figure 44) shows the displacement of the ribbon along its total length.

It can be seen from the displacement differences between 300 Hz and 3 kHz that the ribbon with two corrugations displays a large resonance at 300 Hz. The ribbon with one corrugation has a low resonance at 300 Hz and the ribbon with no corrugation is not resonating at all. The ribbon with no corrugation displays a standing wave in a similar fashion to that of a vibrating string. The ribbon with one corrugation displays similar behaviour, but with slight twisting of the ribbon. The ribbon with two corrugations twists and turns even more along its long straight section. The ribbons do not twist at the corrugations, but only along the flat pieces. Although the ribbon without corrugation has the longest straight section, it is too tightly strung to twist at these frequencies. With the movement of Figure 41 in mind, it can be deduced that the corrugations along the length of the ribbon adds mechanical stabilisation to the ribbon to prevent it from twisting and turning in the sound wave; thereby preventing unwanted harmonics in the sound recording. The mean displacement along the complete surface area of the ribbon is calculated by the simulation software. The displacement results of the four ribbons at 3 kHz are 13.98 nm, 14.18 nm, 13.56 nm and 13.79 nm for the ribbons with 10, 2, 1 and zero corrugations respectively. Although the physical behaviour of the four ribbons is very different, the standard deviation for their displacement amplitudes is only 0.23 nm (i.e. less than 1.7% of the amplitudes) at 3 kHz. The calculated displacement results at 300 Hz (where two ribbons resonate) are 1.60 µm, 0.77 µm, 0.17 µm and 0.14 µm respectively.

It is clear that the corrugations in the ribbon play an important role in the stability of the ribbon. Without regular corrugations the ribbon twists and turns (on a micro-scale) instead of moving in parallel lines between the two magnets. It does not play much of a role in the displacement of the ribbon at non-resonant frequencies however. Logarithmic plots of the displacement (averaged over the total surface area of the ribbon) vs. frequency are shown in Figure 45 and Figure 46 for the ribbons with ten corrugations and zero corrugations. The resolution of the graph is 20 Hz. The resonance frequencies of the ribbons differ significantly, but the displacement values over the 60 Hz to 20 kHz range are of the same magnitude at the non-resonating frequencies. It could be expected that the ribbon with ten corrugations will have a larger displacement value at lower frequencies than the ribbon with no corrugations. However, the displacement is not governed by

the flexibility of the ribbon alone, but also by the weight of the ribbon. More corrugations equal more flexibility, but also more weight. Displacement that is gained by flexibility is lost again because of additional weight. The ribbon may be compared to a vibrating string - the lighter the string, the higher its natural frequency. The ribbon with many corrugations resembles a heavier, more loosely strung string and the ribbon with no corrugations resembles a lighter, more tightly strung string. Figure 45 and Figure 46 are good illustrations to demonstrate how the lower resonant frequencies are more predominant with the corrugated ribbon (Figure 45) while the higher resonant frequencies are more dominant with the non-corrugated ribbon (Figure 46).

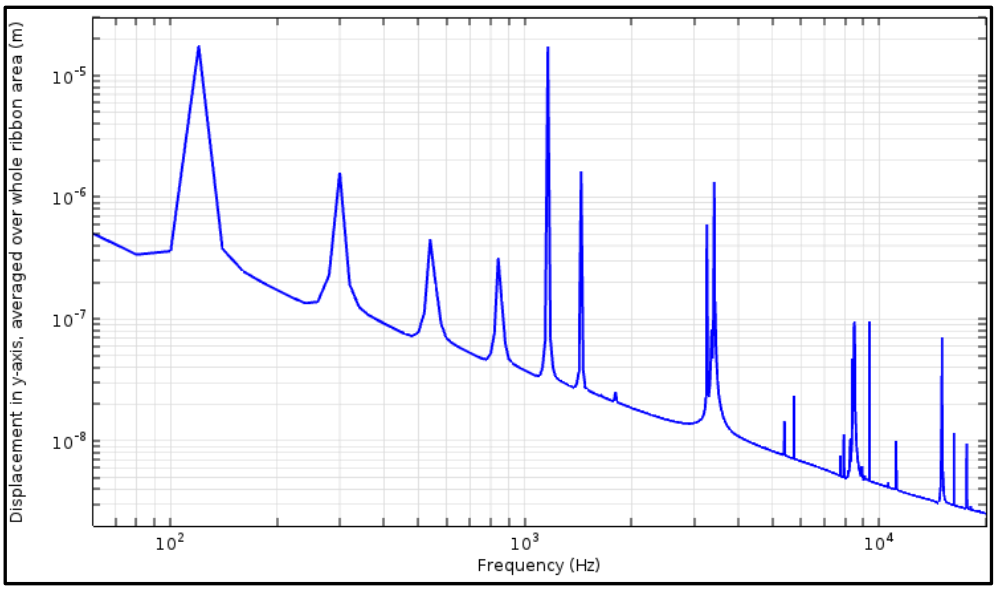

Figure 45: Displacement vs. frequency for ribbon with ten corrugations

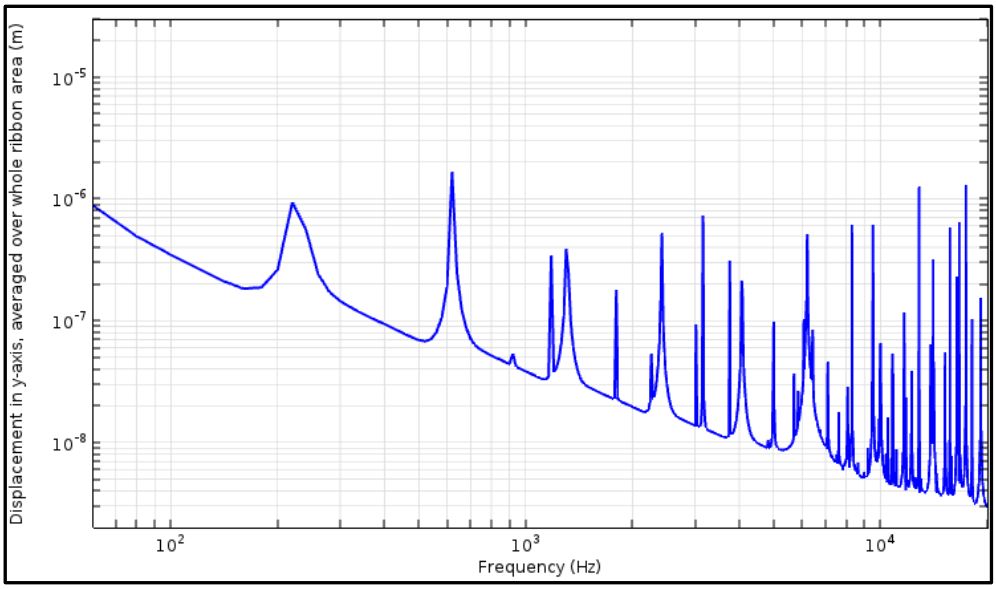

Figure 46: Displacement vs. frequency for ribbon with zero corrugations

This behaviour is in accord with Akino's statement in his gold plated ribbon patent that the ribbon is folded in a zigzag form to lower the resonance frequency of the diaphragm [43]. The 300 Hz frequency at which the ribbon in Figure 41 resonates can also be seen distinctly in the

displacement graph of Figure 45. The ribbon with no corrugations shows no peak at 300 Hz. This agrees with the results of the 3D visualization of the ribbon in Figure 44.

7.2.2 Velocity of the Ribbon

The amplitude of the emf that is generated by the ribbon is not determined by the extent of its displacement, but rather by the velocity of the ribbon. Besides the length of the ribbon and the intensity of the magnetic field, the velocity of the ribbon is the only other determining factor in the magnitude of the generated emf in the following version of Faraday's law:

$$\varepsilon = vBl \tag{45}$$

where ε is the emf, v the velocity, B the magnetic field, and l the length of the conductor [66].

Figure 47 shows the velocity amplitude of the ribbon in the y-axis (averaged over the whole area of the ribbon) plotted against frequency for the ribbon with ten corrugations. At 300 Hz the velocity is 3.67×10^{-3} m/s and at 3 kHz it is 0.32×10^{-3} m/s. For a magnetic field of 1 T and a ribbon length of 40 mm, the generated emf at 300 Hz is therefore 147 µV and at 3 kHz it is 13 µV. The emf generated by the ribbon at its resonant frequencies is much higher than the emf at non-resonant frequencies. This can cause unwanted harmonics in the sound recording.

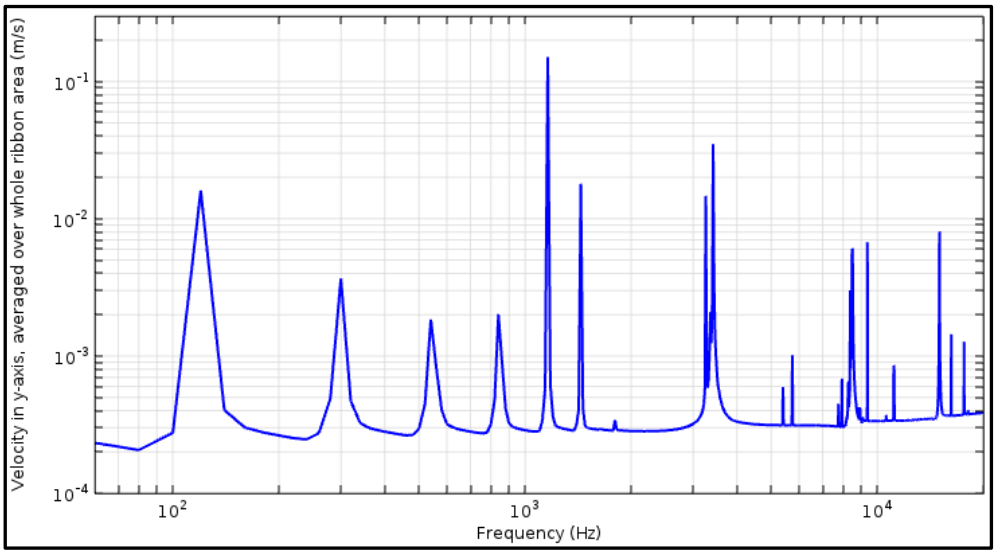

Figure 47: Velocity amplitude vs. frequency for ribbon with ten corrugations

It can be seen in Figure 47 that the velocity of the ribbon increases slightly towards the higher frequencies except for the self-resonance frequencies where there are large increases. The difference in velocity at 100 Hz and 1 kHz is 5%. Between 1 kHz and 10 kHz the difference increases to 17%. At the resonant frequencies the ribbon travels longer distances in the same time period - therefore it travels at higher velocities.

7.3 Testing

Simulations show that there is a difference in frequency response between a corrugated ribbon and a straight ribbon. To support this finding a comparative test is conducted to determine whether the differences are similar in a real-world setup.

7.3.1 Ribbon Corrugation

To perform the experiment for comparing different ribbons, a simple test setup is constructed with the aid of a personal computer (PC). The test setup consists of the following:

- A speaker set connected to the output of a PC's built-in sound card.
- Ribbon microphone connected to the input of the PC's sound card.
- REW software installed on the PC.

To perform the experiment, frequency scans are performed with two different ribbons – a corrugated ribbon and a straight ribbon. Both ribbons are manufactured from 10 µm aluminium foil.

Although the test setup is not ideal, it is sufficient for this experiment because it is used for a comparative test where only one of the variables is changed (the ribbon in this case) while the rest of the variables remain fixed. Any deficiencies in the system that are visible with the corrugated ribbon will have the exact same effect on the straight ribbon. The test is performed a few times with the corrugated ribbon to confirm that the test results are consistently repeatable. Then the corrugated ribbon is replaced with a straight ribbon and the same tests are repeated.

The result of the frequency scans of the two ribbons is shown in Figure 48. The dB scale in the figure indicates the sound pressure level relative to the threshold of hearing. Smoothing of 1/12 octave is applied to the measurements to match the smoothing of Stanley's graph for the hammered ribbon (Figure 49). The human ear perceives loudness with a smoothing effect between 1/3 and 1/6 octave. Due to its corrugations the corrugated ribbon is in effect longer, heavier and more flexible than the straight ribbon. Therefore is has a lower resonance frequency. The result of the real-world ribbon tests in Figure 48 confirms that the ribbon with corrugations has a better low frequency response than the straight ribbon. The amplitude that falls towards the higher frequencies in Figure 48 is the opposite of what is seen in the simulation results of Figure 47. The difference in behaviour is attributed to the fact that the microphone baffle is not included in the simulations. The influence of the baffle is demonstrated in paragraph 6.2.10. The simulated ribbons in paragraph 7.2 are treated in isolation from the rest of the microphone and not all the effects of the microphone design are taken into consideration. Furthermore, the physical ribbons are not exact replicas of the simulated ribbons due to tooling and skill constraints when manufacturing the DIY ribbons. Therefore resonance of the real-world ribbon will not be at the same frequency than the simulated ribbon. The aim of the experiment is however to compare a corrugated ribbon to a

straight ribbon to illustrate that the same effects that are observed with the simulated ribbons are also seen with the laboratory tests. There is no indication in the REW documentation what the reference level of dB-scale on the sound pressure level graph is. It is however not important for comparative tests.

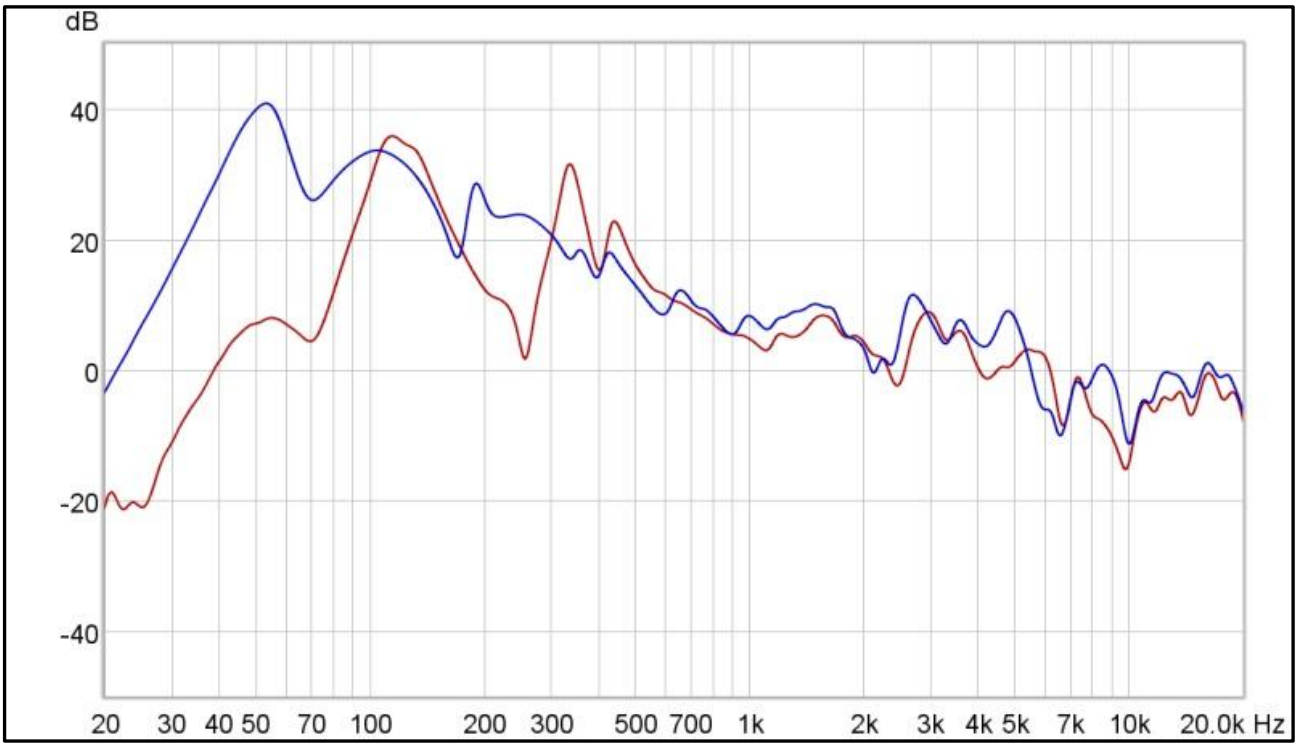

Figure 48: Frequency response of corrugated ribbon (blue) and straight ribbon (red)

7.3.2 Cold Working of an Aluminium Ribbon

No other tests were conducted to illustrate how the mechanical properties of the ribbon influence the microphone's frequency response, but during the literature study a test by Stanley was found that fits this category [67]. These tests were performed from a materials science point of view.

Stanley first looked at the use of alternative materials for the ribbon of the microphone. Nitinol, a Nickel-Titanium alloy with excellent shape memory and super-elasticity properties would make the ideal ribbon, but it is not available in micrometre range foils and its electrical resistivity is 30 times higher than that of aluminium. Magnesium is lighter than aluminium, but a small piece of magnesium foil is more expensive than a top-of-the-range ribbon microphone.

The next option was to treat the aluminium ribbon to change its physical properties. Stanley conducted tests to determine whether cold working (hammering) of the ribbon would influence the microphone's acoustic performance. Cold working changes the crystalline lattice structure of the ribbon. He conducted the tests with an Apex 205 ribbon microphone. Only minor changes were observed in the acoustic performance of the microphone when treating the ribbon by cold working

it. The only significant change was observed in the non-audible range below 20 Hz. A copy of Stanley's test results is presented in Figure 49.

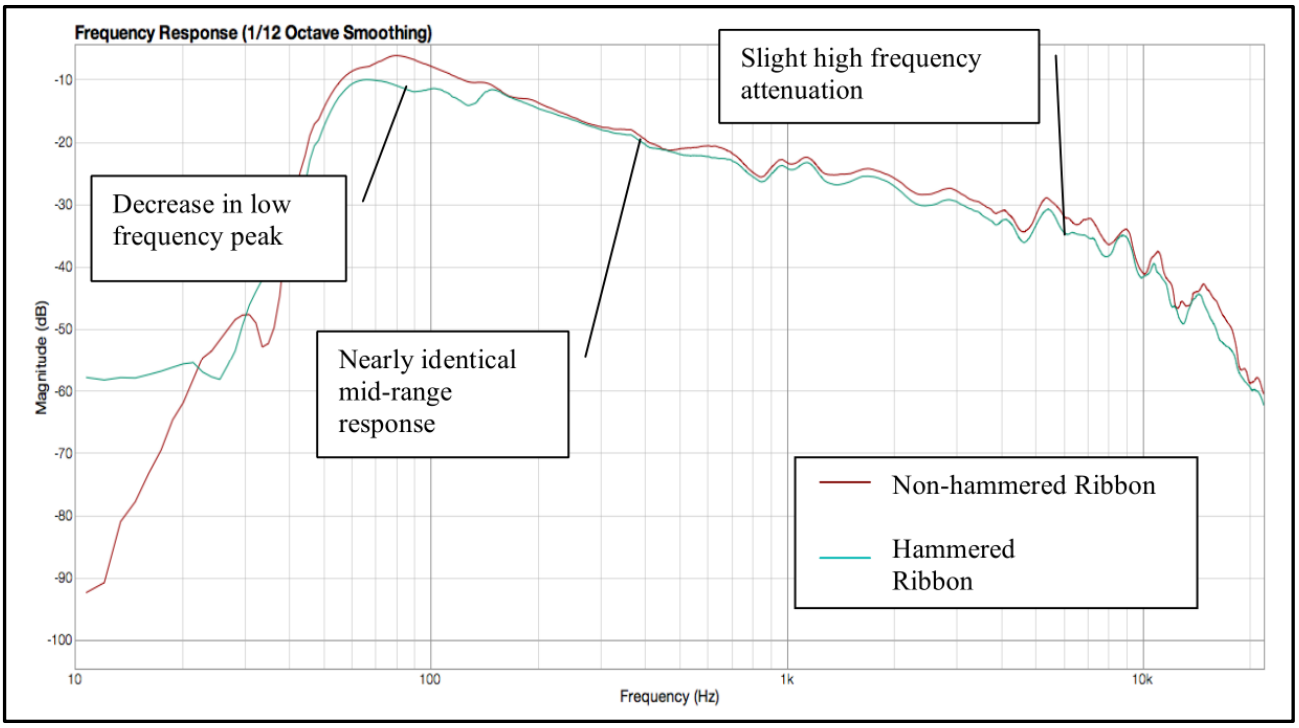

Figure 49: Stanley's frequency response tests for a hammered ribbon **[67]**

7.4 Conclusion

The phenomena of deformation and resonance are clearly illustrated in this chapter by the simulations and laboratory experiments with different ribbon designs. The ribbon microphone is a good vehicle to illustrate how the mechanical properties of a structure influence its response to sound waves of different frequencies. Students can use simulation software to view the response of a ribbon to sound waves over a wide frequency range and then verify the results experimentally with readily available sound equipment, a PC and a DIY ribbon microphone.

8 MAGNETICS

The next physics area for which the ribbon microphone can be used as demonstration tool, is that of magnetics. The propagation of a magnetic field in space and through obstacles, manipulation of the magnetic field to meet the microphone's requirements and the effect of the physical structure of the microphone, is visualised effectively through modelling and simulation.

The microphone requires high magnetic field strength inside the microphone, but low field strength outside of the microphone. Modelling and simulation can be used to check new designs and design parameters that are difficult to measure otherwise. A magnetic design can be characterised for example, by taking hundreds of measurements with a Gauss meter and mapping it painstakingly on a graph. For each new design all the measurements have to be performed all over again. A more elegant solution is to create a simulation model and verify the simulation results with a limited number of laboratory measurements.

This chapter presents 4 experiments which can be performed using the ribbon microphone.

- Two simulation experiments modelling magnetic field lines and magnetic field strength. Here the focus is on the magnetic aspect of the microphone assembly. The aim is to illustrate mainly the impact of magnetic field manipulation.
- Two laboratory experiments showing the magnetic field lines in the vicinity of the microphone and the magnetic field strength in and around the microphone baffle. These are of a modest nature and presented here to highlight the value of computer simulation when expensive test equipment is not readily available, or experiments require cumbersome test procedures.

8.1 Theory

8.1.1 Background

The term magnetic field describes the influence of two similar forces on its surroundings. The one force is that of a magnet and the other, that of charges in motion. A magnetic field can be created by a permanent magnet and it can also be created by an electric current.

The magnetic field is formed by force lines running from the north-pole to the south-pole of a magnet. These force lines are called magnetic flux. It is denoted by the symbol ϕ and is measured in the Système International d'Unités (SI unit) weber (Wb). The term magnetic flux density refers to the amount of flux per unit area perpendicular to the magnetic field.

$$\boldsymbol{B} = \frac{\phi}{A} \tag{46}$$

where $\boldsymbol{B}$ is the magnetic flux density, ϕ the magnetic flux and A the area.

Magnetic flux density is denoted by the symbol $\boldsymbol{B}$ and is measured in tesla (T).

$\boldsymbol{B}$ is sometimes also called magnetic induction, or simply referred to as the magnetic field. The term magnetic field should not be confused with the term magnetic field intensity denoted by $\boldsymbol{H}$ (described later in this text).

One tesla is defined as the amount of magnetic induction that will produce a force of one newton, on a charge of one coulomb, moving at a velocity of 1 m/s in a direction perpendicular to $\boldsymbol{B}$. This definition is consistent with the equation

$$\boldsymbol{B} = \frac{\boldsymbol{F}}{qv} \tag{47}$$

where q is the charge, v is the velocity and $\boldsymbol{B}$ the magnetic flux density.

The force acting on a moving charge is called the Lorentz force and is described by the equation

$$\boldsymbol{F} = qv \times \boldsymbol{B} \tag{48}$$

Another unit that is commonly used for magnetic flux density is the gauss (G). Gauss is the unit that is used in the CGS (centimetre-gram-second) convention. The conversion factor is 1 T = 10 000 G.

The effect of a magnetic field on its surroundings may be expressed in terms of either its magnetic flux density $\boldsymbol{B}$, or its magnetic field intensity $\boldsymbol{H}$. The magnetic field intensity $\boldsymbol{H}$ is defined as

$$\boldsymbol{H} = \frac{\boldsymbol{B}}{\mu_0} - \boldsymbol{M} \tag{49}$$

where μ_0 is the vacuum magnetic permeability (a constant equal to $4\pi \times 10^{-7}$H/m (Henrie per metre) (SI) or 1 Oersted (CGS)) and $\boldsymbol{M}$ is the magnetisation of the body measured in ampere per metre (A/m) or Weber per square metre (Wb/m2) in SI units and Oersted (Oe) in the CGS system. Magnetic permeability is a measure of the response of a medium to a magnetic field. $\boldsymbol{H}$ has the same dimension as $\boldsymbol{M}$ and is therefore expressed either in A/m, Wb/m2 or Oe. $\boldsymbol{H}$ refers to the internal magnetic field intensity of the material. The term magnetic induction (flux density) $\boldsymbol{B}$ is more regularly used than the term magnetic field intensity $\boldsymbol{H}$, although both can be used to characterise the effect of a magnetic field.

The permeability of a soft magnetic material has a similar relation to its magnetic field than the relation between a metal's conductivity and its electrical current. Magnetic flux density corresponds to electrical current density. Free space is an excellent *electrical* insulator, but not a *magnetic* insulator at all. The magnetic equivalent of an electric insulator is a superconductor that no flux penetrates, i.e. its permeability is zero.

Magnetic materials may also be characterised by their polarisation $\boldsymbol{J}$ (intensity of magnetisation), which is defined as

$$\boldsymbol{J} = \mu_0 \boldsymbol{M} \tag{50}$$

The different measuring units in SI and CGS become quite confusing. Table 2 summarises the different units and their conversion factors [68]. Literature dating back to the nineteen-sixties [69] and earlier refer to the MKSA system instead of the SI system. MKSA stands for metre-kilogram-second-ampere. For the remainder of this text only SI units will be used.

Table 2: CGS vs. SI units and its conversion factors

Unit	Symbol	CGS	SI	Conversion
Magnetic flux	$\boldsymbol{B}$	Gauss (G)	Tesla (T)	10^{-4}
Magnetic field intensity	$\boldsymbol{H}$	Oersted (Oe)	A/m	$10^3/4\pi$
Magnetisation (magnetic dipole moment per unit volume)	$\boldsymbol{M}$	erg/G/cm^3	A/m	10^3
Magnetic permeability	μ	G/Oe	H/m	$4\pi \times 10^{-7}$
Magnetic polarisation	$\boldsymbol{J}$	none	Tesla	None

8.1.2 Ferromagnetic Hysteresis Loop (Magnetisation Curve)

The ferromagnetic hysteresis loop is well described in [70] and [68]. A condensed version is provided below.

The characteristics of a ferromagnetic material are determined by placing the material in an applied external magnetic field and observing how the material's own magnetism changes as the external field is increased, decreased or reversed. The results are plotted on a graph with the external magnetic field $\boldsymbol{H}$ on the x-axis and the material's own magnetic field $\boldsymbol{M}$ on the y-axis. The hysteresis loop is therefore also referred to as the M-H loop of the material (Figure 50).

$\boldsymbol{M}$ and $\boldsymbol{H}$ are both measured in ampere per metre (A/m). The unit of A/m is a relatively small unit considering that the earth's magnetic field is approximately 50 A/m. The magnetic field of natural magnetite (Fe_3O_4) is 480kA/m.

The four ideal types of magnetic material will behave as follow:

- The ideal *nonmagnetic* material is not magnetic at all and it will not be magnetised by an external field, no matter how large the external field. Its hysteresis curve is a straight horizontal line on the x-axis ($\boldsymbol{M} = \boldsymbol{0}$).

- The ideal *hard magnetic* material is permanently magnetised and its own magnetism will not increase or decrease in the presence of an external field. Its hysteresis curve is a straight horizontal line at a certain value of $\boldsymbol{M}$. No matter how large or how small that value of $\boldsymbol{M}$ is, it will not be changed by an external magnetic field of any magnitude.
- The ideal *soft magnetic* material will be magnetised instantaneously by an external magnetic field. Its hysteresis curve is a vertical line along the y-axis ($\boldsymbol{H} = \boldsymbol{0}$).
- The ideal *diamagnetic* material will be magnetised by an amount that changes linearly with the external magnetic field. Its hysteresis curve is a straight line at a 45° angle.

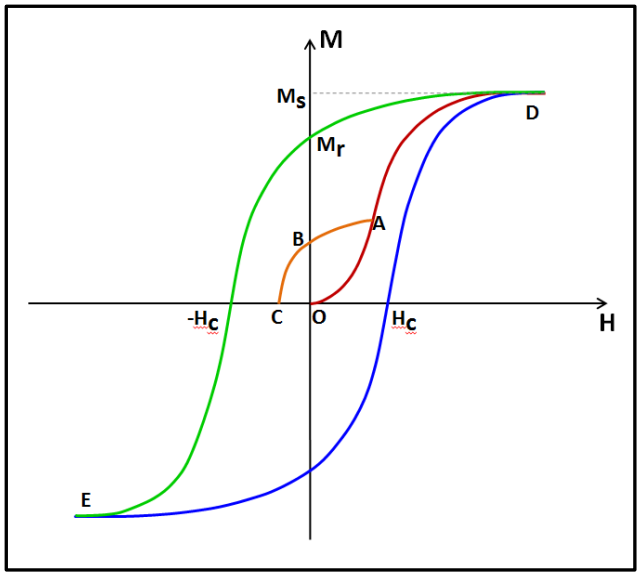

Figure 50: Magnetisation hysteresis loop

The magnetisation of a sample that has never been magnetised before will follow the curve along the red line (the virgin curve) in Figure 50 while $\boldsymbol{H}$ is increased. If $\boldsymbol{H}$ is increased only until reaching point **A** on the curve and then decreased to zero again, the material will retain an amount of magnetism of $\boldsymbol{M} =$ **B**. To demagnetise the sample again, an external field $\boldsymbol{H}$ needs to be applied with magnitude **C** in the opposite direction. If $\boldsymbol{H}$ is increased beyond point **A** the sample will reach magnetic saturation near point **D**. Beyond point **D** the magnetism of the sample will no longer increase. As the external field $\boldsymbol{H}$ is decreased, the magnetism of the sample will follow the green curve. When the external field is removed ($\boldsymbol{H} = \boldsymbol{0}$) a magnetisation strength of $\boldsymbol{M} = \mathbf{M_r}$ will remain in the sample. If a reverse field of increasing magnitude is applied externally, the sample's magnetism will decrease along the green curve until $\boldsymbol{H}$ reaches the value $\mathbf{-H_C}$. At this point the sample will be demagnetised ($\boldsymbol{M} = \boldsymbol{0}$). If the magnitude of the reverse field is further increased ($\boldsymbol{H}$ becomes more negative), the sample will become magnetised with opposite polarity. When point **E** is reached the sample is saturated in the opposite direction. When the external field is increased again, the sample's magnetism will follow the blue curve from point **E** to point **D**.

Three points of particular interest are noted on the M-H curve:

- $\mathbf{M_S}$ – *saturation* or spontaneous magnetisation. This is the value of $\boldsymbol{M}$ beyond which the magnetisation of the material does not increase any further with an increase in the externally applied $\boldsymbol{H}$.
- $\mathbf{M_r}$ – *remanence* or retentivity. The amount of magnetisation that remains in the material after the external magnetic field has been removed, i.e. the amount of magnetisation that the material retains.
- $\mathbf{H_C}$ – *coercivity*. The intensity of an external field that is required to change the direction of magnetisation of a material.

These parameters are used in calculations and simulation models for magnetic material. Another quantity that is regularly used is the energy product $(BH)_{max}$ of a magnet. $(BH)_{max}$ is equal to the area of the largest rectangle that can fit inside the second quadrant of the B-H curve. The B-H curve is similar to the M-H curve, but the material's induction $\boldsymbol{B}$ instead of its magnetisation $\boldsymbol{M}$ is plotted against $\boldsymbol{H}$.

Soft magnetic materials have narrow loops and lose their magnetisation as soon as the external field is removed. The H-field penetrates soft magnetic materials only partially. Magnetic dipoles at the surface of the sample are arranged in such a way that they shield the internal structure from any external fields. Soft magnetic materials are fit for use as magnetic shields. Soft magnetic materials have high permeability, low coercivity and small hysteresis losses and are therefore also ideal for transformer cores and cores for motors and generators. Iron-cobalt-vanadium alloy (Fe-C-V), iron-nickel alloy (Fe-Ni), amorphous alloy, silicon steel and ferrites are examples of soft magnetic materials.

Hard magnetic materials have wide, square M-H curves. Once magnetised by applying an external field, these materials will keep their magnetised state after the H-field has been removed. The H-field penetrates hard magnetic materials completely. They are fit for use as permanent magnets. Their high coercivity, high remanence and large hysteresis losses are the characteristics that make these materials good permanent magnets. Neodymium-iron-boron alloy (NdFeB), samarium-cobalt alloy (SmCo) and aluminium-nickel-cobalt alloy (AlNiCo) are examples of hard magnetic materials.

Permanent magnets gets demagnetised by vibration, opposing fields and high temperatures. The temperature above which a magnet completely loses its magnetism is known as its Curie temperature. At 1388 Kelvin, cobalt is the material with the highest Curie temperature. The extremely strong NdFeB magnets that are most commonly in use today (N33 grade for example) have a relatively low Curie temperature of 353 K (80°C). Special grades of these magnets (N33AH for instance) may have Curie temperatures up to 513 K (240°C).

The spontaneous magnetisation, remanence and coercivity of magnetic materials depend on many factors. The rate at which $\boldsymbol{H}$ is swept, its thermal history, the shape of the material, surface roughness and microscopic defects are just a few of these factors. Physicists are trying to explain the hysteresis loop. Materials scientists are figuring out how to improve it. Engineers are working together to make the best use of it.

8.1.3 Ribbon Corrugation

Horng et al. states in their patent [47] that the ribbon is corrugated to lengthen the ribbon in order for a larger part of the ribbon to cut the magnetic field, thereby enhancing the sensitivity. This is not the case however. The emf is generated perpendicular to the movement of the ribbon and the magnetic field. The corrugation changes the angle of the ribbon relative to the magnetic field lines – thereby reducing the magnitude of the emf. The greatest electrical excitation is achieved when the movement of the ribbon cuts the field lines perpendicularly. Any change in angle reduces the amplitude of the generated emf, thereby counteracting the gain in ribbon length. The simplified equation for the generated emf is

$$\varepsilon = vBl \tag{51}$$

where ε is the emf, v the velocity, B the magnetic field, and l the length of the conductor [66].

This equation is however only true for perpendicular movement. The complete equation for other angles of movement is

$$\varepsilon = vBl \sin\theta \tag{52}$$

where θ is the angle between the direction of movement and the magnetic field.

For a straight ribbon that is 50 mm long, vibrating at an average speed of 1.25 um/s, in a magnetic field of 1.2 T, the generated emf will be

$$\varepsilon = 1.25 \times 10^{-6} \times 1.2 \times 0.05 = 75 \times 10^{-9}\text{Volt}$$

If the ribbon is fully corrugated with corrugations at 45° to the length of the ribbon, then the ribbon length will increase to 70.710678 mm. The generated emf will be

$$\varepsilon = 1.25 \times 10^{-6} \times 1.2 \times 0.070710678 \sin 45 = 75 \times 10^{-9}\text{Volt}$$

The calculations show that no sensitivity is gained by corrugating the ribbon. Calculations for corrugations at other angles produce the same results.

The ribbon is in fact corrugated because the corrugations add flexibility to the ribbon for its forward-backward movement while simultaneously providing mechanical stability to the ribbon in the other directions. The corrugations have a large influence on the frequency response of the microphone and the resonant frequencies of the ribbon as shown earlier in paragraph 7.

8.2 Modelling and Simulation

Simulation results of the magnetic field lines in (and around) the ribbon microphone of 5.2.1.1 are illustrated here and manipulation of the field lines with yokes of different metals is demonstrated.

8.2.1 Direction of Field Lines

The magnetic field needs to cut the ribbon perpendicular to its direction of motion to generate the highest emf. Figure 51 illustrates the magnetic field lines between the two magnets of the microphone and also in the area surrounding the magnets. It can be seen from the size of the arrows that the flux density is at its highest between the two magnets and inside the magnets themselves. Figure 52 provides a graph of the magnetic flux density along the x-axis (cutting through the centre of both magnets) and a graph of the flux density along the y-axis (cutting through the open space between the two magnets where the ribbon will move). Figure 53 illustrates with a different visualisation effect how the pole piece design influences the flux density and the flow of the magnetic field lines by comparing a design with square-bar magnets to a design with round-bar magnets. The slice is made on the x-y plane in the same position as for Figure 51.

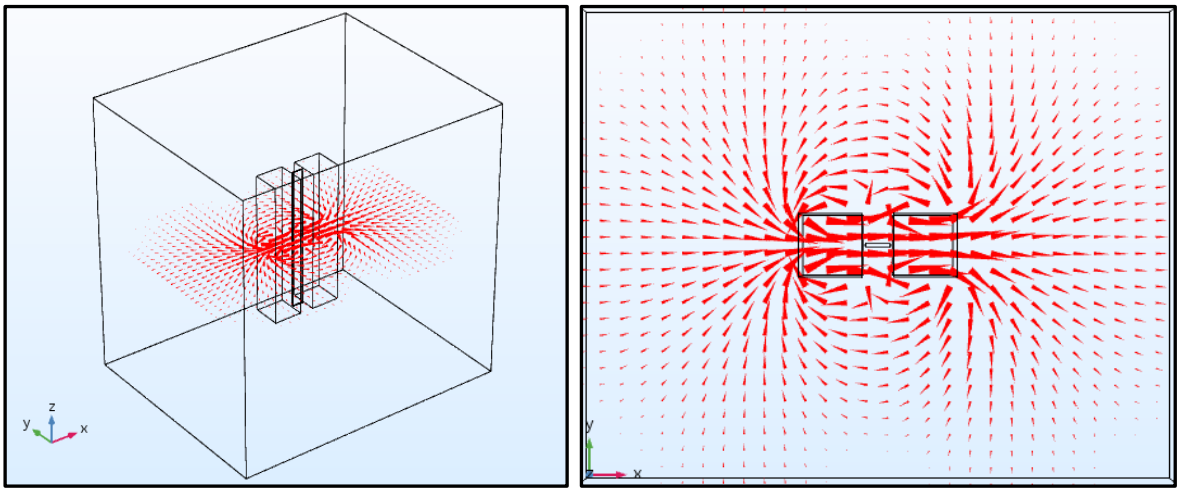

Figure 51: Magnetic field lines – perspective view and top view of slice on x-y plane

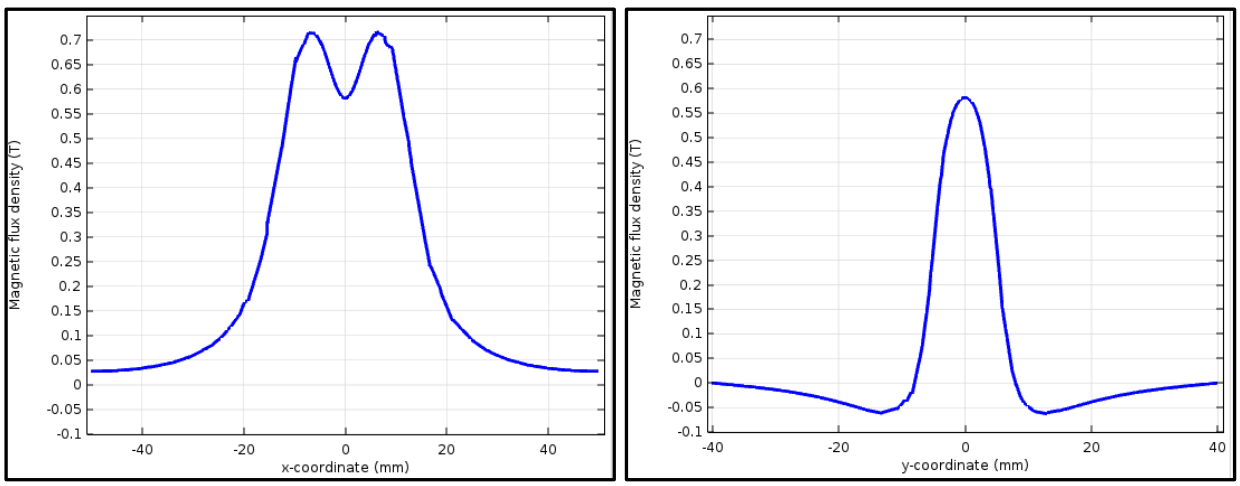

Figure 52: Magnetic flux density on z-x plane (left) and y-z plane (right)

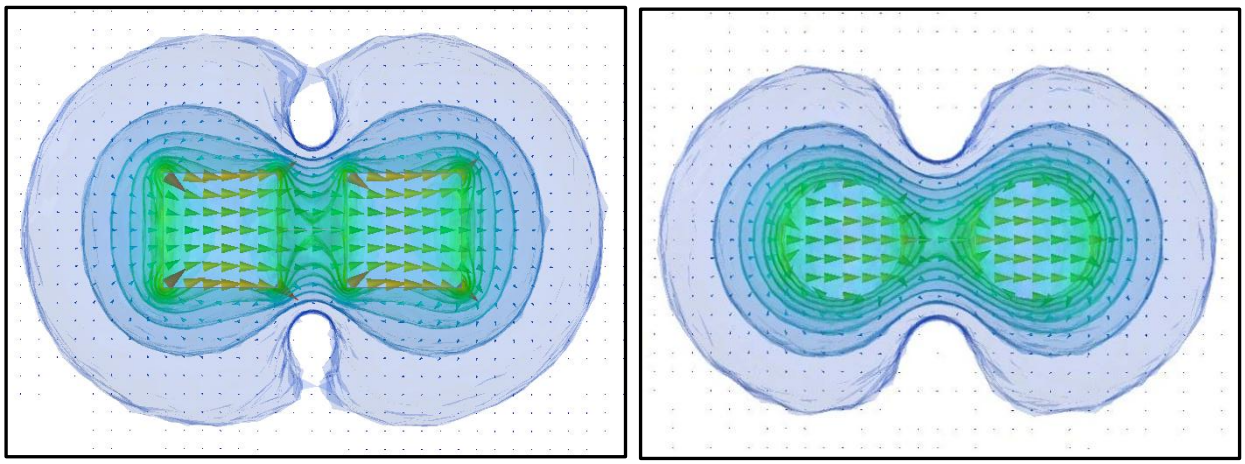

Figure 53: Influence of pole piece design on magnetic flux density and field lines **[1]** © 2016 IEEE

8.2.2 Magnetic Field Strength

The magnetic field can be guided through magnetic material. By placing an iron yoke around the two magnets most of the magnetic field lines are constrained within the path that the yoke provides. The yoke has a twofold benefit – the magnetic field strength in the area around the outside of the magnets is reduced and the magnetic field strength between the two magnets is increased. The field strength is thus increased where it is needed for the ribbon to generate a higher emf and decreased in the area outside where it is unwanted. Figure 54 is used to compare the magnetic field strength for magnets without a yoke and for magnets with a yoke. The slice for visualisation is made on the z-x plane through the centres of the two magnets. The peak intensity is between 0.5 T and 0.6 T for the model without a yoke, while it increases to a peak intensity between 0.7 T and 0.8 T for the model with an iron yoke. The yoke therefore increases the magnetic field strength across the ribbon between 30% and 40%.

Pure iron is a better magnetic conductor than mild steel because of its high permeability. Its relative permeability is up to 100 times higher than that of mild steel, depending on the purity of the iron. Figure 55 provide simulation results for the less effective mild steel yoke.

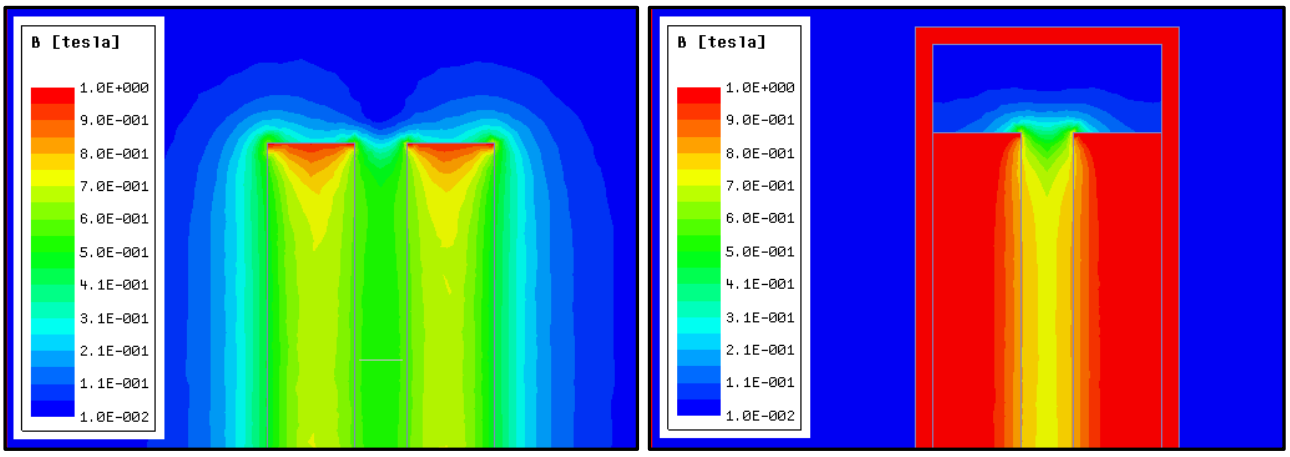

Figure 54: Magnetic field strength without yoke (left) and with iron yoke (right) on the z-x plane

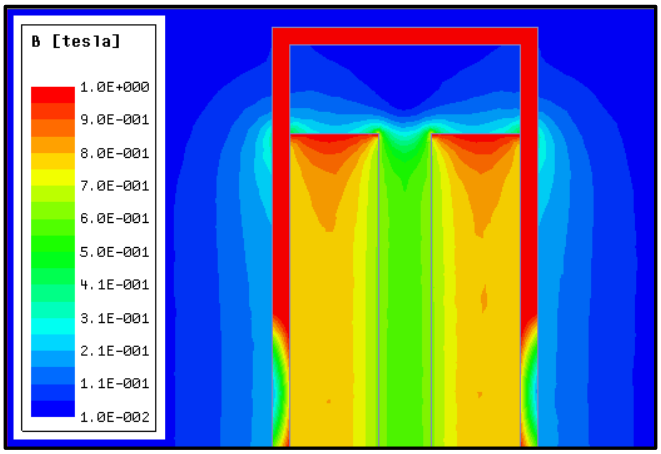

Figure 55: Magnetic field strength with mild steel yoke

The yoke is not only beneficial for the magnetic field strength, but it also serves as a convenient structure to hold the magnets in place. Because the magnets are so much closer to the yoke than to each other, the magnets are attracted more to the yoke then to each other and remains stuck to the yoke instead of snapping together.

8.3 Testing

Two experiments are performed to illustrate the magnetic effects of the microphone assembly. One of the tests is used to demonstrate the direction of the magnetic field lines, and the other test is used to measure the strength of the magnetic field.

8.3.1 Magnetic Field Lines

The magnetic field lines are checked with a handheld magnetic search pole consisting of a small bar magnet on a gimbal (Figure 56). The gimbal allows the bar magnet to swivel freely in any direction in order to align itself with the magnetic field lines.

Figure 56: Magnetic search pole

A simple check with this device (Figure 57) confirms that the magnetic field lines run in the same pattern that the simulation shows in Figure 51. The red coloured side of the search pole is its north pole and the blue side is its south pole.

A magnetic compass (Figure 58) can also be used, but the movement of the compass is restricted to a single plane. Although *most* compass needles have a red north pole, there is not a clear standard in this regard. The north pole of the compass in Figure 58 is the white side of the needle.

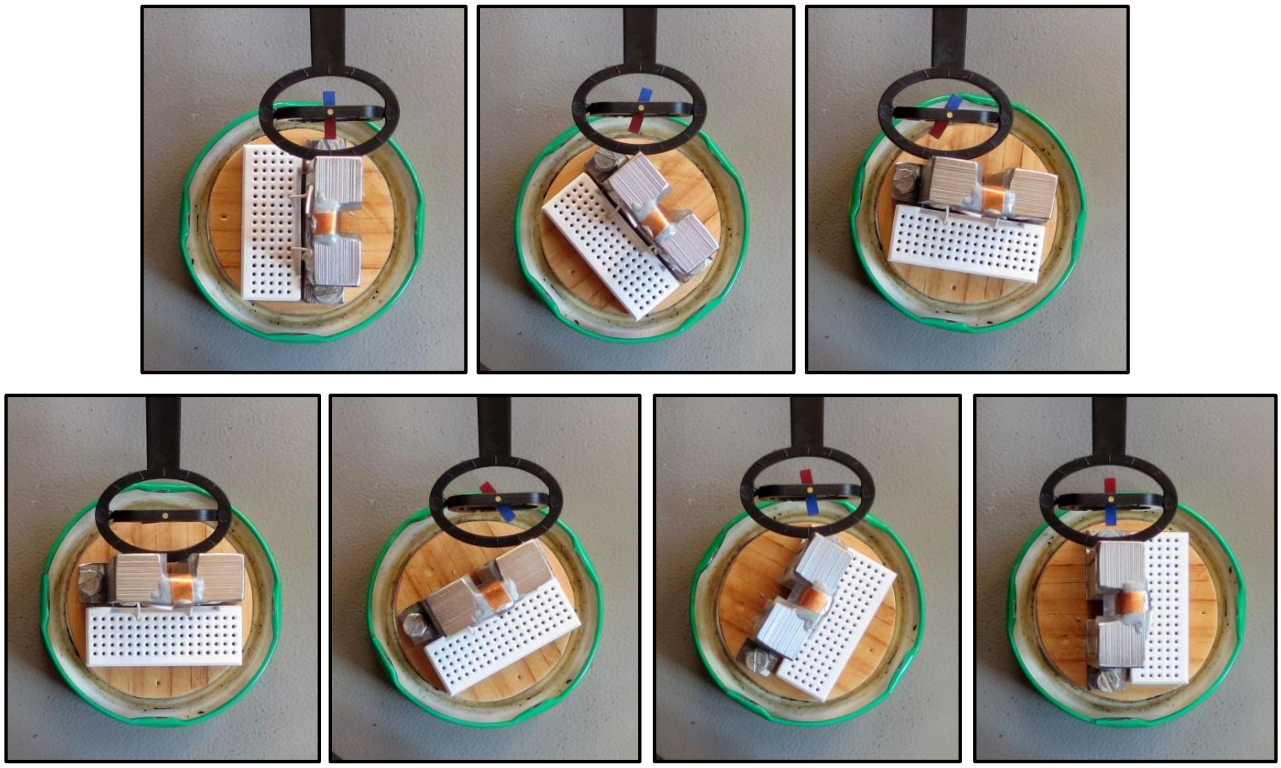

Figure 57: Magnetic field lines indicated by search pole

Figure 58: Magnetic field lines indicated by magnetic compass

8.3.2 Magnetic Field Strength

Gauss meters that measure magnetic field strength are not only expensive, but are also difficult to find. Only a limited number of laboratories are equipped with a Gauss meter.

A simple custom made device is constructed in order to measure the field strength. The device consists of a Honeywell SS49E linear hall-effect sensor IC wired to a battery and a multimeter (Figure 60). The output from the SS49E varies linearly in proportion to the magnetic field strength According to its datasheet the typical output is 1.4 mV per Gauss. Using the conversion factor in Table 2 gives 1.4 mV per $1x10^{-4}$ Tesla, or 14 V per Tesla. The SS49E's limited supply voltage only allows a magnetic range of ±1 000 Gauss (±0.1 T). Its range is well below the maximum field strength of the simulation, but it is still useful in the areas of weaker magnetic field strength.

The output of the SS49E for zero Gauss is a voltage halfway between its supply lines. For a 3 V supply the zero Gauss reading will be 1.5 V and for a 6 V supply it will be 3 V for example. The device is also sensitive to the direction of the field lines. When the field lines are running perfectly parallel to the device then it measures no magnetic field strength. When the field lines run perpendicular to the device as indicated in Figure 59 the output voltage will increase or decrease depending on the direction of the magnetic field. The voltage will increase for field lines running south to north through the device and decrease for field lines running north to south through the device.

A couple of spot-checks with this measuring device, as shown in Figure 61, confirms that the magnetic field on the outside of the soft-iron yoke is weaker than the magnetic field between the two magnets inside the yoke. These checks agree with the simulation results of Figure 55.

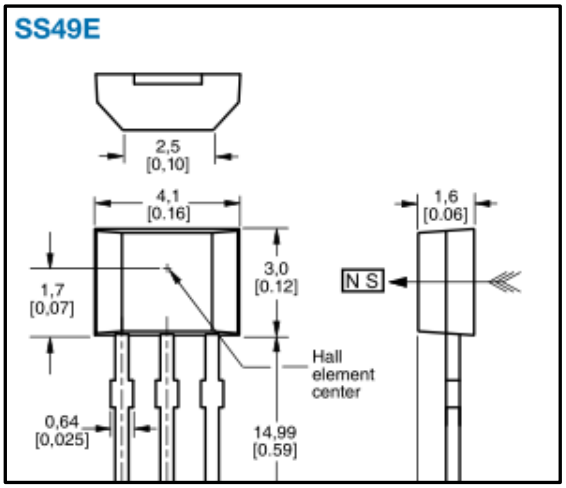

Figure 59: SS49E field line direction

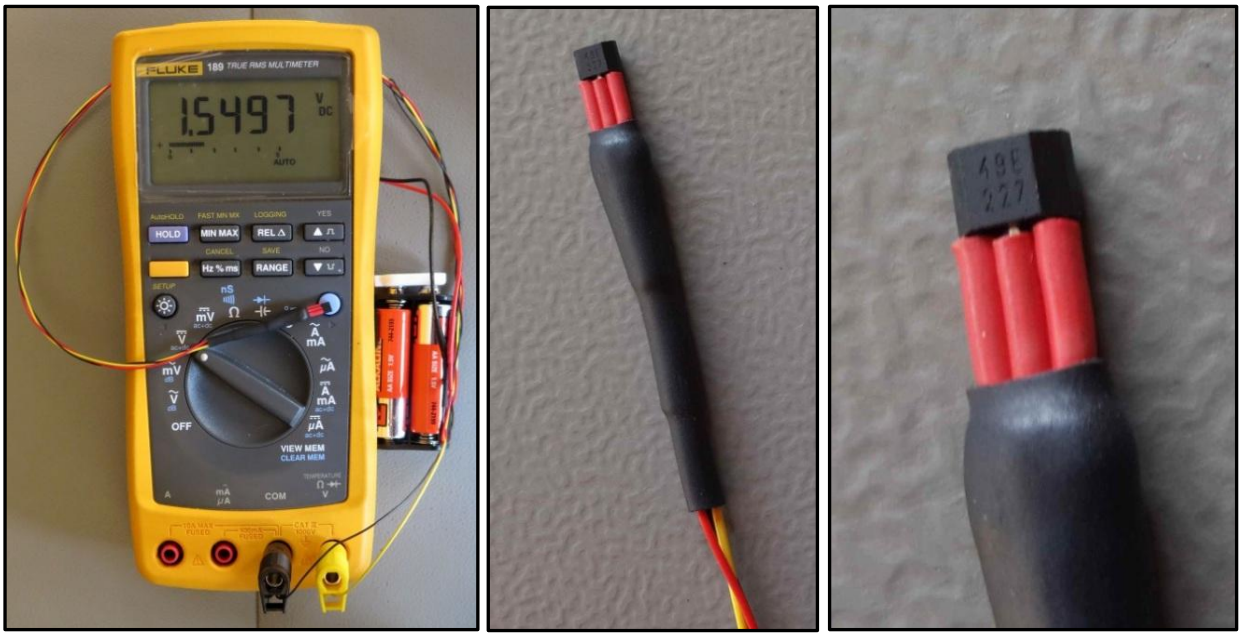

Figure 60: DIY Gauss meter with SS49E hall sensor

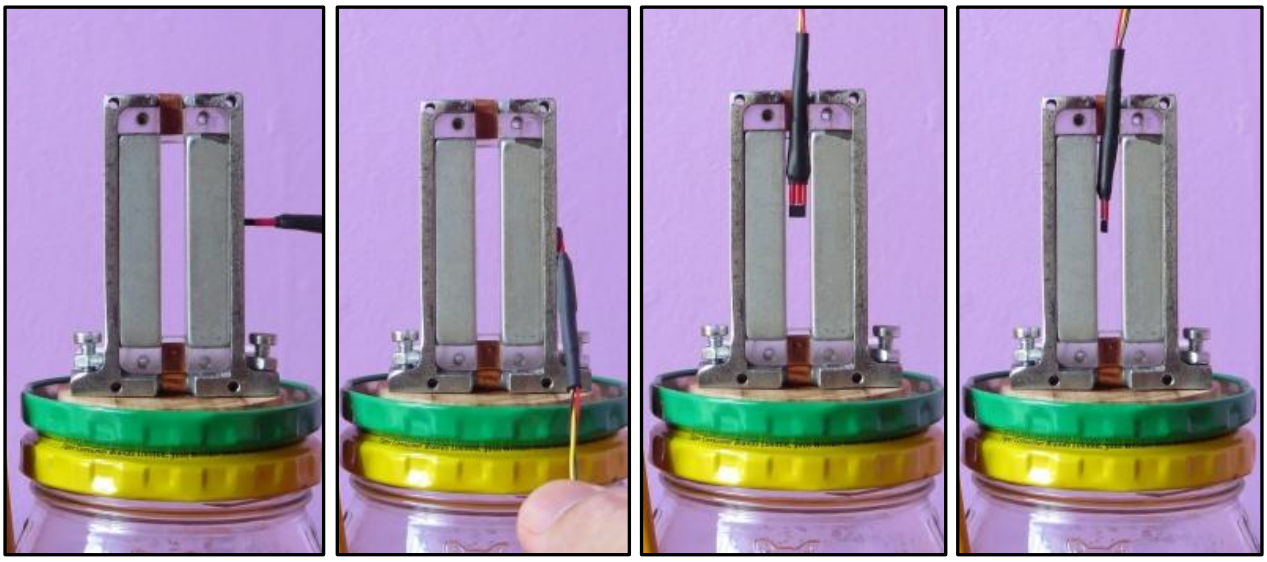

Figure 61: Magnetic field strength measurements outside and inside yoke

8.4 Conclusion

It is demonstrated by simulation and testing that magnetic design can be aided by computer software modelling to save time and effort.

9 ELECTROMAGNETICS

The last of the physics areas for which the ribbon microphone is used as demonstration tool, is that of electromagnetics.

The complete microphone system can be used to include circuit and system concepts in the teaching model. The two techniques by which useful signal levels can be obtained from a ribbon microphone, namely via a transformer or an amplifier, both offer excellent opportunities for teaching circuit concepts through experimentation and simulation. In the case of the transformer, concepts like transformation ratios, impedance matching and the frequency dependence of real-world transformers can be illustrated, while for amplifiers concepts like noise, input impedance and bandwidth can be shown.

This chapter presents 4 experiments which can be performed using transformers and electronic amplifiers with the ribbon microphone.

- A simulation experiment modelling two audio transformers of differing size, winding ratio and impedance. Here the focus is on the components that complete the microphone system. The aim of the simulation is to illustrate the impact that winding turns and core material have on transformer frequency response and to show transformer behaviour under various loads.
- Laboratory experiment with transformers showing the effects of impedance matching. The aim of this practical experiment is to illustrate the importance of impedance matching.
- Laboratory experiment with electronic amplifiers. The aim of this experiment is to demonstrate the effect of an RC filter and noise handling with electronic amplifiers.
- Laboratory experiment with the microphone. The aim of this experiment is to provide a test environment consisting of a complete microphone system, to compare the performance of transformers and electronic amplifiers on a system level.

9.1 Theory

The ribbon microphone is a classic example of electromagnetic induction. By means of a micro-meter-thin aluminium ribbon that is suspended in a magnetic field, it converts sound energy into electric energy. The audio transformer that is used with the microphone is an excellent example of low frequency electromagnetic coupling.

9.1.1 Faraday's Law

Electromagnetic analysis is handled on a macroscopic level during simulation by solving Maxwell's equations within a set of boundary conditions. The four Maxwell equations that form the basis for fundamental electromagnetism calculations are Ampère's law, Faraday's law, Gauss' law for

electric fields and Gauss' law for magnetic fields. For the purpose of this chapter, only Faraday's law is required. The differential form and the integral form of the equation are provided in Table 3.

Table 3: Faraday's law

Differential Form	Integral Form
$\nabla \times \boldsymbol{E} = -\frac{\partial \boldsymbol{B}}{\partial t}$	$\oint_C \boldsymbol{E} \cdot d\boldsymbol{l} = -\frac{d}{dt}\oint_S \boldsymbol{B} \cdot \hat{n}\, da$ $\oint_C \boldsymbol{E} \cdot d\boldsymbol{l} = -\int_S \frac{\partial \boldsymbol{B}}{\partial t} \cdot da$

Faraday's law describes the relationship between an electric field and a changing magnetic field. Changing magnetic flux through a conducting surface induces an emf across the conductor. The symbols that are used in Faraday's law are listed in Table 4. For further reading and a concise introduction to Maxwell's equations see [71].

Table 4: Symbols used in Faraday's law

Symbol	SI unit	Quantity name or description	SI unit, non-abbreviated
$\boldsymbol{E}$	V/m N/C	Electric Field Intensity	Volt per metre Newton per Coulomb
$\boldsymbol{B}$	T	Magnetic Flux Density Magnetic Induction Magnetic Field	Tesla

9.1.2 Transformers

The amplitude of the emf generated in the vibrating ribbon of the microphone is too low for transmission through a long cable without being drowned by ambient electromagnetic interference. The signal-to-noise-ratio of the microphone output can be improved by amplifying its voltage by means of a step-up transformer close to the microphone ribbon. The transformer is also vital for impedance matching with amplifiers and recording equipment on the other end of the cable.

The ideal transformer is a device that will step an AC voltage up or down in the same ratio over all frequencies and independent of any source or load impedance. With practical transformers there are however many factors that influence the performance of the transformer. These influences are so severe that transformers have to be designed specifically for different applications. A summary of the factors that influence the characteristics of a transformer is provided in this paragraph [72].

9.1.2.1 Turns-ratio

The turns-ratio of a transformer causes the following transformations in an ideal transformer:

- *Voltage* transformation is directly proportional to the turns-ratio.
- *Current* transformation is inversely proportional to the turns-ratio.
- *Impedance* transformation is proportional to the square of the turns-ratio.

The turns-ratio of a transformer is the most basic part of its function, but it can also be the most misleading parameter on the transformer's datasheet. The immediate thought of a transformer with a 1:2 turns-ratio is that it will double the voltage. It is however only true for a limited frequency range and is also dependent on the impedances of the circuits that are connected to the windings.

9.1.2.2 Magnetising Current and Core Loss

The current in the primary winding of the transformer sets up the mutual flux in the core and it balances the demagnetising effect of the load current in the secondary winding. The net magnetomotive force is related to the reluctance in the transformer core according to the equation

$$N_1 I_1 - N_2 I_2 = \varphi_m \mathcal{R} \tag{53}$$

where N is the number of turns in the primary and secondary windings, I is the current in these windings, φ_m is the magnetic flux in the core and $\mathcal{R}$ is the reluctance of the core.

There is a magnetising inductance associated with the reluctance of the core and the core has finite permeability. The flux in the core is established by the instantaneous magnetising current which is determined by the magnetic properties of the core. When the core goes into saturation the distorted magnetising current contains odd harmonics. The magnetising current increases rapidly as the transformer go further into saturation. Hysteresis is a cause of power loss in the core at high frequencies. Eddy current losses add to the hysteresis loss in high power applications.

9.1.2.3 Winding Resistance

Besides the DC resistances of the wires that are used for the transformer windings, there is also an AC resistance component due to the internal flux of the wires (conductors). The AC resistance can by approximated as

$$R_{ac} = R\varphi_{dc}\left[1 + \frac{\left(\frac{r_0}{\delta}\right)^4}{48 + 0.8\left(\frac{r_0}{\delta}\right)^4}\right] \tag{54}$$

where δ is the skin depth of the conductor and r_0 is the radius of the conductor.

AC losses in the form of skin effect and proximity effects have to be taken into account for high-frequency operation of transformers.

9.1.2.4 Magnetic Leakage

Ideally the same magnetic flux will link the primary and secondary windings of the transformer (mutual flux). In reality however, there is always an amount of flux limited to one winding that does not link all the windings (leakage flux). Because of leaking flux there is not 100% power transfer between windings and power is wasted.

9.1.2.5 General Transformer Equations

High-frequency loss in transformers is not of much concern in the audible frequency range. Therefore the equations to follow are more than adequate for the purpose of the thesis.

Voltage Equation: The impressed voltage (v) on a winding is related to the rate of change of flux density according to Faraday's law.

$$v = NA_m \frac{dB}{dt} \tag{55}$$

where N is the number of winding turns, A_m the effective cross-sectional area of the magnetic core and B the flux density.

Power Equation: The total VA rating of a transformer can be related to its physical, electrical and magnetic properties according to the equation

$$\sum VA = K_v f B_{max} J_0 k_f k_u A_p \tag{56}$$

where K_v is the voltage waveform factor, f the frequency, B_{max} the maximum flux density, J_0 the current density, k_f the core stacking factor, k_u the window utilisation factor and A_p the product of the window winding area and cross-sectional area.

Winding Loss: The total resistive loss P_{cu} in the windings of the transformer is

$$P_{cu} = \rho_w V_w k_u J_0^2 \tag{57}$$

where ρ_w is the electrical resistivity and V_w the winding volume.

Core Loss: The total core loss under sinusoidal excitation can be calculated with the general Steinmetz equation

$$P_{fe} = K_c f^{\alpha} B_{max}^{\beta} \tag{58}$$

where P_{fe} is the time-average core loss per unit volume and B_{max} the peak value of the flux density at a sinusoidal frequency f. K_c, α and β are constants that can be found in the manufacturer's datasheet.

9.1.3 Resistance of the Ribbon

The resistance of the ribbon does not feature in Faraday's law (45) because emf is the potential difference when no current is flowing from the source [73]. The resistance of the ribbon only becomes a factor when an external path is created for a current to flow. When an external current path exists, the current in the circuit will be limited by the combined resistance of the load and the ribbon. The current flowing in the circuit can be calculated as:

$$I = \varepsilon \, / \, (R + r) \tag{59}$$

where I is the current, ε the emf, R the resistance of the external circuit (load), and r the resistance of the ribbon itself.

The amplitude of the signal across the load is:

$$V_R = IR \tag{60}$$

where V_R is the voltage across the load, I the current, and R the resistance of the load.

Substituting I with (59) yields:

$$V_R = \varepsilon \, / \, (1 + \frac{r}{R}) \tag{61}$$

The amplitude of the emf that is seen across a load will therefore increase when lowering the resistance of the ribbon. The material that the ribbon is made of as well as its thickness and width, will determine the resistance of the ribbon. The following trade-offs have to be considered for the design of the ribbon:

- A thicker ribbon will have lower electrical resistance but it will present higher mechanical resistance to the sound wave because of the additional weight.
- A wider ribbon will have lower resistance and will present a larger area for the sound wave to impose on, but once again it will be heavier.
- Lower resistance of the ribbon will result in higher amplitudes, but also in higher currents that will increase the effect of Eddy currents on the ribbon. The Eddy currents act like a magnetic brake on the ribbon and adversely affect its velocity, thereby limiting the generated emf.

There is only a limited amount of energy present in a sound wave that has to overcome both the mechanical inertia of the ribbon and the effect of the Eddy currents. The design of the ribbon is therefore a balancing act between electrical resistance, physical area and weight. If the external load has relatively low impedance, like a transformer for instance, the resistance of the ribbon plays an important role, but if the external circuit has very high impedance (like an instrumentation amplifier) then the resistance of the ribbon has very little effect on the signal amplitude.

9.2 Modelling and Simulation

9.2.1 Transformer

Transformers that are used to step up the voltage of a ribbon microphone are good examples of low frequency electromagnetic coupling. The transformer is not only used to step up the output voltage of the microphone, but also for impedance matching with the audio equipment that is connected to the microphone.

Two transformers from different manufacturers are chosen for simulation and testing.

- The RMX-1 transformer from EDCOR is chosen because it is a transformer that is specifically designed for ribbon microphones.
- The SP-48 transformer is chosen because it is a miniature MIL-SPEC audio transformer that will fit neatly inside a microphone enclosure.

Little of the information that is necessary for modelling these transformers is available from the datasheets. Some of the unknown parameters can be measured on the physical RMX-1 model without any damage, but the SP-48 transformer is completely encapsulated in epoxy. The same parameters can therefore not be measured on the SP-48.

COMSOL® provides a physics interface that gives the user full control over the core and coil geometries and the materials of the transformer model. ANSYS® PEmag on the other hand provides the user with comprehensive lists of commercial parts (cores, bobbins, wires and winding topologies) that can be used to design a transformer from standardised commercially available components. The RMX-1 and SP-48 are specialised transformers that do not contain the standard parts found in PEmag. ANSYS® also has an Electronic Transformer Kit (ETK) for Maxwell, but the ETK is intended for ferrite core transformers in the 100 kHz range and not for the low frequency range of the audio band. The coil design toolkit for Maxwell can be used to calculate coil resistance and number of turns that fit on a bobbin. The toolkit accepts coil dimensions in millimetre, but the wire thickness must be entered in American Wire Gauge (AWG). Many conversion tables are available on the internet, but most of these tables have the thinnest wire size of 30 AWG or 32 AWG. Only a few tables indicate wire sizes as thin as 40 AWG. For thinner wires a conversion calculation is necessary. The equation to convert from metric wire diameter to AWG is

$$n = -39log_{92}\left(\frac{d_n}{0.127}\right) + 36 \tag{62}$$

where n is the AWG number and d_n the wire diameter in millimetre [74].

9.2.1.1 Simulation models

The simulation models for the transformers in the experiments here are based on the E-core transformer example that is supplied by COMSOL® as a tutorial. The basic example is taken as a starting point and then customised to suit the RMX-1 and SP-48 transformers.

The following factors have a distinct influence on the simulation models and will be discussed in more detail later in this section:

- Number of turns on the primary winding
- Source impedance
- Load
- Core material

9.2.1.2 EDCOR RMX-1 transformer

The parameters that are used to model the RMX-1 transformer are listed in Table 5.

Table 5: RMX-1 transformer parameters

Parameter	Magnitude	Source
Turns-ratio	1:37	Datasheet
DC Resistance	Primary : 0.4 Ohm Secondary : 87 Ohm	Datasheet
Core material	Super Q 80 Nickel (80%)	Datasheet
E-core dimensions	Outer : 25.5 mm x 19.0 mm x 6.65 mm Inner : 18.5 mm x 12.5 mm Centre : 7.0 mm x 12.5 mm	Measured
Wire diameter	Primary : 380 µm, double wound. Secondary : 120 µm, single wound. Wire thickness includes insulation. Heavy insulation on primary, light insulation on secondary.	Measured
Bobbin	Outer diameter (including shielding foil) : 17.2 mm Inner diameter : 9.8 mm Winding height : 11 mm	Measured
Number of turns	Primary : 38 Secondary : 1395	Calculated

The Maxwell® 3D Coil Design Toolkit from ANSYS® is used to calculate the number of turns on the RMX-1 coil windings. The RMX-1 does not consist of a simple inner and outer winding. The primary winding has two wires - one wire winding around the outside of the coil and the other wire somewhere in-between the windings of the secondary coil. The parameters for the inner diameter of the bobbin, the coil height and the wire thickness for the secondary coil are first entered in the toolkit. Then the outer diameter of the coil is adjusted until the coil resistance equals the datasheet value. This method yields an answer of 1395 turns on the secondary winding. There are then 38 turns on the primary winding according to the turns-ratio of the transformer.

The parameter entry window of Maxwell® is shown in Figure 62 and the geometry of the coil is illustrated in Figure 63.

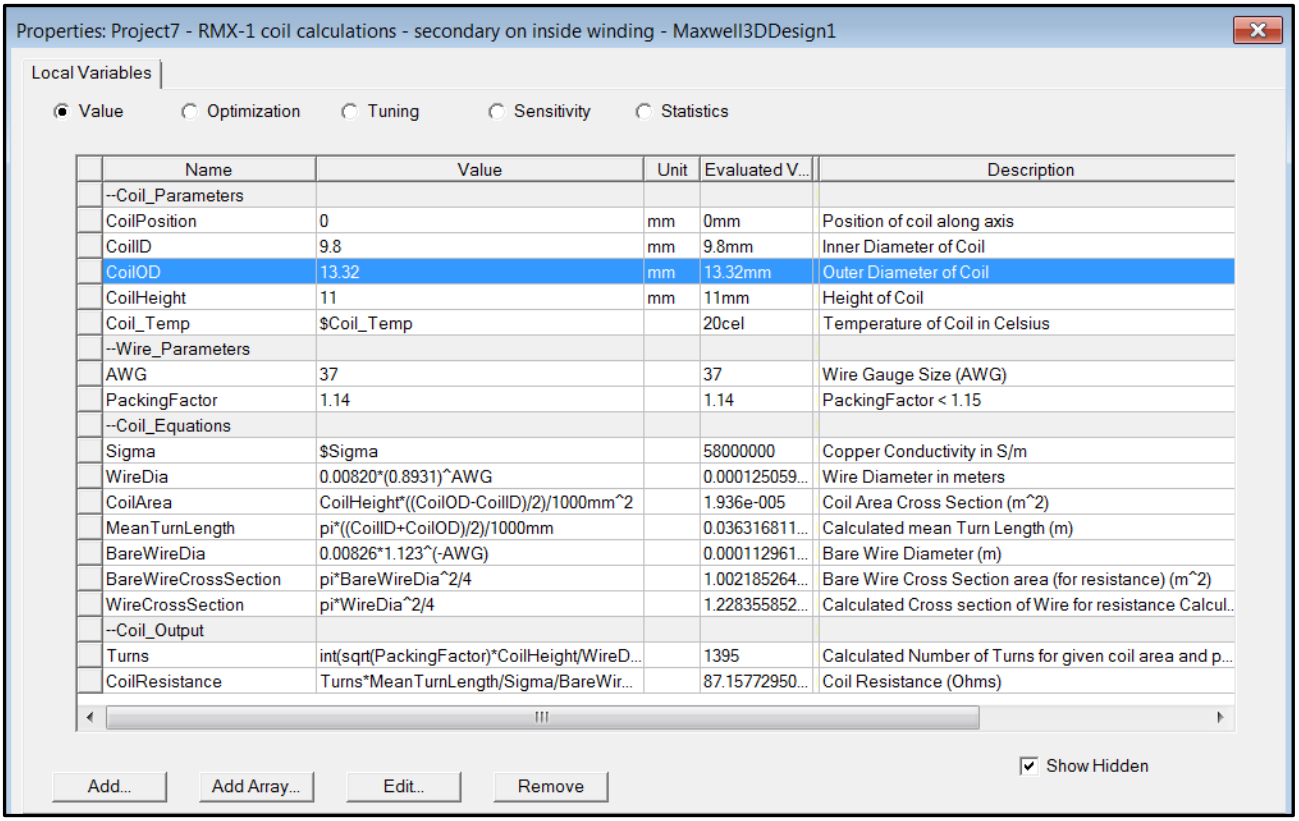

Figure 62: Maxwell® coil design toolkit – parameter entry

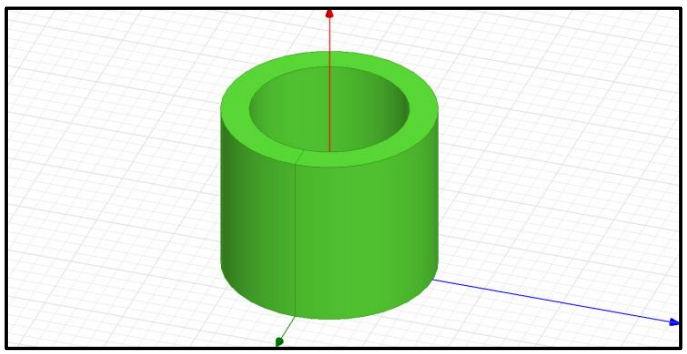

Figure 63: Maxwell® coil design toolkit – coil geometry

Once the necessary parameters of the transformer are determined with the aid of ANSYS® Maxwell®, a model for the transformer is created in COMSOL®. The mesh of the transformer model and a simulation of the magnetic flux density are illustrated in Figure 64. Students can create animations with the simulation software to visualise how the flux density and the current changes as a function of time, to gain an even better understanding of the functioning of transformers.

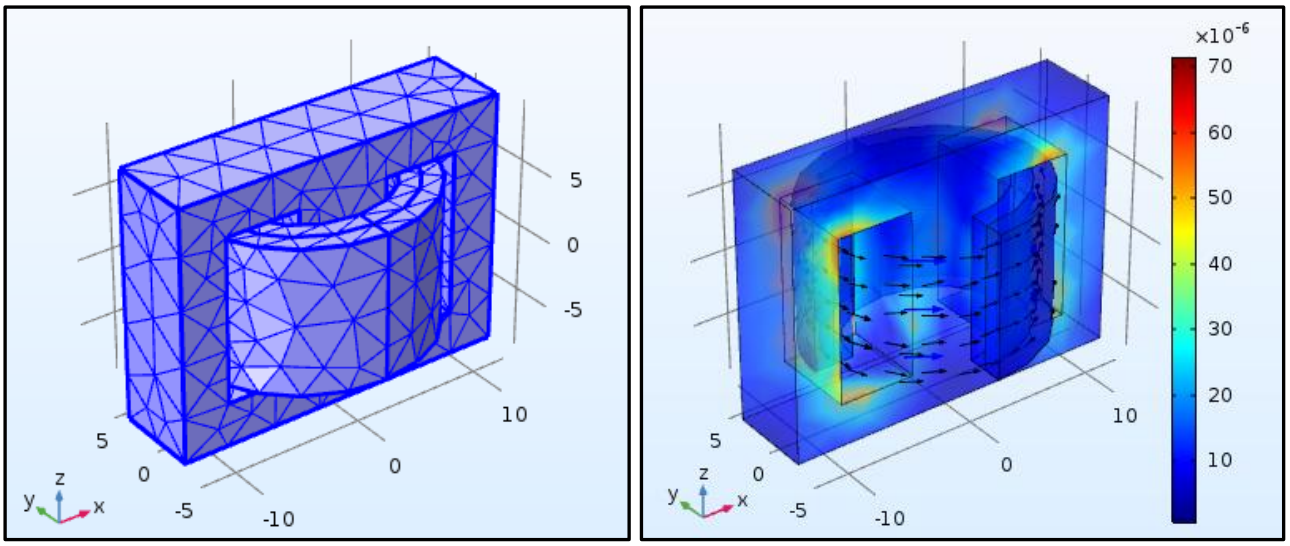

Figure 64: Mesh of RMX-1 model (geometry in mm) and magnetic flux density (Tesla)

To demonstrate the influence that the number of turns of the primary winding has on the transformer's performance, a set of simulations is run with different numbers of turns. Simulations are done for frequencies ranging from 10 Hz to 30 kHz and for the number of turns on the primary winding ranging from 5 turns to 140 turns. The simulation results are exported from COMSOL® and then processed in Microsoft Excel for display in graphical format. The results for a 10 mV (RMS) sinusoidal excitation of the primary winding with 2kΩ and 3 kΩ loads are presented in Figure 65 and Figure 66. The load on the output of the transformer also plays a role in the outcome of the simulations.

It is clear from the simulations that a low number of turns have a negative effect on the output of the transformer. A higher number of turns causes the output voltage to increase but if the number of turns is increased beyond a certain point, then the output voltage starts to decrease at higher frequencies. The reason is that the inductance increases with the increasing number of turns. The point where the graphs of all the frequencies intersect is a good choice for the number of turns to use. For the simulations that are presented here the ideal number of turns is somewhere between 35 and 41, depending on the load conditions. The earlier calculation of 38 turns fits well within this range.

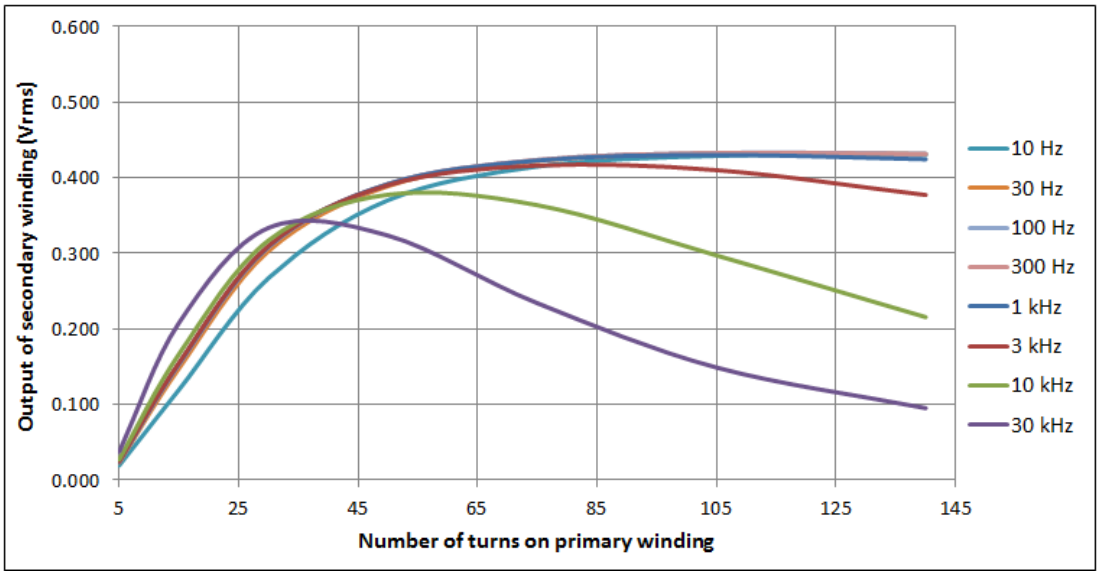

Figure 65: Number of turns on primary winding vs. output voltage (2kΩ load)

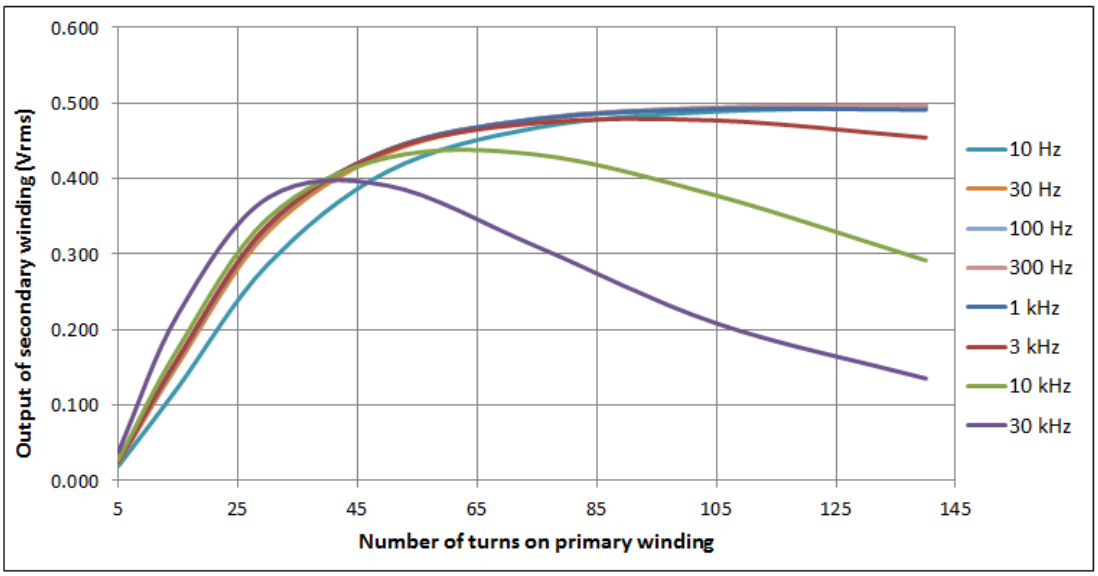

Figure 66: Number of turns on primary winding vs. output voltage (3kΩ load)

In COMSOL® the source of the test signal has zero impedance and there are no resistive losses between the source and the transformer. In a laboratory test setup however, the source has a fixed impedance and there is considerable resistance between the source and the transformer due to the connections and wires to the test equipment. A series resistance of 0.3 Ω between the signal source and the transformer is added for this reason during simulation. To illustrate the influence that the source impedance has on the results, a set of simulations are run where the source impedance is changed from 0.1 Ω to 6.4 Ω. The results for a 2 kΩ load are shown in Figure 67 and for a simulation with a 3 kΩ load in Figure 68. With a source impedance somewhere between 0.2 Ω to 0.4 Ω the transformer should have a relatively flat frequency response depending on the load. The selection of a 0.3 Ω series resistance for the simulation is therefore an acceptable choice.

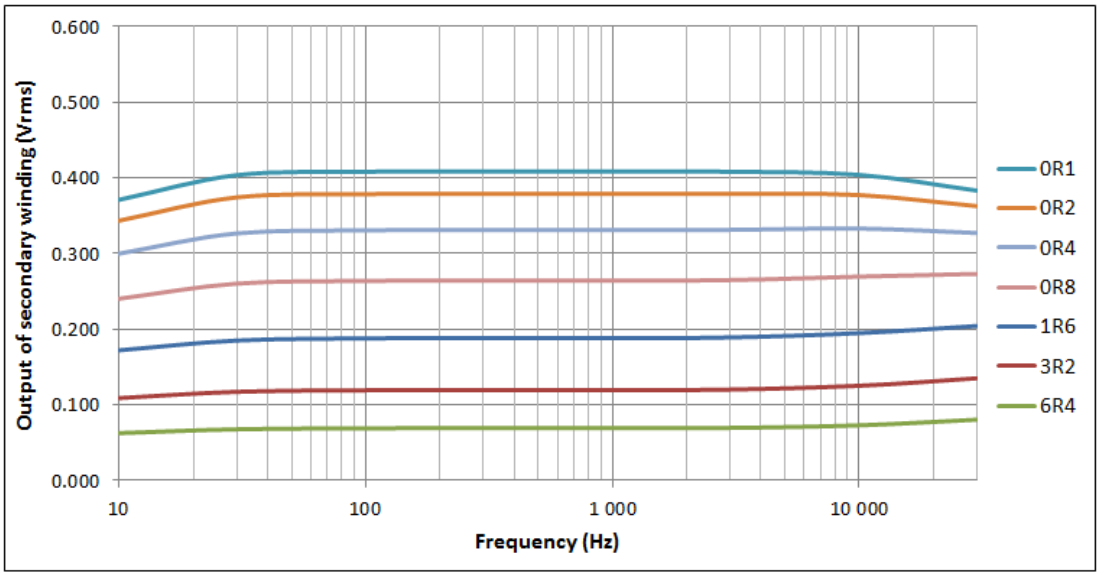

Figure 67: Influence of source impedance on output voltage (2 kΩ load)

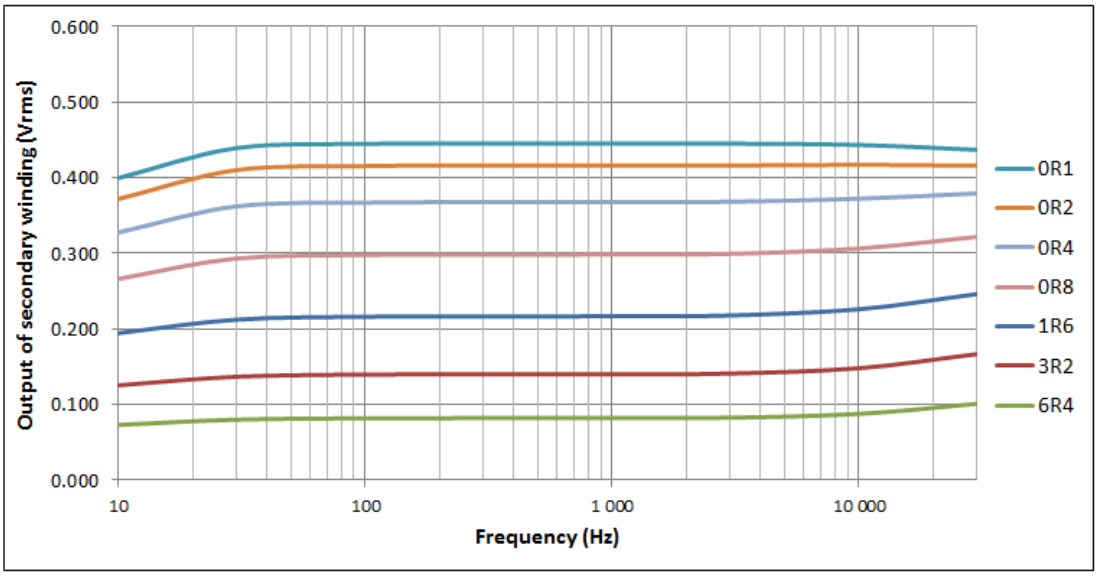

Figure 68: Influence of source impedance on output voltage (3 kΩ load)

These results are for simulations that are performed with a mu-metal transformer core. Nickel alloys that contain high percentages of nickel (around 79%) have high initial permeability and high maximum permeability, with very low hysteresis losses. The addition of molybdenum or copper further promotes specific magnetic properties. MolyPermalloys (typical 80% Ni, 4 to 5% Mo, balance Fe) and mu-metals (typical 77% Ni, 5% Cu, 2% Cr, balance Fe) are popular high permeability alloys [75]. The magnetic characteristics of these alloys make them ideal for transformer cores. The RMX-1 datasheet specifies Super Q 80 Nickel (80%) as the core material. The closest match in the simulation software's materials library is "Nickel Steel Mumetal 80% Ni". The HB curve for this material is included in the library. Figure 69 shows a comparison between the simulation results with a mu-metal core and a soft iron core. This comparison illustrates that the magnetic characteristic (given by the HB curve) is an important factor in the transformer design. Of

all the parameters that can be changed in the simulation model, the core material selection has the greatest contribution towards an ideal flat frequency response.

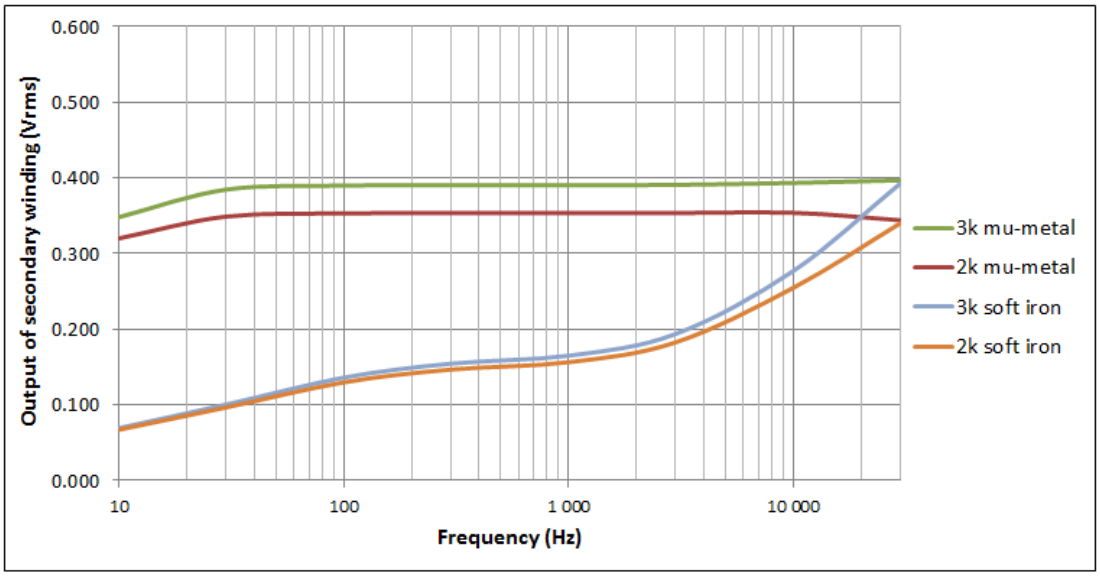

Figure 69: RMX-1 results with mu-metal core and soft iron core (2 kΩ & 3 kΩ loads)

To create the frequency response graphs the simulation results have to be exported and then manipulated in an external editor like Microsoft Excel to display the results on a graph. COMSOL® can perform a simulation in the frequency domain, but for this particular simulation there are a few hurdles to overcome. Simulation in the frequency domain cannot be performed directly on the HB/BH curve of the core material. The HB curve must first be interpolated to replace the nonlinear material with an inhomogeneous linear material that is described by a magnetic permeability constant in time, but which can be space dependent [76]. COMSOL® provides an application that computes the effective HB curve from a material's known HB relations. The application (*Effective Nonlinear Magnetic Curves Calculator*) is part of COMSOL's built-in application libraries. It creates an effective curve with the local linearized relation between the magnetic field $\boldsymbol{H}$ and the magnetic flux density $\boldsymbol{B}$ for frequency domain (time-harmonic) simulations. In the COMSOL® model the Magnetic Fields (mf) physics properties must be edited to use the effective HB curve instead. The material's HB curve must then be exported, converted to an effective HB curve and imported again to set up the correct material properties. This solves the magnetic field problem when simulating the magnetic part without the electrical circuit. When the electrical circuit is added to the frequency domain however, the *Frequency Domain solver* gives an error that "The DAE is structurally inconsistent". The solution to this problem is to change the voltage source type from a sine source to an AC-source. When the source type is changed however, then the *Coil Geometry Analysis solver* complains about the same problem. Note that COMSOL® does not allow for this experiment to be solved in the frequency domain. Therefore simulations can only be performed at discrete frequencies with post-processing in Microsoft Excel.

A cheaper Shinhom T25 transformer is available from China as a replacement for the more expensive RMX-1 from America. According to the T25 specification sheet, the RMX-1's frequency response is as depicted in Figure 70. This graph is for an unknown load.

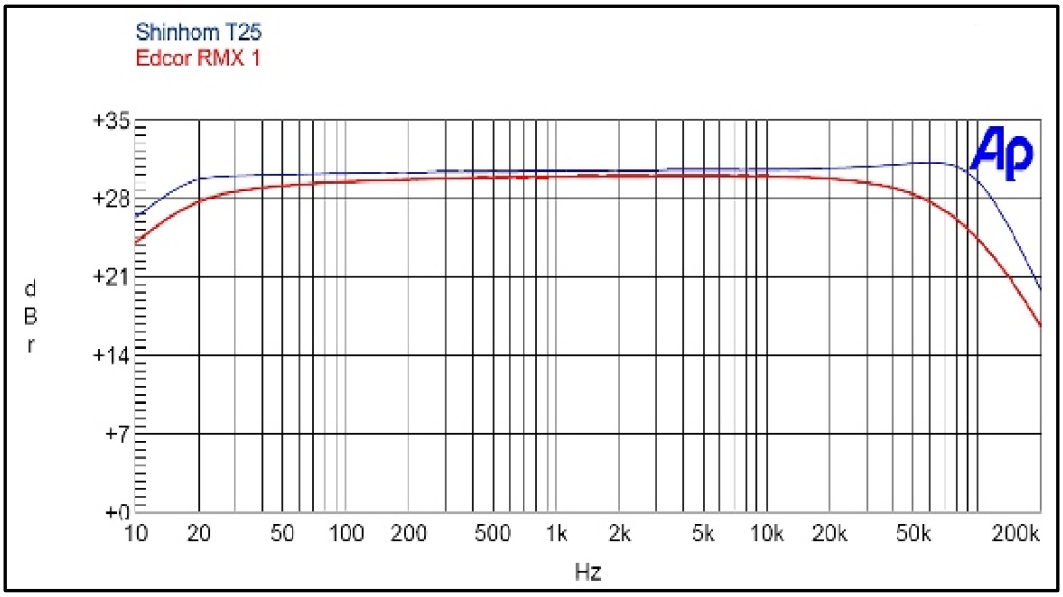

Figure 70: Frequency response of RMX-1 according to its competitor of the T25

9.2.1.3 Triad SP-48 transformer

The SP-48 transformer is not analysed and simulated in as much detail as the RMX-1 transformer. The SP-48 is completely encapsulated in epoxy and it is therefore not possible to measure the wire thicknesses of the windings. The construction of a Triad SP-13 transformer that is similar to the SP-48 is shown in Figure 71. The core dimensions of the SP-13 are the same as the SP-48, but the wire thickness is different.

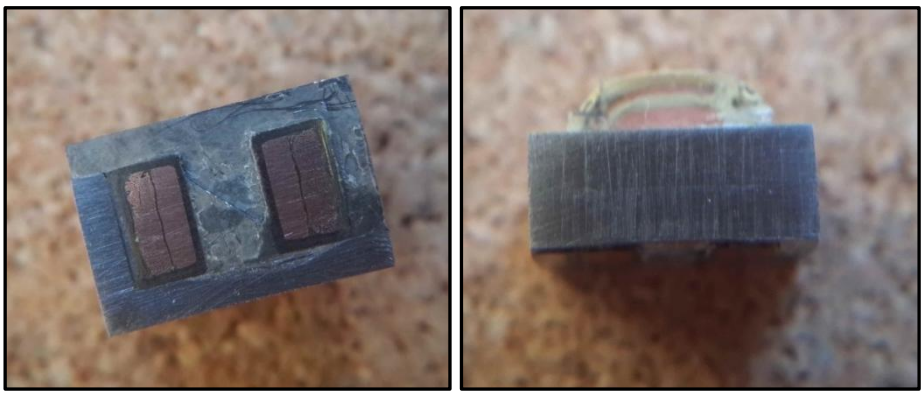

Figure 71: Cross section of Triad SP-13 transformer

A simulation model of the SP-48 is created with the same number of primary windings and core material than the RMX-1, but with different turns-ratio, smaller core and higher winding resistance. The parameters of the SP-48 transformer are listed in Table 6 alongside the parameters of the RMX-1 transformer. Figure 72 shows a comparison between the simulation results of the SP-48 and RMX-1 transformers.

Table 6: SP-48 and RMX-1 transformer parameters

Parameter	SP-48	RMX-1
Turns-ratio	1:25	1:37
DC Resistance	Primary : 2.9 Ohm Secondary : 796 Ohm	Primary : 0.4 Ohm Secondary : 87 Ohm
Core material	Unknown	Super Q 80 Nickel (80%)
E-core dimensions	Outer : 9.6 mm x 6.4 mm x 4.0 mm Inner : 7.4 mm x 4.2 mm Centre : 2.4 mm x 4.2 mm	Outer : 25.5 mm x 19 mm x 6.65 mm Inner : 18.5 mm x 12.5 mm Centre : 7.0 mm x 12.5 mm
Wire diameter	Primary : Unknown Secondary : Unknown	Primary : 380 µm, double wound. Secondary : 120 µm, single wound.
Bobbin	Outer diameter : 4.6 mm Inner diameter : 3.0 mm Winding height : 3.4 mm	Outer diameter : 17.2 mm Inner diameter : 9.8 mm Winding height : 11 mm
Number of turns	Primary : 38 Secondary : 950	Primary : 38 Secondary : 1395

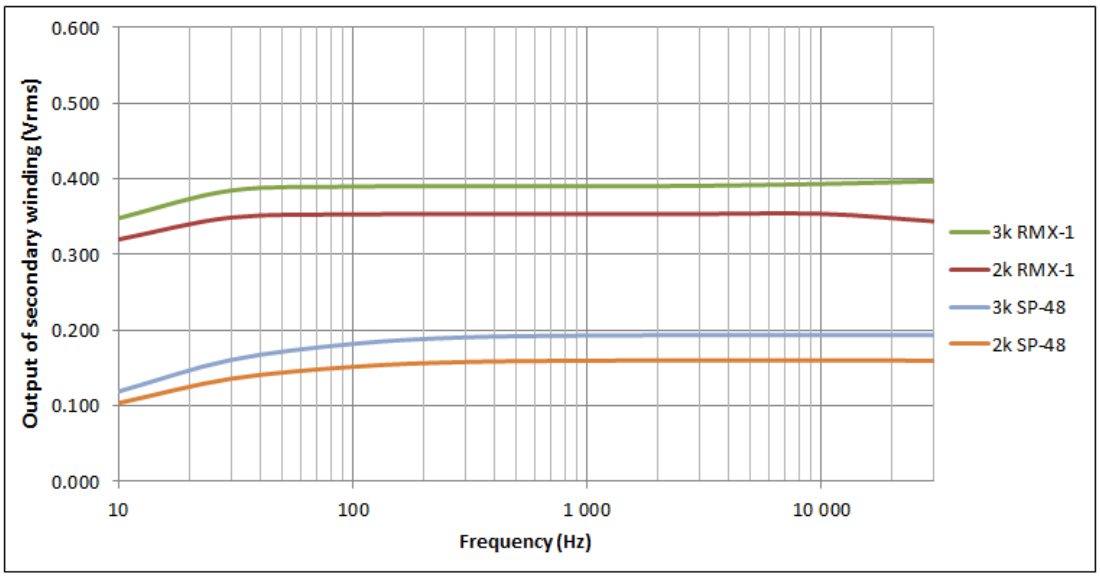

Figure 72: SP-48 simulation results vs. RMX-1 simulation results (2 kΩ & 3 kΩ loads)

9.2.2 Microphone

No simulations demonstrating the emf generated by the microphone are provided here. Simulation of the induced emf in the ribbon is not simple. The ribbon can be simulated by using the single-turn coil model and the Magnetic Fields (mf) Study in COMSOL®. To compute the emf of the ribbon, the

two ends of the ribbon must touch the external walls of the air domain surrounding the conductor. When the geometry of the model is changed so that the ribbon touches the boundary walls however, multiple other problems arise and the model causes mutually conflicting conditions.

9.3 Testing

9.3.1 Transformer

The emf generated by the ribbon microphone is extremely low – in the order of a few hundred microvolt and less. To work at voltages this low is extremely difficult because of ambient electromagnetic noise and the sensitivity of the test equipment that is required. Therefore the laboratory tests are performed with signals in the millivolt range rather than the microvolt range. The RMX-1 and SP-48 transformers Figure 73 are used in the experiments.

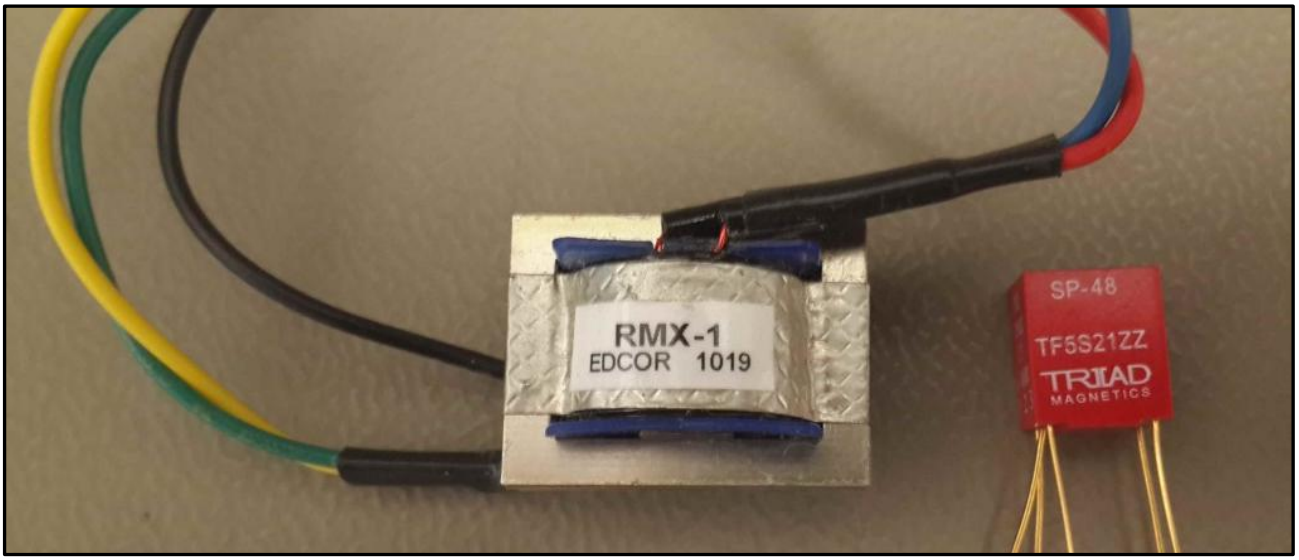

Figure 73: RMX-1 and SP-48 transformers

9.3.1.1 Manual Measurements

To verify the simulated results in section 9.2.1 a selection of discrete measurements are taken with a simple test setup. The Wavetek function generator and the Fluke multimeter are used for this experiment. The minimum output voltage of the function generator is 650 mV AC. To reduce the test voltage into the millivolt range a resistor divider network is used to reduce the output voltage of the function generator. A diagram of the test setup is provided in Figure 74. The output of the function generator is adjusted until 10 mV (RMS) is measured across the 1.1 ohm resistor while a 10 kΩ load is connected to the secondary side of the transformer. The voltages are then measured across the load on the secondary winding of the transformer for different loads and frequencies. The test results are provided in Table 7 for the RMX-1 transformer and in Table 8 for the SP-48 transformer. See Figure 75 and Figure 76 for graphical representations of these measurements and comparisons of measured versus simulated results.

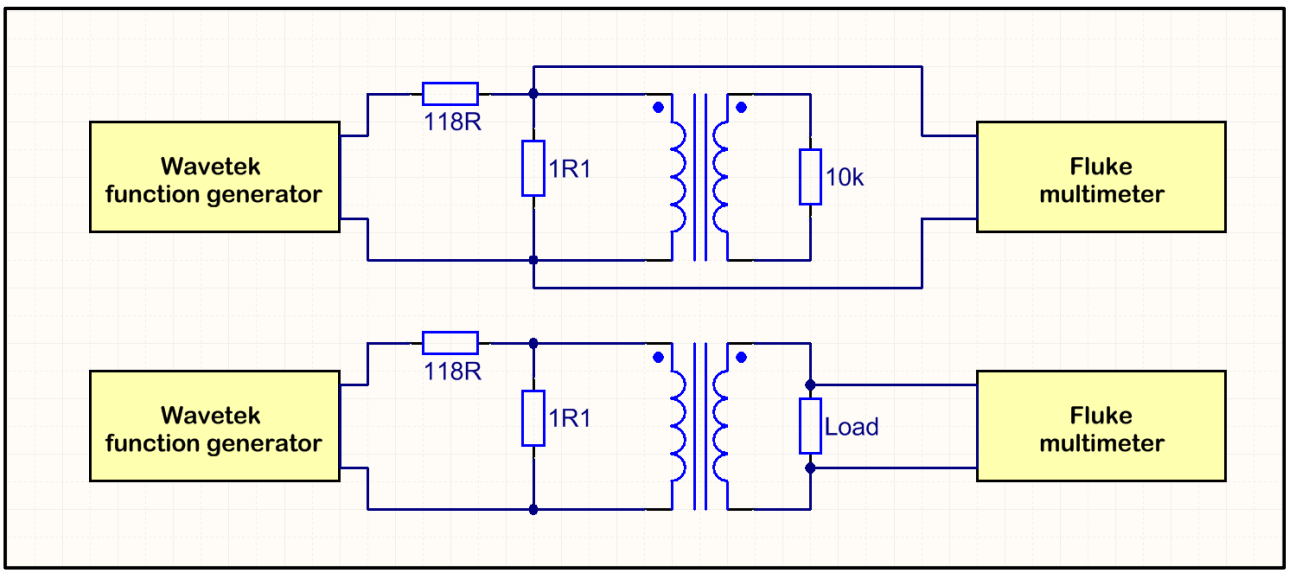

Figure 74: Test setup for manual transformer measurements

Table 7: RMX-1 measurements

Freq	RMX-1 output (mV RMS) at loads of				
(Hz)	1k2	2k	3k	10k	Open circuit
10	128	162	188	240	268
30	140	184	217	290	338
100	144	189	224	305	360
300	145	191	227	310	368
1 000	146	192	229	314	372
3 000	147	194	231	318	378
10 000	148	195	234	322	383
30 000	145	193	232	324	386

Table 8: SP-48 measurements

Freq	SP-48 output (mV RMS) at loads of				
(Hz)	1k2	2k	3k	10k	Open circuit
10	50	65	77	103	118
30	65	89	110	161	200
100	70	97	121	185	238
300	71	98	123	190	248
1 000	71	99	124	192	250
3 000	71	99	125	194	253
10 000	69	98	124	195	257
30 000	55	83	109	194	269

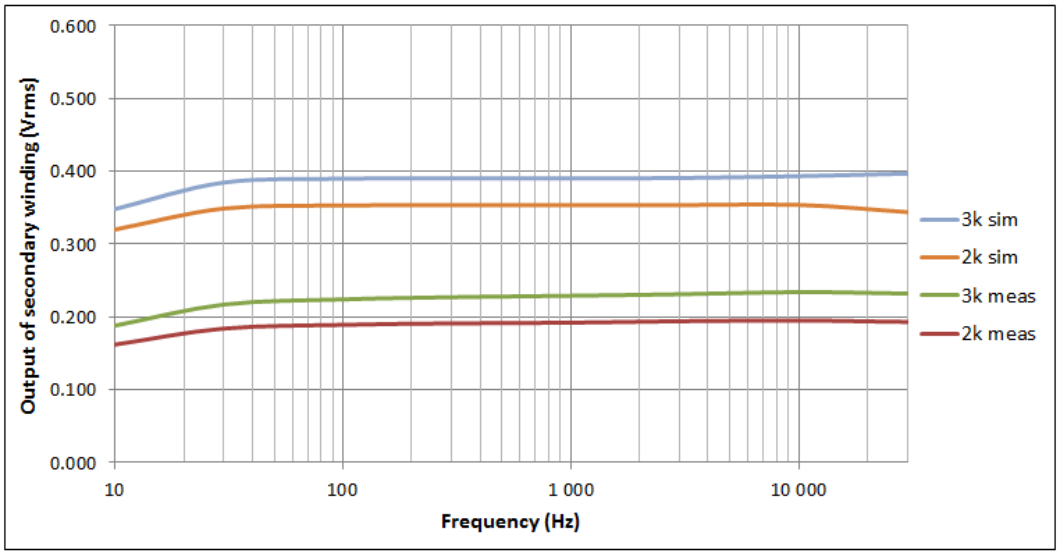

Figure 75: RMX-1 simulated results (sim) vs. measured results (meas)

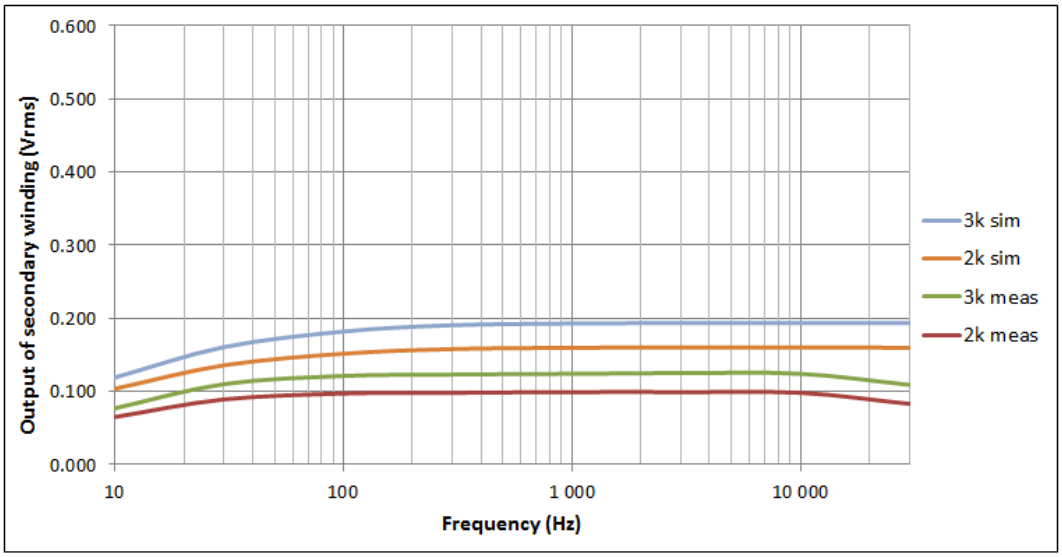

Figure 76: SP-48 simulated results (sim) vs. measured results (meas)

9.3.1.2 Automated Measurements

The number of measurements done by hand is limited to a few discrete frequencies. A wide range of frequencies can be covered in a short period of time by automated testing. Every student that owns a personal computer (PC) with a sound card can perform automated tests with little effort. With a similar resistor divider network as used in 9.3.1.1 an automated test is set up with the aid of a PC and software. John Mulcahy's REW software is used for this purpose. The test setup is shown in Figure 77.

First an automated loop-back calibration test is performed to compensate for the sound card's own non-linearity. The output of the sound card is connected directly to the input of the sound card for calibration. Thereafter, the divider network and transformer with 10 kΩ load are connected. The output level of the sound card is adjusted until 10 mV (RMS) is measured with a multimeter across

the 1.1 ohm resistor. Use a 1 kHz sinusoidal signal for this purpose. The impedance of an ordinary set of headphones is 33 ohm, so the soundcard should be able to drive the impedance of the resistor network in Figure 77. It is however still advised to check with an oscilloscope that no clipping or deformation of the sinusoidal signal occurs on the primary or secondary winding of the transformer.

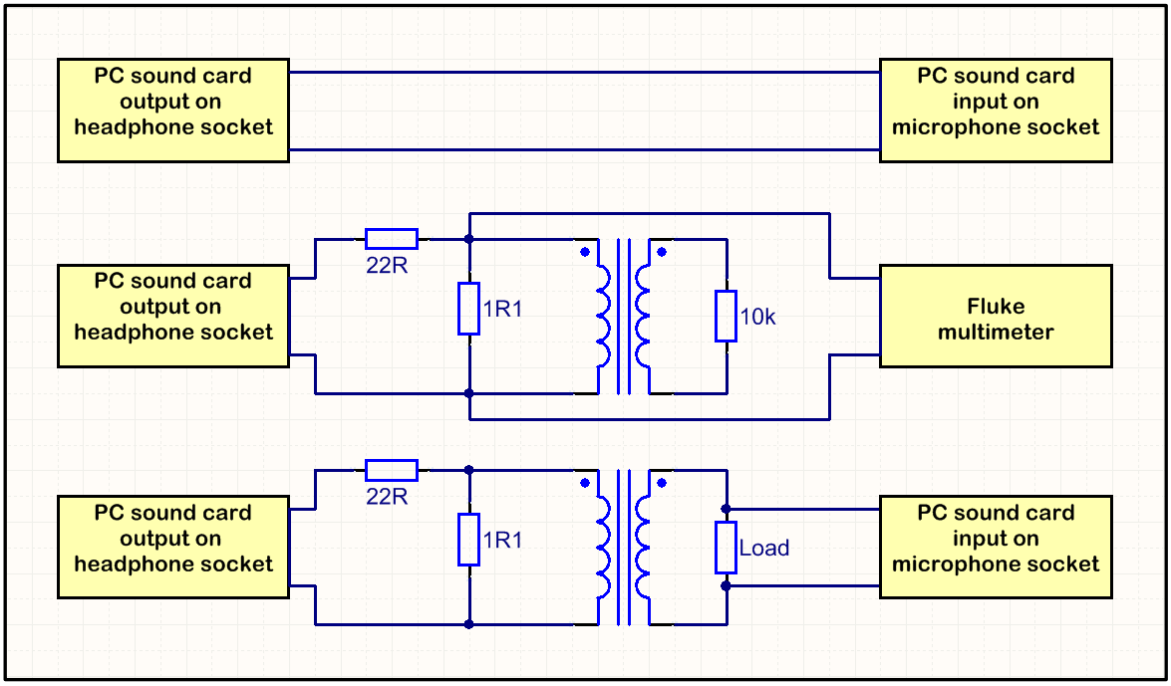

Figure 77: Test setup for automated transformer measurements

Finally the microphone input of the sound card is connected to the load on the secondary side of the transformer and the automated measurements are performed. The test results with 10 kΩ, 3 kΩ, 2 kΩ and 1.2 kΩ loads are shown in Figure 78 and Figure 79.

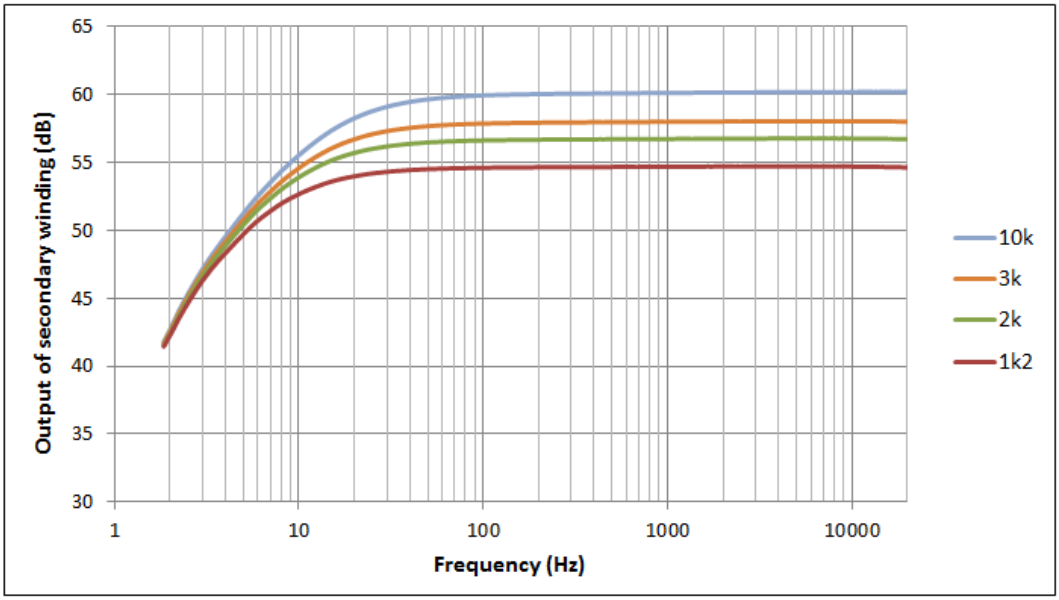

Figure 78: RMX-1 frequency response (automated test)

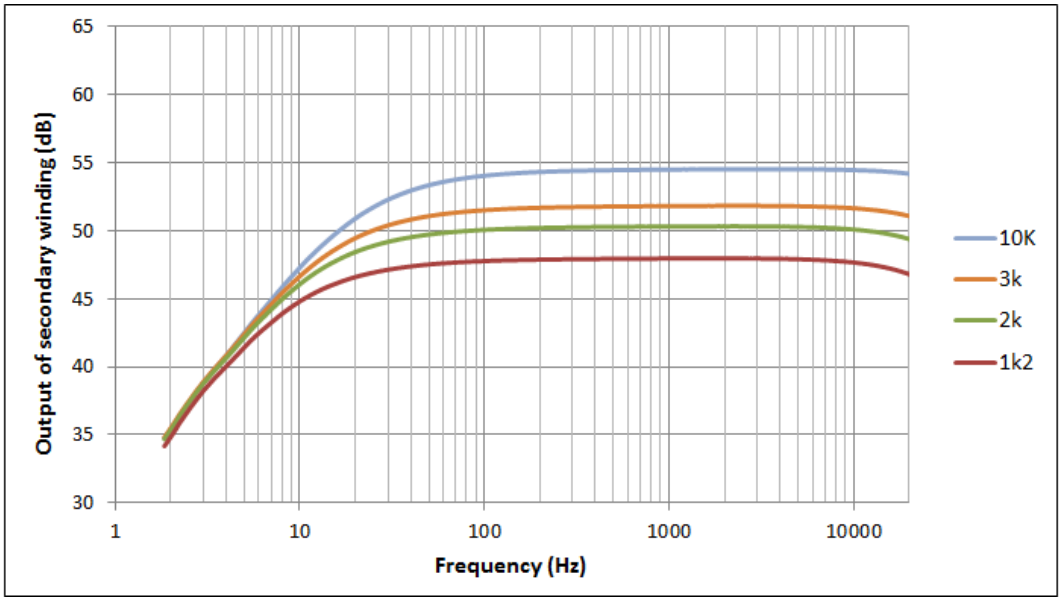

Figure 79: SP-48 frequency response (automated test)

With the soundcard's input connected to the 1.1 ohm resistor in the same position as the multimeter, in order to check the signal level on the primary winding of the transformer, the soundcard reads 33.4 dB while a 10 kΩ load is connected. The RMX-1 provides therefore a 26.6 dB gain (i.e. 21 times gain factor) instead of the ideal 37 times gain (31.4 dB) as per it turns-ratio. The SP-48 provides a gain of 21.1 dB (i.e. 11 times gain factor). It can be seen that even with a high impedance load such as 10 kΩ, the voltage gain provided by a transformer is substantially less than the ideal gain based on its turns-ratio.

9.3.1.3 Impedance Matching

The output impedance of a ribbon microphone is typically less than one ohm and the input impedance of an amplifier can range anywhere between 1 kΩ and 10 kΩ depending on the model. A transformer may be used to match the impedance between the microphone and the amplifier of a sound system. With the wide range of amplifiers that are available a single transformer will unfortunately not always match the impedance of the amplifier. The laboratory test results and the simulated results discussed earlier illustrate how source and load impedances have an influence on the signal transfer from source to load. The loads that are chosen represent two selectable impedances of the Focusrite Scarlett 2i2 computer audio interface and two selectable impedances of the Buzzaudio MA-2.2 professional microphone amplifier.

A complete table of impedances versus frequencies for the RMX-1 and SP-48 secondary windings is provided in Table 9. The impedances on the secondary winding are measured while a 1.1 Ω resistor remains connected to the primary winding.

Table 9: Impedances of secondary transformer winding at different frequencies

Freq (Hz)	DC	10	30	100	300	1 000	3 000	10 000	30 000
RMX-1 impedance (Ω)	88	1 620	1 758	1 826	1 858	1 889	1 945	2 065	2 249
SP-48 impedance (Ω)	787	1 898	2 825	2 994	3 058	3 096	3 215	3 802	7 463

The maximum power transfer theorem states that maximum power is transferred from a source to a load when the impedances of the source and the load are equal [72]. A transformer may be used to match the impedance between a source and its load. Reflected impedance is commonly used in electronic circuits to achieve maximum power transfer. To test the validity of this theorem in the current test setup the test results in Table 7 and Table 8 are used to calculate the power transfer to each load. The results of the power calculations that are presented in Table 10 and Table 11 support the maximum power theorem. These results are good illustrations that most power is transferred to the load that match the output impedance of the transformer. The same can be illustrated for the input of the transformer, but it is more difficult to perform measurements on the low voltage signals of the primary winding. This experiment illustrates how the electromagnetic properties of a transformer can be utilized to minimize energy losses when transferring energy from a low impedance source to a high impedance load.

Table 10: RMX-1 power transfer (μW) to different loads

Freq (Hz)	10	30	100	300	1 000	3 000	10 000	30 000
1.2 kΩ load	13.65	16.33	17.28	17.52	17.76	18.01	18.25	17.52
2 kΩ load	13.12	16.93	17.86	18.24	18.43	18.82	19.01	18.62
3 kΩ load	11.78	15.70	16.73	17.18	17.48	17.79	18.25	17.94
10 kΩ load	5.76	8.41	9.30	9.61	9.86	10.11	10.37	10.50

Table 11: SP-48 power transfer (μW) to different loads

Freq (Hz)	10	30	100	300	1 000	3 000	10 000	30 000
1.2 kΩ load	2.08	3.52	4.08	4.20	4.20	4.20	3.97	2.52
2 kΩ load	2.11	3.96	4.70	4.80	4.90	4.90	4.80	3.44
3 kΩ load	1.98	4.03	4.88	5.04	5.13	5.21	5.13	3.96
10 kΩ load	1.06	2.59	3.42	3.61	3.69	3.76	3.80	3.76

9.3.2 Electronic Amplifier

The same tests that are performed with the two transformers are also performed with two electronic amplifiers.

The first amplifier is the AD8231 instrumentation amplifier from Analog Devices. An instrumentation amplifier is chosen because of its high common mode rejection ratio (100-120 dB). The AD8231 in particular is chosen for its low voltage operation (±1.5V to ±2.5V), low input offset (4-15 μV) and the fact that it has binary selectable gains of 1 to 128.The schematic for the AD8231 electronic amplifier circuit is provided in Figure 80.

The second amplifier is the INA103 instrumentation amplifier from Texas Instruments. The INA103 is chosen because it is a high fidelity amplifier, specifically designed for low noise operation. The schematic for the INA103 electronic amplifier circuit is shown in Figure 81. The gain resistor (47 Ω) on the INA103 is selected to match the highest gain (128) of the AD8231.

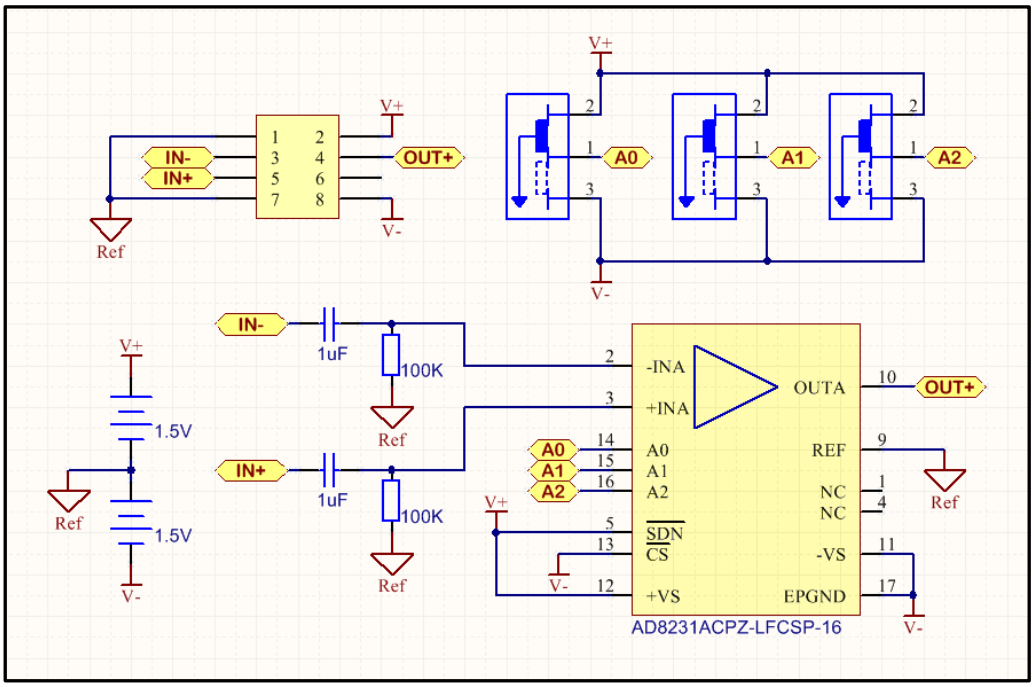

Figure 80: AD8231 amplifier schematic

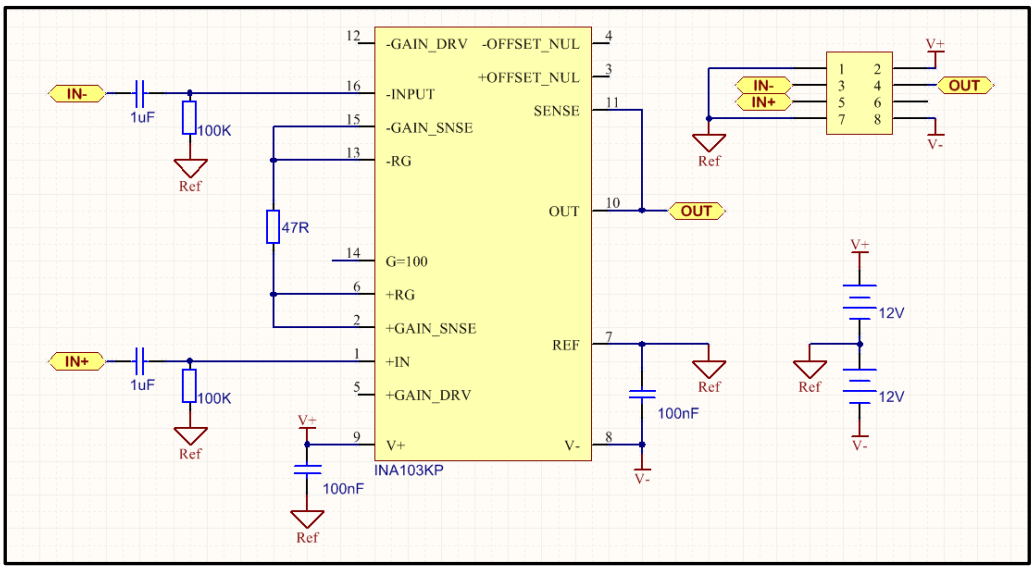

Figure 81: INA103 amplifier schematic

The same automated test setup (Figure 77) that is used for the transformers is also used with the amplifiers.

The AD8231 is tested at different gains, since the gain can be easily changed with just a few switches. The test results are displayed in Figure 82. The gain of the AD8231 is independent of the load. Load tests that are done with loads ranging from 1.2 kΩ to 10 kΩ all give identical results than Figure 82 across all gains. With a gain of one on the AD8231, the sound card reads 29.6 dB for a 1 kHz sine wave. The detailed data of Figure 82 shows a level of 59.9 dB at 1 kHz for a gain selection of 32 on the AD8231. The effective gain is then 30.3 dB. This is very close to the theoretical gain of 30 dB. See Table 12 for a quick conversion between gain as a multiplication factor and gain in dB.

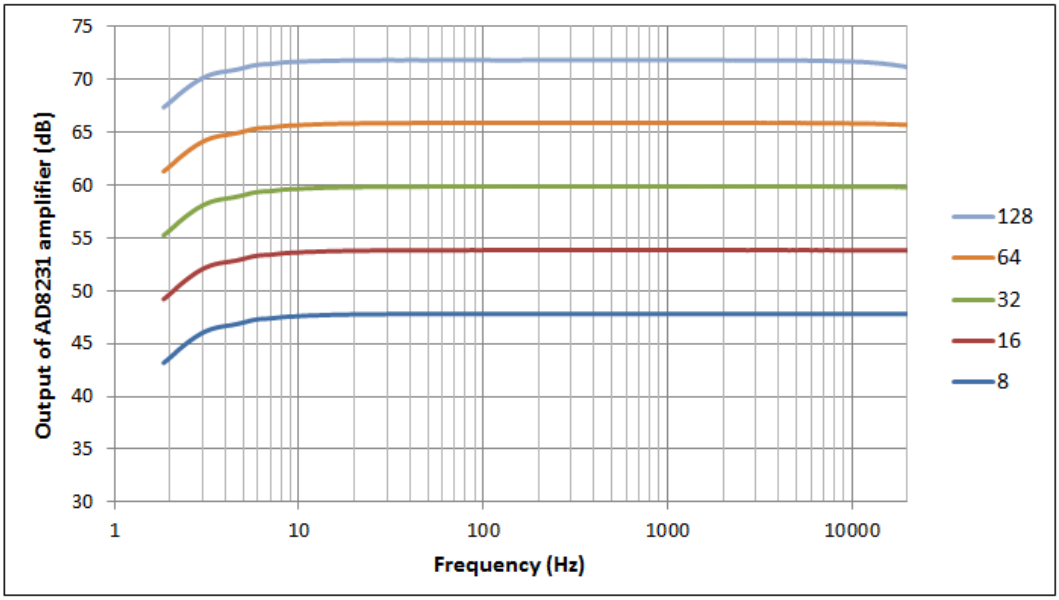

Figure 82: AD8231 amplifier gain test

To illustrate the influence of the RC-filter on the input of the amplifier the 100 kΩ resistors on the AD8231's inputs are changed to 10 kΩ. The result is a filter that suppresses the lower frequencies. This is clearly illustrated in Figure 83.

An electronic amplifier has the advantage that it adds energy to the signal during amplification. That energy is taken from the circuit's power supply.

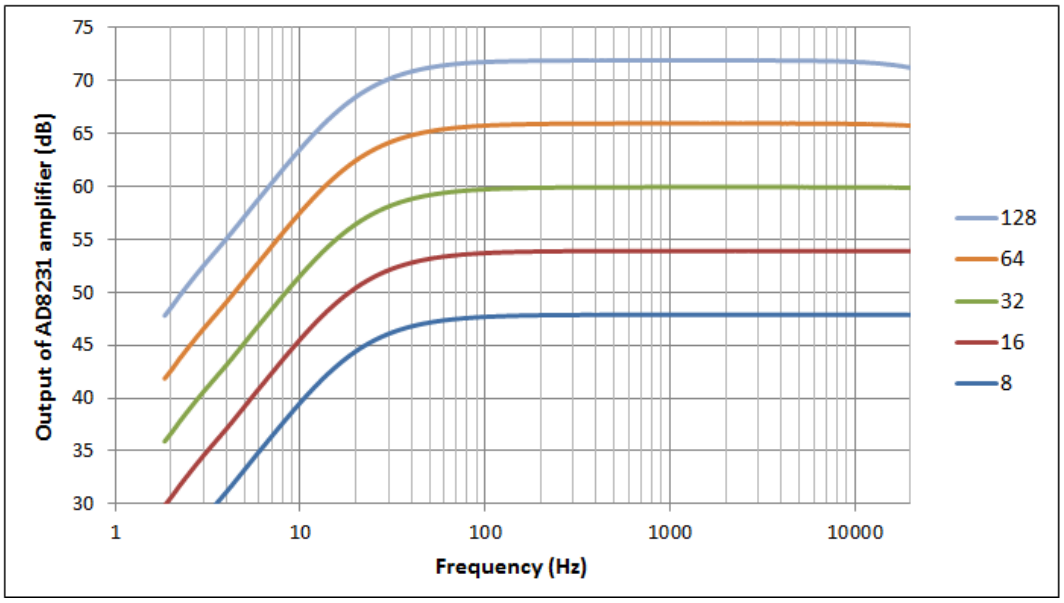

Figure 83: AD8231 amplifier gain test with high pass filter

The electronic amplifier does not only add energy to the signal, but it also adds noise in the process. Each of the components in the amplifier adds noise into the circuit and this noise is amplified together with the microphone signal through all the consecutive stages of the amplifier. The noise is clearly audible as a “hiss” when the signal is further amplified by the final stage amplifier. For this reason there are high fidelity amplifiers available that are specifically designed for low noise operation. The INA103 instrumentation amplifier is one example of such an amplifier. Listening tests conducted with the INA103 confirm that the noise level of this low noise amplifier is orders of magnitude lower than the AD8231. The noise level of the INA103 is comparable with that of a transformer. The frequency response of the IN103 versus the AD8231 at a gain of 128 is given in Figure 84.

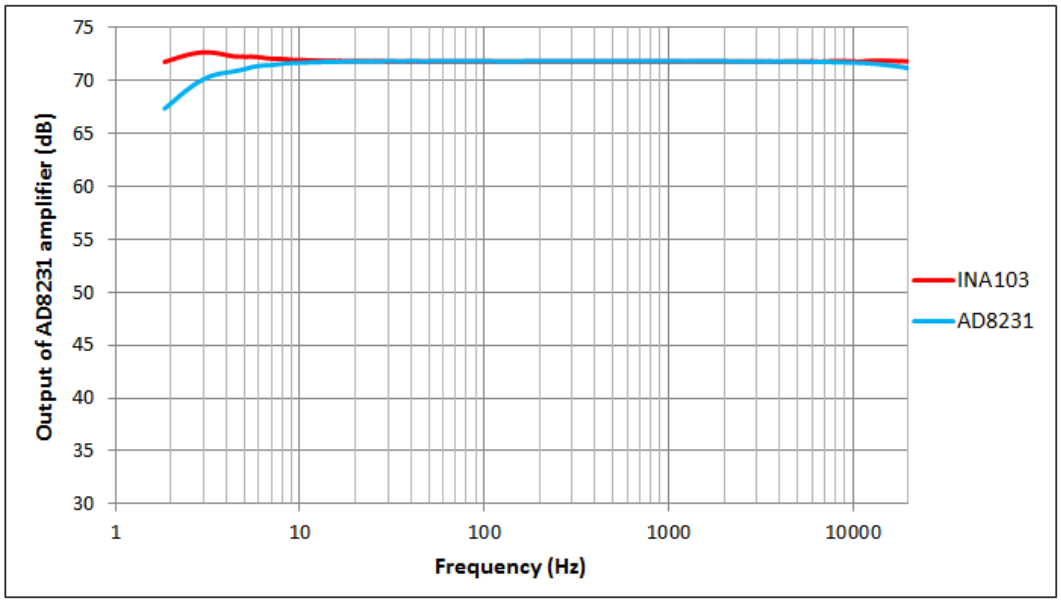

Figure 84: INA103 vs. AD8231 frequency response at gain of 128

Table 12: Voltage gain multiplication factor to voltage gain in dB

Gain multiplier	Gain in dB
128	42
100	40
64	36
37	31
32	30
25	28
16	24
8	18

9.3.3 Microphone

To conclude the hardware tests the ribbon microphone is connected to each transformer and amplifier for a frequency sweep.

The test setup consists of the following:

- Ribbon microphone
- RMX-1 and SP-48 transformers
- AD8231 and INA103 amplifier circuits
- Dell Optiplex 9020 PC
- Logitech S-220 speaker set
- REW software

Figure 85: Test setup with ribbon microphone and RMX-1 transformer

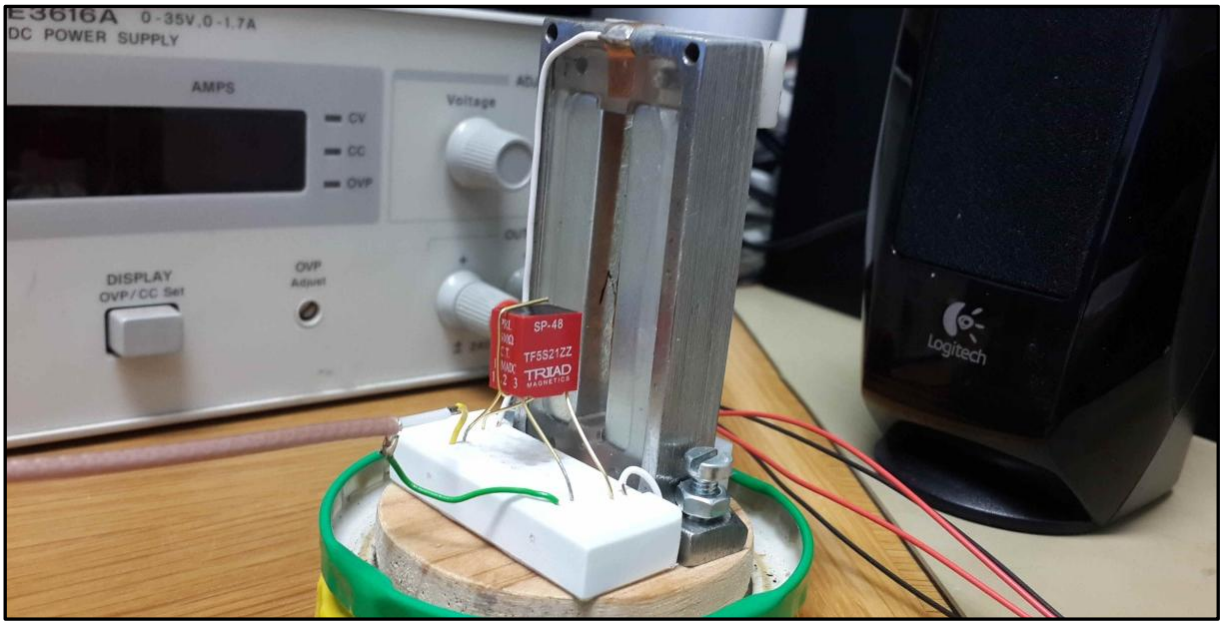

Figure 86: Ribbon microphone and SP-48 transformer

The frequency sweeps with the two transformers are shown in Figure 87. The frequency responses are very similar, only with the RMX-1 providing a higher gain than the SP-48.

The frequency dip between 50 Hz and 90 Hz is not a function of the transformers or the microphone. It is a problem with the transition between the subwoofer and the main speakers of the S-220 set. This is a frequency band that is poorly covered by both speakers.

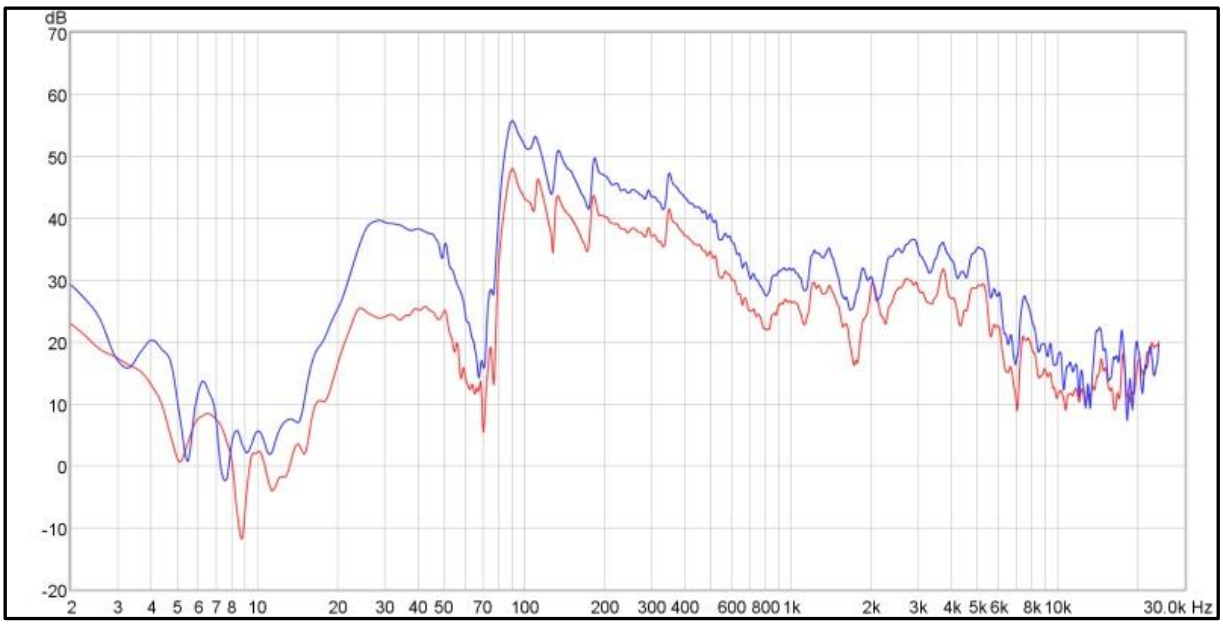

Figure 87: Microphone frequency response with RMX-1 (blue) and SP-48 (red)

The RMX-1 is compared to the AD8231 amplifier with a gain setting of 32 in Figure 88. Once again the frequency responses are very similar. Although the gain of the AD8231 is lower than the 1:37 turns-ratio of the RMX-1, the AD8231 provides a higher gain because it is not influenced like the transformer by the load impedance.

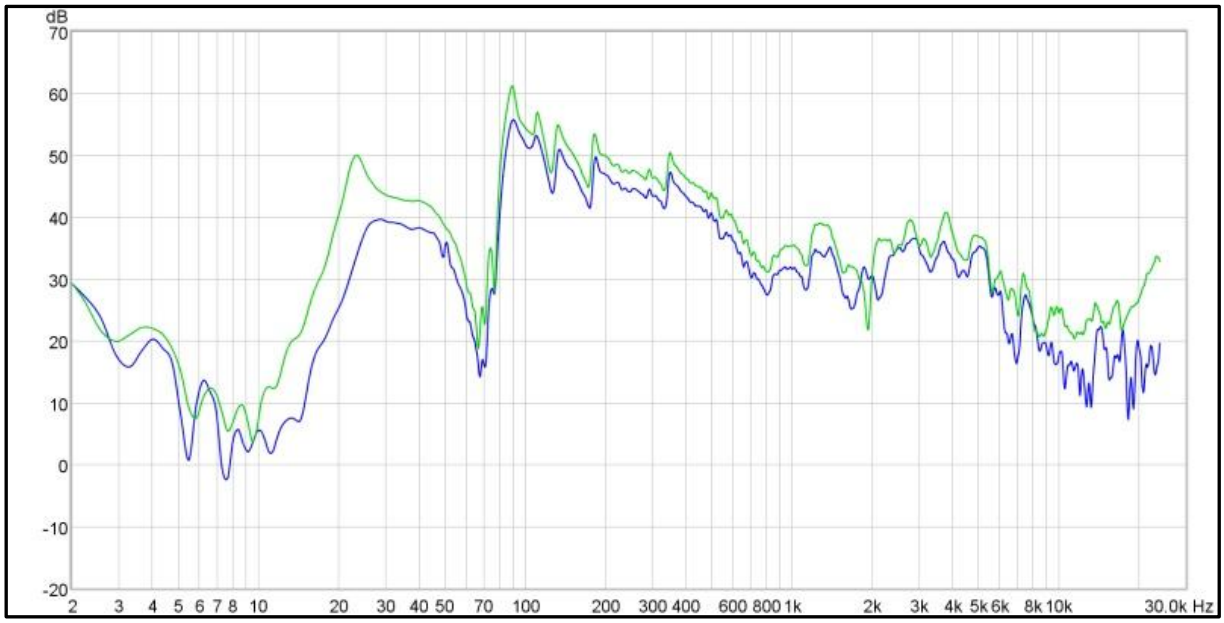

Figure 88: Microphone frequency response with RMX-1 (blue) and AD8321 (green)

In Figure 89 the AD8231 results are shown for gains of 32 and of 128. In the last illustration (Figure 90) the results of the AD8231 and INA103 are illustrated with gains of 128. Although it cannot be seen on the frequency response graphs, the INA103 has much less background noise than the AD8231 when listening to the microphone. The noise level of the INA103 is almost as low as the two transformers, but its gain is much higher, making it ideal as a ribbon microphone amplifier.

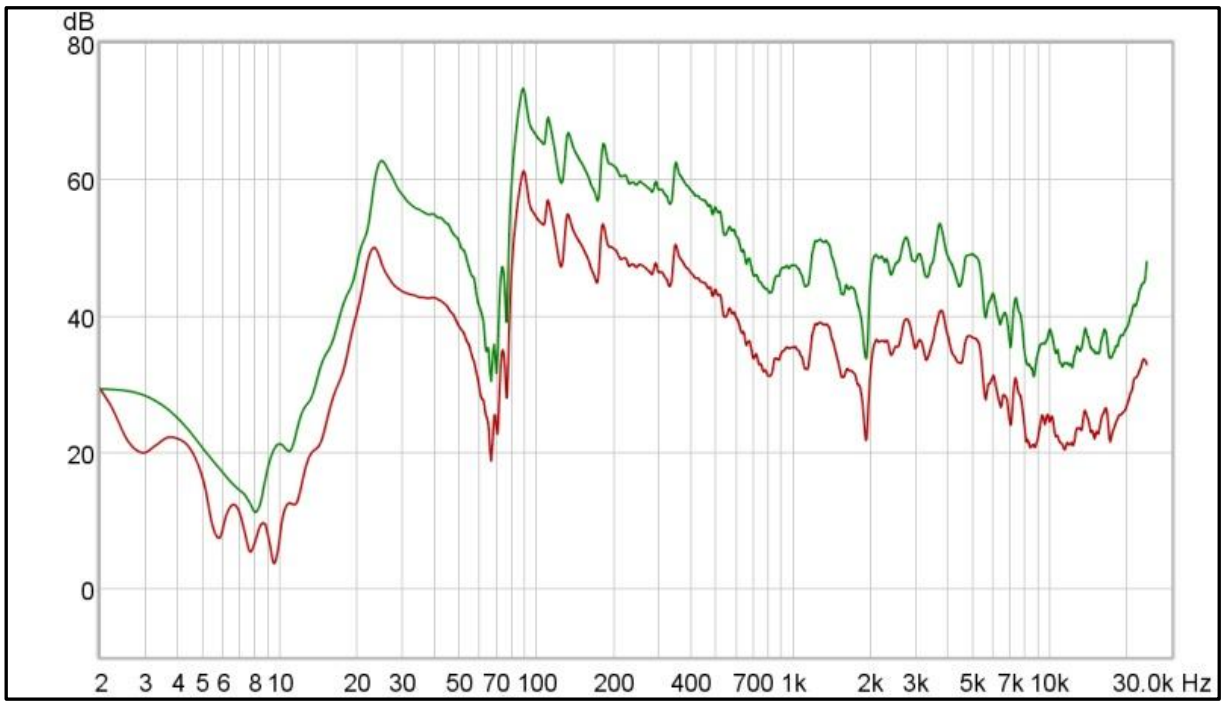

Figure 89: Microphone with AD8231 amplifier at gains of 32 and 128

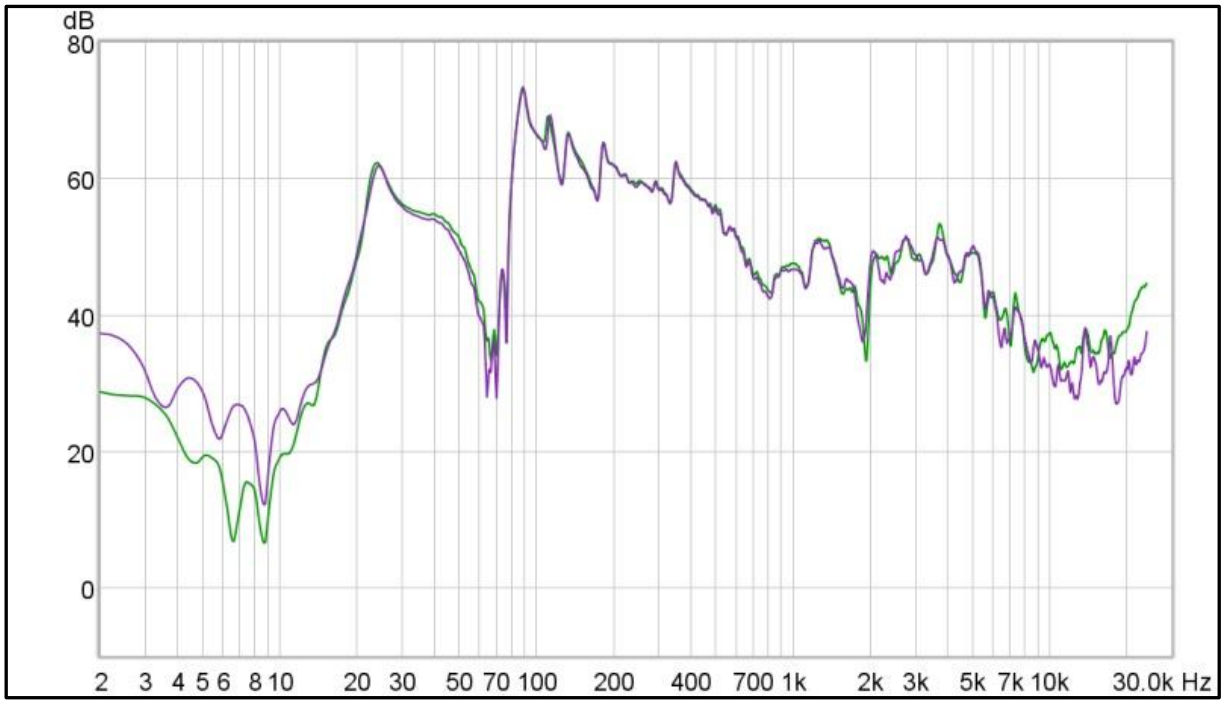

Figure 90: Microphone with AD8231 (green) and INA103 (purple)

9.4 Conclusion

One of the benefits of simulations is that parameters can be changed that are not always possible with the hardware at hand. The core material of the transformer is such an example. Although it cannot be verified with an experiment, the simulation exercises show that the choice of material for the transformer core plays a more important role in its performance than any of the other parameters that can be changed.

The following comparisons can be drawn between transformers and electronic amplifiers according to the tests results in 9.3:

- Transformers work well for impedance matching, but the output signal amplitude is load dependent. It is however a passive component that requires no external power.
- Electronic amplifiers work well for impedance matching and the amplitude of the output signal is not load dependent. It is however an active component that requires external power.
- A properly shielded transformer adds almost no audible noise to the signal, but most electronic amplifiers, even when properly shielded from ambient electrostatic noise, adds a substantial amount of audible noise to the signal. Only specially designed low noise amplifiers can match the noise levels of a transformer.

The impedance difference of a transformer between a DC signal and an AC signal clearly illustrates the importance of frequency when it comes to impedance matching. DC tests are much simpler to perform and the mathematics is less complicated than AC tests, but it can be totally

misleading. Transformer tests over a wide frequency range, like audio signals, provide the student with a better understanding of the role that frequency response plays in the design of a system.

The high input impedance of the electronic amplifier has a specific benefit for the ribbon microphone in a laboratory test setup. Instead of a low resistance aluminium ribbon, a polyethylene terephthalate (PET) film with vaporized aluminium can be used in the laboratory. The resistance of the vaporized aluminium is much higher than that of a 2 µm aluminium ribbon, but with the high input impedance of the amplifier it is no longer a problem. PET is about half the weight of aluminium, but much more tear resistant. So a stronger ribbon can be used in demonstrations to make the microphone more durable for laboratory use.

Audio tests with electronic amplifiers and transformers can be used by students to experience the effect of noise in different systems. The tests can be expanded to include demonstrations of the effect that short cables versus long cables, cable screening and differential signals have on noise levels.

The ribbon microphone serves as a good low energy source of emf that can be amplified through the electromagnetic properties of transformers or with low power electronic amplifiers.

Simulation models can provide students, without the need for hardware, with a better understanding of the effects that various parameters have on the design of a system. The hardware provides a method to verify with a limited number of experiments that the simulations and theory are correct. Students can perform relatively accurate first-order tests with the minimum amount of test equipment by using the built-in sound cards of their personal computers.

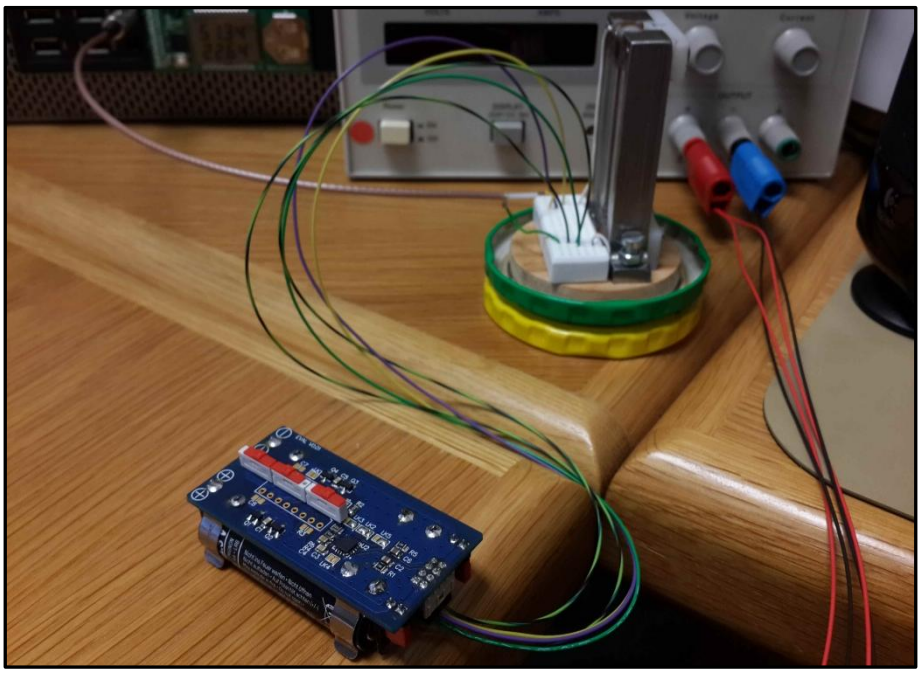

Figure 91: Ribbon microphone and AD8231 amplifier running from two AA cells

10 A FINAL WORD

Considering the minute movement of an aluminium ribbon in a sound wave, it is a truly amazing accomplishment that someone could, more than eighty years ago, detect and amplify the voltage generated by this tiny movement in a magnetic field.

Of all the theory that was mastered and the discoveries that were made during the work for this thesis, none was as valuable as witnessing first-hand how many consistent, seemingly insignificant efforts, over a long period of time, come together to accomplish a task that seemed so insurmountable at times.

11 REFERENCES

[1] M. van Wyk and P. Meyer, “The Ribbon Microphone - An Educational Aid,” in *3rd International Conference on Advances in Computational Tools for Engineering Applications (ACTEA)*, Zouk Mosbeh, Lebanon, 2016.

[2] National Academy of Engineering, “Engineering in K-12 Education,” National Academic Press, Washington D.C., 2009.

[3] National Research Council, “Engineering Graduate Education and Research,” NATIONAL ACADEMY PRESS, Washington, D.C., 1985.

[4] National Academies of Science, Engineering & Medicine, “Undergraduate Research Experiences for STEM Students: Successes, Challenges and Opportunities,” National Academies Press, Washington, D.C., 2017.

[5] National Research Council, “Engineering Undergraduate Education,” National Academy Press, Washington, D.C, 1986.

[6] B. H. Ferri, A. A. Ferri, D. M. Majerich and A. G. Madden, “Effects of In-class Hands-On Laboratories in a Large Enrollment, Multiple Section Blended Linear Circuits Course,” *Advances in Eingineerin Education,* pp. 1-27, 2016.

[7] National Research Council, “Improving Indicators of the Quality of Science and Mathematics Education in Grades K-12,” National Academy press, Washington, D.C., 1988.

[8] N. Savage, R. Birch and E. Noussi, “Motivation of engineering students in higher education,” *Engineering Education,* pp. 39-46, 2011.

[9] National Research Council, “Transforming Undergraduate Education in Science, Mathematics, Engineering, and Technology,” National Academy Press, Washington, D.C., 1999.

[10] National Research Council, “Discipline-Based Education Research,” National Academies Press, Washington, D.C., 2012.

[11] National Research Council, “Education and learning to think,” Nationl Academy Press, Washington, D.C, 1987.

[12] National Research Council, “From Analysis to Action: Undergraduate Education in Science, Mathematics, Engineering and Technology,” National Academy Press, Washington, D.C., 1996.

[13] L. D. Feisel and A. J. Rosa, “The Role of the Laboratory in Undergraduate Engineering Education,” *Journal of Engineering Education,* pp. 121-130, 2005.

[14] X. Liu, “Effects of Combined Hands-on Laboratory and Computer Modeling on Student Learning of Gas Laws: A Quasi-Experimental Study,” *Journal of Science Education and Technology,* pp. 89-100, 2006.

[15] D. Heise, “Asserting the inherent benefits of hands-on laboratory projects vs. computer simulations,” in *Consortium for Computing Sciences in Colleges (CCSC)*, Central Plains Conference, 2006.

[16] B. Taylor, P. Eastwood and B. Jones, “Development of a Low-cost, Portable Hardware Platform to Support Hands-on Learning in the Teaching of Control and Systems Theory,” *Engineering Education,* pp. 62-73, 2014.

[17] S. Lee, M. C. Harrison and C. L. Robinson, “Engineering students’ knowledge of mechanics upon arrival: Expectation and reality,” *Engineering Education,* pp. 32-38, 2006.

[18] F. W. Sears, M. W. Zemansky and H. D. Young, University Physics, USA: Addison-Wesley, 1982.

[19] R. T. Beyer, Sounds of Our Times, New York: Springer, 1999.

[20] P. White, Basic Microphones, London: Sanctuary Publishing Limited, 1999.

[21] J. Eargle, The Microphone Book, Burlington: Focal Press, 2005.

[22] G. Ballou, J. Ciaudelli and V. Schmitt, Handbook for Sound Engineers, Burlington: Focal Press, 2008.

[23] H. F. Olson, “Apparatus for converting sound vibrations into electrical variations”. US Patent 1885001, 31 March 1931.

[24] J. F. Schneider, Bay Area Radio (Images of America), Charleston: Arcadia Publishing, 2012.

[25] W. Dooley, “Evolution of an icon,” *Technology,* pp. 58-60, September 2008.

[26] D. E. Royer and R. T. Perrotta, “Ribbon-microphone transducer”. US Patent 2006/0078135, 8 October 2004.

[27] R. Cloud and S. Sank, “Ribbon microphone with rounded magnet motor assembly, backwave chamber, and phantom powered JFET circuit”. US Patent 8433090, 9 October 2010.

[28] H. F. Olson, “Apparatus for converting sound vibrations into electrical variations”. United States Patent 1885001, 25 October 1932.

[29] H. F. Olson and J. Weinberger, “Sound Pick-up Device”. US Patent 19115, 4 April 1933.

[30] L. J. Anderson, “Electroacoustical apparatus”. US Patent 2173219, 29 May 1937.

[31] S. Ruttenberg, “Acoustic Compensator”. US Patent 2196342, 15 January 1938.

[32] L. G. Bostwick, “Acoustic device”. US Patent 2230104, 20 December 1938.

[33] H. F. Olson, “Sound Translating Apparatus”. US Patent 2301638, 2 January 1940.

[34] L. J. Anderson, “Magnetic Equalization of Sensitivity in Ribbon Microphoen Assemblies”. US Patent 2476396, 29 April 1942.

[35] E. W. Rogers, “Microphone device”. US Patent 2361656, 9 February 1942.

[36] H. F. Olson, “Directional microphone”. US Patent 2539671, 28 February 1946.

[37] L. J. Anderson, “Pressure gradient responsive microphone”. US Patent 2527344, 30 January 1947.

[38] H. F. Olson and J. Preston, “Velocity microphone”. US Patent 2699474, 29 December 1950.

[39] L. J. Anderson, “Magnetic structure”. US Patent 2963557, 1 June 1954.

[40] C. P. Fisher, “Ribbon microphone”. US Patent 3435143, 2 August 1965.

[41] E. D. Royer and T. R. Perrotta, “Ribbon Microphone”. US Patent 6434252, 20 September 1999.

[42] D. E. Royer and R. T. Perrotta, “Ribbon microphoe incorporating a special-purpose transformer and/or other randsucer-output circuitry”. US Patent 2006/0078152, 8 October 2004.

[43] H. Akino, “Moving ribbon microphone”. US Patent 7430297, 1 March 2005.

[44] R. J. Crowley, “Acoustic ribbon transducer arrangements”. US Patent 7894619, 3 October 2005.

[45] H. A. Tripp and R. J. Crowley, “methods for forming and usin thin film ribbon microphone elements and the like”. US Patent 8218795, 16 March 2007.

[46] H. Akino, “Ribbon for ribbon microphone, manufacturing method of the same, and ribbon microphone”. US Patent 2009/0208038, 12 February 2009.

[47] R.-H. Horng, C.-C. Chang, M.-L. Ke, G.-W. Chen and Y.-C. Tsai, “Acoustoelectric transformation chip for ribbon microphone”. US Patent 2009/0245544, 24 March 2009.

[48] H. Akino, “Ribbon Microphone”. US Patent 8744090, 30 March 2012.

[49] M.-L. Ke, R.-H. Horng, Y.-C. Tsai, G.-W. Chen and C.-C. Chang, “Design and simulation of miniature ribbon microphones,” *J. Micro/Nanolinth MEMS MOEMS,* vol. 8, no. 2, pp. 021160-1 to 021160-5, Apr-Jun 2009.

[50] R.-H. Horng, “Study on Miniature Ribbon Microphone,” in *6th IEEE International Conference on Nano/Micro Engineered and Molecular Systems*, Kaohsiung, Taiwan, 2011.

[51] Y. W. Kwon and J. Honorato, “AN INVESTIGATION OF THE PERFORMANCE OF A RIBBON AND SMALL PLANAR MAGNETIC TRANSDUCER, MADE FOR USE IN AIR, AS AN UNDERWATER ACOUSTIC VELOCITY SENSOR,” Naval Postgraduate School, Monterey, California, 2016.

[52] ANSYS, *ANSYS AIM,* ANSYS 2015, 2017.

[53] Shure Incorporated, 6 April 2009. [Online]. Available: http://www.shure.com/americas/news-events/press-releases/crowley-and-tripp-acquisition. [Accessed 15 October 2016].

[54] D. Rochman, “Roswellite – What Is This Stuff?,” 29 April 2010. [Online]. Available:

http://blog.shure.com/what-is-this-stuff/. [Accessed 15 October 2016].

[55] A. Fisher, “Bumblebee diy pro audio,” 22 November 2015. [Online]. Available: http://www.bumblebeepro.com/ribbon-microphone/ribbon-microphone-foil-thickness/. [Accessed 14 May 2017].

[56] M. D. Kelzenberg, “Software: 4192A Sweep Utility,” 2015. [Online]. Available: http://mkelzenb.caltech.edu/software/4192A/. [Accessed 27 June 2016].

[57] R. A. Serway and J. W. Jewett, Physics for Scientists and Engineers with modern Physics, Belmont: Brooks/Cole - Thomson Learning, 2004.

[58] H. F. Olson, Acoustical Engineering, Princeton: D. van Nostrand Company, 1957.

[59] L. E. Kinsler, A. R. Frey, A. B. Coppens and J. V. Sanders, Fundamentals of Acoustics, New York: John Wiley & Sons, 1982.

[60] H. Kuttruff, Room Acousics, London: Applied Science Publishers, 1979.

[61] COMSOL, *COMSOL Multiphysics Reference Manual 5.0,* COMSOL, 2014.

[62] A. M.-J. Lamarche, “Putting the Singing Voice on the Map,” KTH School of Computer Science and Communication, Stockholm, 2009.

[63] H. F. Olson, Music, Physics and Engineering, New York: Dover Publications, 1967.

[64] COMSOL, *Structural Mechanics Module User's Guide 5.2,* COMSOL, 2015.

[65] A. Meiring, “Design of a Ribbon Microphone,” Department of Mechanical and Mechatronic Engineering, Stellenbosch University, Stellenbosch, 2015.

[66] H. Q. Fuller, R. M. Fuller and R. G. Fuller, Physics, Including Human Applications, New York: Harper & Row, 1978.

[67] A. Stanley, “An Exploratory Investigation into How Cold Working Can Affect the Acoustic Performance of Thin Aluminum Foil in a Ribbon Microphone,” California Polytechnic State University, San Luis Obispo, 2012.

[68] A. Guimaraes, Magnetism and Magnetic Resonance in Solids, Rio de Janeiro: John Wiley &

Sons, Inc., 1998.

[69] S. Chikazumi, Physics of Magnetism, New York: John Wiley & Sons, 1964.

[70] J. M. D. Coey, Magnetism and Magnetic Materials, Cambridge: Cambridge University Press, 2010.

[71] D. A. Fleisch, A Student's Guide to Maxwell's Equations, Cambridge: Cambridge University Press, 2008.

[72] W. G. Hurley and W. H. Wölfle, Transformers and Inductors for Power Electronics, John Wiley & Sons, 2013.

[73] Boundless, " "EMF and Terminal Voltage." Boundless Physics," Boundless Physics, 8 August 2016. [Online]. Available: https://www.boundless.com/physics/textbooks/boundless-physics-textbook/circuits-and-direct-currents-20/resistors-in-series-and-parallel-151/emf-and-terminal-voltage-537-1104/. [Accessed 29 March 2017].

[74] Wikipedia, "Wikipedia," 29 May 2017. [Online]. Available: https://en.wikipedia.org/wiki/American_wire_gauge. [Accessed 17 June 2017].

[75] ASM International, "ASM Specialty Handbook: Nickel, Cobalt, and Their Alloys (#06178G)," 2017.

[76] COMSOL, *AC/DC Module User's Guide version 5.2a,* COMSOL, 2016.

12 PERMISSIONS

Rightslink® by Copyright Clearance Center - Chromodo

https://s100.copyright.com/AppDispatchServlet#formTop

Copyright Clearance Center RightsLink®

Home | Create Account | Help

IEEE Requesting permission to reuse content from an IEEE publication

Title: The ribbon microphone — An educational aid: Use of a ribbon microphone to teach multi-discipline computer simulation skills

Conference Proceedings: Advances in Computational Tools for Engineering Applications (ACTEA), 2016 3rd International Conference on

Author: Marius van Wyk

Publisher: IEEE

Date: July 2016

Copyright © 2016, IEEE

LOGIN

If you're a copyright.com user, you can login to RightsLink using your copyright.com credentials. Already a RightsLink user or want to learn more?

Thesis / Dissertation Reuse

The IEEE does not require individuals working on a thesis to obtain a formal reuse license, however, you may print out this statement to be used as a permission grant:

Requirements to be followed when using any portion (e.g., figure, graph, table, or textual material) of an IEEE copyrighted paper in a thesis:

1) In the case of textual material (e.g., using short quotes or referring to the work within these papers) users must give full credit to the original source (author, paper, publication) followed by the IEEE copyright line © 2011 IEEE.
2) In the case of illustrations or tabular material, we require that the copyright line © [Year of original publication] IEEE appear prominently with each reprinted figure and/or table.
3) If a substantial portion of the original paper is to be used, and if you are not the senior author, also obtain the senior author's approval.

Requirements to be followed when using an entire IEEE copyrighted paper in a thesis:

1) The following IEEE copyright/ credit notice should be placed prominently in the references: © [year of original publication] IEEE. Reprinted, with permission, from [author names, paper title, IEEE publication title, and month/year of publication]
2) Only the accepted version of an IEEE copyrighted paper can be used when posting the paper or your thesis on-line.
3) In placing the thesis on the author's university website, please display the following message in a prominent place on the website: In reference to IEEE copyrighted material which is used with permission in this thesis, the IEEE does not endorse any of [university/educational entity's name goes here]'s products or services. Internal or personal use of this material is permitted. If interested in reprinting/republishing IEEE copyrighted material for advertising or promotional purposes or for creating new collective works for resale or redistribution, please go to http://www.ieee.org/publications_standards/publications/rights/rights_link.html to learn how to obtain a License from RightsLink.

If applicable, University Microfilms and/or ProQuest Library, or the Archives of Canada may supply single copies of the dissertation.

BACK | CLOSE WINDOW

Copyright © 2016 Copyright Clearance Center, Inc. All Rights Reserved. Privacy statement. Terms and Conditions.
Comments? We would like to hear from you. E-mail us at customercare@copyright.com